AD-A189 608 CALCULATED UNSTEADY AERODYNAMICS OF WINGS(U) 1/1
MASSACHUSETTS INST OF TECH CAMBRIDGE DEPT OF
AERONAUTICS AND ASTRONAUTICS J E MCCUNE 15 DEC 87
UNCLASSIFIED AFOSR-TR-88-0031 AFOSR-86-0157 F/G 1/1 NL

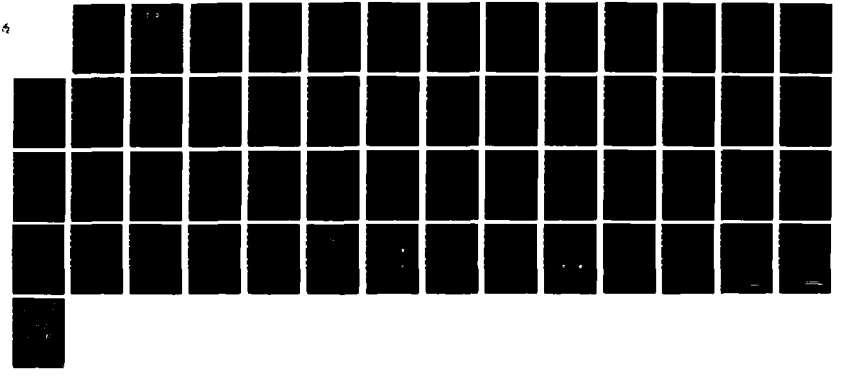

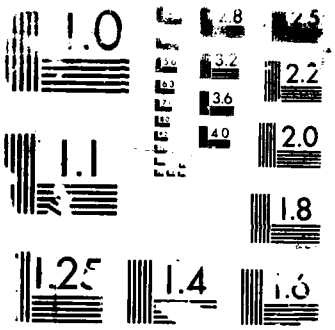
1.0
1.1
1.25
1.4
1.6
1.8
2.0
2.2
3.2
3.6
4.0

SEC

AD-A189 608

IMENTATION PAGE

Form Approved
OMB No. 0704-0188

1a. [illegible] Unclassified

DTIC ELECTE FEB 25 1988 S D H

1b. RESTRICTIVE MARKINGS

2a. SECURITY CLASSIFICATION AUTHORITY

3. DISTRIBUTION / AVAILABILITY OF REPORT
Approved for Public Rel.
Distribution is unlimited

2b. DECLASSIFICATION / DOWNGRADING SCHEDULE

4. PERFORMING ORGANIZATION REPORT NUMBER(S)

5. MONITORING ORGANIZATION REPORT NUMBER(S)
AFOSR-TR- 88-0031

6a. NAME OF PERFORMING ORGANIZATION	6b. OFFICE SYMBOL (If applicable)	7a. NAME OF MONITORING ORGANIZATION
M.I.T.		AFOSR/NA

6c. ADDRESS (City, State, and ZIP Code)	7b. ADDRESS (City, State, and ZIP Code)
77 Massachusetts Ave. 33-214 Cambridge, MA 02139	Building 410 Bolling AFB, DC 20332

8a. NAME OF FUNDING / SPONSORING ORGANIZATION	8b. OFFICE SYMBOL (If applicable)	9. PROCUREMENT INSTRUMENT IDENTIFICATION NUMBER
AFOSR/NA	NA	AFOSR-86-0157

8c. ADDRESS (City, State, and ZIP Code)	10. SOURCE OF FUNDING NUMBERS			
	PROGRAM ELEMENT NO.	PROJECT NO.	TASK NO	WORK UNIT ACCESSION NO.
Building 410 Bolling AFB, DC 20332	61102F	2307	A3	--

11. TITLE (Include Security Classification)
(U) "Calculated Unsteady Aerodynamics of Wings"

12. PERSONAL AUTHOR(S)
J.E. McCune

13a. TYPE OF REPORT	13b. TIME COVERED	14. DATE OF REPORT (Year, Month, Day)	15. PAGE COUNT
Annual (18 mos.)	FROM 5/86 TO 11/87	12/15/87	52 pages

16. SUPPLEMENTARY NOTATION
N/A

17. COSATI CODES			18. SUBJECT TERMS (Continue on reverse if necessary and identify by block number)
FIELD	GROUP	SUB-GROUP	Aerodynamics of Wings, Unsteady Wing Theory, Wake Evolution, Vortex Core Evolution, Wings in Maneuver, Unsteady Wing Loads

19. ABSTRACT (Continue on reverse if necessary and identify by block number)

Progress is reported for the contract period covering the past 18 months. Substantial advances in the analysis of the large-amplitude unsteady aerodynamics of wings have been achieved and are summarized in the attached papers. Special focus has been placed on developing techniques for describing the exact non-linear convection, deformation, and roll-up of the vorticity wakes above and behind active wing surfaces. Using a combination of analytic and computer-interactive methods, new insights and more exact aerodynamic performance results have been generated. The effects of dissipative internal "cores" in the overall 3D wake structures above deltas have been analyzed in the slender-wing limit. New paths for further computer-assisted advances, including improved understanding of wing-wake interaction in severe maneuver, vortex core formation and break-up, and aerodynamic history effects have been charted.

20. DISTRIBUTION / AVAILABILITY OF ABSTRACT	21. ABSTRACT SECURITY CLASSIFICATION
☒ UNCLASSIFIED/UNLIMITED ☐ SAME AS RPT ☐ DTIC USERS	Unclassified

22a. NAME OF RESPONSIBLE INDIVIDUAL	22b. TELEPHONE (Include Area Code)	22c. OFFICE SYMBOL
Capt. Henry E. Helin	(202) 767-0471	AFOSR/NA

DD Form 1473, JUN 86 — Previous editions are obsolete. — SECURITY CLASSIFICATION OF THIS PAGE

UNCLASSIFIED

AFOSR Grant Nr. AFOSR-86-157

Annual Technical Report

Period: May, 1986 - November, 1987

"Calculated Unsteady Aerodynamics of Wings"

J.E. McCune

Masssachusetts Institute of Technology

Department of Aeronautics and Astronautics

Abstract

Progress is reported for the contract period covering the past 18 months. Substantial advances in the analysis of the large-amplitude unsteady aerodynamics of wings have been achieved and are summarized in the attached papers. Special focus has been placed on developing techniques for describing the exact non-linear convection, deformation, and roll-up of the vorticity wakes above and behind active wing surfaces. Using a combination of analytic and computer-interactive methods, new insights and more exact aerodynamic performance results have been generated. The effects of dissipative internal "cores" in the overall 3D wake structures above deltas have been analyzed in the slender-wing limit. New paths for further computer-assisted advances, including improved understanding of wing-wake interaction in severe maneuver, vortex core formation and break-up, and aerodynamic history effects have been charted.

Statement of Progress

The papers attached summarize as carefully as we are able the sequential aspects of the progress made during the above contract period. In addition to these three papers, two key Master of Science thesis reports (see attached list) have proved to be major contributors to our understanding of wing aerodynamics involving both large-scale unsteady motion and viscous-related phenomena such as leading-edge separation, bubble formation and reattachment and vortex core evolution.

In paper 1 "Nonlinear Aerodynamics of Two-Dimensional Airfoils in Severe Maneuver" (Scott/McCune), advanced computer-interactive techniques for studying large-amplitude unsteady wake motion behind host airfoils is described. The nonlinear generalization of the classical Wagner equation is included.

In paper 2 "Interactive Aerodynamics of Wings in Severe Maneuver" (McCune, Colorado Springs), analysis of exact nonlinear unsteady wake convection over slender delta wings in severe maneuver is described. Application of paper 1 to that problem is detailed.

In paper 3 "Slender Wing Theory Including Regions of Embedded Total Pressure Loss" (McCune, Tavares, Lee, Weissbein), self-consistent wake development over slender wings including the development of dissipative, low-total-pressure core regions is described. Viscous related criteria for the sizing and evolution of core size shape and intensity are discussed. The importance of the "history" effect of wake development on wing performance is pointed out.

List of Publications Prepared During Subject Period

1. Scott, Matthew T., J.E. McCune, "Nonlinear Aerodynamics of Two-Dimensional Airfoils in Severe Maneuver", AIAA Paper Nr. 88-0129, AIAA 26th Aerospace Sciences Meeting, Reno NV, Jan., 1988. Attached.

2. McCune, J.E., "Interactive Aerodynamics of Wings in Severe Maneuver." To be included in Proceedings of Workshop II on Unsteady Flow, United States Air Force Academy, July 28-30, 1987. To be published. Attached.

3. McCune, J.E., T.S. Tavares, N.K.W. Lee, and D. Weissbein, "Slender Wing Theory Including Regions of Embedded Total Pressure Loss", AIAA Paper Nr. 88-0320, AIAA 26th Aerospace Sciences Meeting, Reno NV, Jan., 1988. Attached.

List of Related M.I.T. Theses (Master of Science)

1. Weissbein, D., "Embedded Vortical Regions Within Otherwise Irrotational Flows", M.I.T. S.M. Thesis, June 1987.

2. Scott, M., "Nonlinear Airfoil Wake Interaction in Large Amplitude Unsteady Flow", M.I.T. S.M. Thesis, June 1987.

List of of Recent Interactions Away From M.I.T.

Jan., 1987 AIAA Annual Aerosciences Meeting, Reno NV.

June, 1987 Visit to Cambridge Univ., Cambridge U.K., esp. Sir W. Hawthorne concerning general aerodynamic theory.

July, 1987 AFOSR Workshop on Aerodynamic Separation, Colorado Springs.

Aug., 1987 Visit to DFVLR in Göttingen, W. Germany esp. Dr. B. Müller, et. al., concerning CFD studies of delta wings.

NONLINEAR AERODYNAMICS OF TWO-DIMENSIONAL AIRFOILS IN SEVERE MANEUVER+

Matthew T. Scott*
Engineer, Aerodynamic Technology
Bell Helicopter Textron, Fort Worth, Texas

James E. McCune**
Professor, Dept. of Aeronautics and Astronautics
Massachusetts Institute of Technology, Cambridge, Massachusetts

Abstract

This paper presents a nonlinear theory of forces and moment acting on a two-dimensional airfoil in unsteady potential flow. Results are obtained for cases of both large and small amplitude motion. The analysis, which is based on an extension of Wagner's integral equation to the nonlinear regime, takes full advantage of the trailing wake's tendency to deform under local velocities. Interactive computational results are presented that show examples of wake-induced lift and moment augmentation on the order of 20 percent of quasi-static values. The expandability and flexibility of the present computational method are noted, as well as the relative speed with which solutions are obtained.

Nomenclature

$\alpha(t)$	Angle of attack
$h(t)$	Height of airfoil midchord above reference axis
v_r , v_θ	Radial and tangential components of velocity in the transformed (circle) plane
a	Radius of airfoil in transformed (circle) plane
β , τ	Angular running variables in transformed (circle) plane
Γ	Circulation strength
x , y	Cartesian coordinates fixed on global reference axes in the physical (airfoil) plane
ξ , η	Cartesian coordinates parallel and normal to the airfoil
$Y_c(x,t)$	Position of the airfoil or camber line in physical (airfoil) plane
$\hat{u}(\beta)$	Total tangential velocity on the airfoil
$u_w(\beta)$	Wake-induced tangential velocity on the airfoil
$v_w(\beta)$	Wake-induced velocity normal to the airfoil
s	Distance along the wake from the trailing edge
$s_{max}(t)$	The location of the end of the wake farthest from the trailing edge
$\gamma_w(s,t)$	Strength of vorticity in the wake
$\langle\hat{u}(\beta)\rangle$	Average tangential (parallel) velocity component on the airfoil: $\langle\hat{u}(\beta)\rangle = (\hat{u}(\beta) + \hat{u}(\beta+\pi))/2$
$\Delta\hat{u}(\beta)$	The difference in velocity components on the upper and lower surfaces of the airfoil; equal to the strength of the vorticity on the airfoil: $\Delta\hat{u}(\beta) = \hat{u}(\beta) - \hat{u}(\beta+\pi) = \gamma(\beta)$
U_∞ , ρ_∞	Free stream velocity and density, respectively
Φ	Potential function
$L(t)$, $M(t)$	Lift and moment on the airfoil
c	Chord length
$\Gamma_o(t)$	Quasi-steady bound circulation
$\zeta_v(s,t)$	Discrete vortex location in the wake
$x_{t.e.}$	Location of the trailing edge

Introduction

Early studies of the linearized response of the forces and moment acting on an airfoil in unsteady flow, including the effects of its own unsteady wake, have been described by such authors as Theodorsen,[1] von Kármán,[2] Kussner,[3] Sears,[4] and Wagner.[5] Limiting

+ This study was supported by AFOSR Grant No. 86-157 and by NASA Langley Grant No. NAG-1-658.
* Presented at the 26th Aerospace Sciences Meeting of the American Institute of Aeronautics and Astronautics, Reno, Nevada, January 1988.
** Associate Fellow AIAA

assumptions in the classical two-dimensional analysis are that the airflow be idealized as a potential flow, that the wake be approximated as trailed out flat behind the airfoil, and that the amplitude of airfoil motion be correspondingly small. However, modern requirements for aircraft maneuverability now dictate that problems associated with fully nonlinear, large-amplitude, unsteady flows be addressed. Thus, the theoretical basis for the linearized response must be reformulated and extended to allow the inclusion of nonlinear effects, including wake deformation. The wake must be allowed to convect freely, so that an effective "history" of the airfoil motion is present in the wake elements. An extension of Wagner's integral equation[2,5] is necessary to relate, in a time accurate sense, the strengths and positions of each of these wake elements to the circulation on the airfoil.

With the interactive capabilities of a VAX 11-750 computer and solving for only one unknown per time step, it is possible to convect the wake very quickly, and this enables the user of the program to see the wake unfold and flow downstream as the program runs. Output of force and moment histories is generated on-line, enabling a quick test-and-evaluation turnaround time of only a few minutes per case. The following sections outline the derivation and implementation of this interactive nonlinear solution and present results for typical input histories.

Derivation

Laplace's equation in the vicinity of an oscillating airfoil in a two-dimensional flowfield can be solved explicitly by means of the classical Joukowski transformation of the region to complex space.[6,7] By using the theory of conjugate functions, and following the explicit derivation of reference 8, we can describe the radial and tangential components of velocity that exist on the airfoil in the transformed plane as follows:

$$v_r(a,\beta) = +\frac{1}{2\pi}\oint_0^{2\pi} v_\theta(a,t)\cot\left(\frac{t-\beta}{2}\right)dt \qquad (1)$$

$$v_\theta(a,\beta) = -\frac{1}{2\pi}\oint_0^{2\pi} v_\theta(a,t)\cot\left(\frac{t-\beta}{2}\right)dt + \frac{\Gamma}{2\pi a} \qquad (2)$$

To generate the appropriate circulation on the airfoil and in the wake, the Kutta value of circulation is applied, and (2) can be rewritten:

$$v_\theta(a,\beta) = -\frac{1}{2\pi}\oint_0^{2\pi} v_r(a,t)\left|\frac{\sin\beta+\sin t}{\cos\beta-\cos t} - \frac{1+\cos t}{\sin t}\right|dt \qquad (3)$$

Boundary conditions at the surface of the airfoil are prescribed in the manner of reference 9 by the use of an implicit variable formulation. For purposes of simplicity, the airfoil in the present study has been assumed to be a flat plate whose instantaneous position relative to a global reference system can be described by a function η as follows:

$$\eta(x,y,t) = y - Y_c(x,t) \qquad (4)$$

In equation (4), $Y_c(x,t)$ denotes the position of the plate or, more generally, the camber line of a given airfoil. Given this formulation, we note that the substantial derivative $D\eta/Dt$ must vanish at $y=0$.[10] Therefore, if the equation for the position of the airfoil is defined, the velocity on the airfoil at a given time t and position x may be computed. The present formulation of $Y_c(x,t)$ involves the uncoupled use of two parameters: $h(t)$, the height of the midchord above the reference axis, and $\alpha(t)$, the angle of attack relative to the free stream. An input or "forcing" function is defined by setting the variation of these two parameters with time. The input function then yields surface velocity components through the use of the substantial derivative.[8]

Conjugate function theory requires that the velocities impinging upon the airfoil due to the presence of wake vorticity be "removed" from the problem before proceeding. This process is illustrated in Figures 1 through 3.

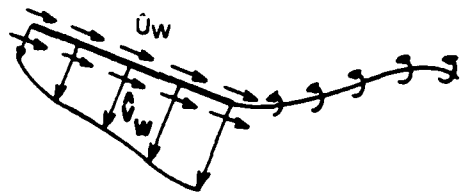

Figure 1. Apparent wake-induced velocity on an airfoil.

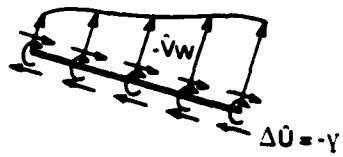

Figure 2. Velocity at airfoil surface due to additional bound vorticity.

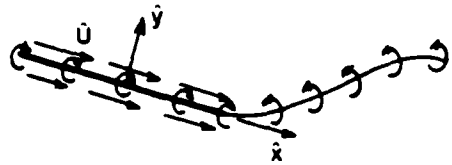

Figure 3. Net flow with normal velocity cancelled at airfoil surface.

Figure 1 shows the apparent wake-induced velocity impinging on the plate. In order to counter the normal velocity a "fictional" problem must be created (Figure 2) in which additional bound vorticity is produced on the surface of the airfoil. When these two solutions are added (Figure 3), the no-flow-through boundary condition of the net flow on the plate is achieved. Conjugate

function theory must create the "fictional" flow by measuring the wake-induced upwash at each station and then inducing the bound vorticity on the plate to counter the upwash. Thus we may write that the total velocity component parallel to the plate, $\hat{u}(\beta)$, is composed of the addition of the wake-induced component, $u_w(\beta)$, and the conjugate function denoted by equation (3).

$$\hat{u}(\beta) = -\frac{1}{2\pi}\oint_0^{2\pi} v_r(\tau)\left[\frac{\sin\beta + \sin\tau}{2\sin\beta}\left|\frac{\sin\beta + \sin\tau}{\cos\beta - \cos\tau} - \frac{1+\cos\tau}{\sin\tau}\right|\right]d\tau + u_w(\beta) \tag{5}$$

$u_w(\beta)$ may be derived by the use of the Biot-Savart law in complex form:

$$u_w - iv_w\Big|_{plate} = \frac{1}{2\pi i}\int_0^{s_{max}(t)} \gamma_w(s,t)\,\frac{1}{\zeta_{plate} - \zeta_w(s,t)}\,ds \tag{6}$$

Since the circulation on the airfoil can be described as the difference between the velocities $\hat{u}(\beta)$ and $\hat{u}(\beta+\pi)$, the loading, lift, and moment can be computed if the velocity $\hat{u}(\beta)$ can be found for values of β between 0 and 2π. One very important outcome of this analysis is that, for the general nonlinear case, the following expression is always true:

$$\langle \hat{u}(\beta)\rangle = U_\infty \cos\alpha(t) + u_w(\beta) \tag{7}$$

where $\langle \hat{u}(\beta)\rangle$ is taken to be the average of the velocities $\hat{u}(\beta)$ and $\hat{u}(\beta+\pi)$. This result proves that the only influencing factors on the average platewise velocity are the free stream, the angle of attack, and the location of the wake's vortex elements. The linearized theory is recovered if the wake is trailed out flat behind the airfoil and the angle of attack is small. Equation (7) then reduces to the familiar expression $\langle \hat{u}(\beta)\rangle = U_\infty$ as required.[2]

The expression for the vorticity on the plate at a position β is more complicated, but still conveys meaning:

$$-\gamma(\beta) = u(\beta) - \hat{u}(\beta+\pi) = 2U_\infty \sin\alpha(t) - 2U_\infty \cos\alpha(t)\left(\frac{1-\cos\beta}{\sin\beta}\right) - 8\dot{\alpha}(t)\sin\beta + \frac{2}{\pi}\left(\frac{1-\cos\beta}{\sin\beta}\right)\oint_0^{\pi} v_w(\xi)\left(\frac{1+\cos\tau}{\cos\tau - \cos\beta}\right)d\tau \tag{8}$$

where $v_w(\xi)$ is measured at a station ξ on the airfoil and is derived by means of equation (6). We notice that the first two terms on the right-hand side of (8) are classical linear terms, while the final two are nonlinear.

Calculation of loading, lift, and moment proceeds along classical lines by means of the unsteady Bernoulli equation:

$$-\Delta p = \rho_\infty\left|\langle \hat{u}(\beta)\rangle\,\Delta\hat{u}(\beta) + \Delta\left(\frac{\partial\Phi}{\partial t}\right)\right| \tag{9}$$

Reduction of the resulting expressions requires a judicious use of the Glauert Integral and ultimately leads to the following final equations:[8]

$$L(t) = \rho_\infty \frac{c}{2}\left\{\int_0^{\pi}\left(U_\infty + \dot{h}(t)\tan\alpha(t) + \frac{u_w(\beta)}{\cos\alpha(t)}\right)\times \left(2U_\infty \sin\alpha(t)(1-\cos\beta) - \mathcal{L}_{c_K}^{EVEN}(\beta)\right)d\beta + \frac{c}{2}\int_0^{\pi}\frac{1-\cos\beta}{\cos\alpha(t)}\times \frac{\partial}{\partial t}\left(2U_\infty \sin\alpha(t)(1-\cos\beta) - \mathcal{L}_{c_K}^{EVEN}(\beta)\right)d\beta\right\} \tag{10}$$

$$M(t) = \rho_\infty\left(\frac{c}{2}\right)^2\left\{\int_0^{\pi}\left(U_\infty\cos\alpha(t)\cos\beta + \dot{h}(t)\sin\alpha(t)\cos\beta + u_w(\beta)\cos\beta\right)\left(2U_\infty\sin\alpha(t)\times (1-\cos\beta) - \mathcal{L}_{c_K}^{EVEN}(\beta)\right)d\beta + \frac{c}{8}\int_0^{\pi}(1-\cos 2\beta)\times \frac{\partial}{\partial t}\left(2U_\infty\sin\alpha(t)(1-\cos\beta) - \mathcal{L}_{c_K}^{EVEN}(\beta)\right)d\beta\right\} \tag{11}$$

where we have defined:

$$\mathcal{L}_{c_K}^{EVEN}(\beta) = +\frac{1-\cos\beta}{\pi}\oint_0^{\pi} v_r(\tau)\left|\frac{1+\cos\tau}{(\cos\tau - \cos\beta)(\sin\tau)}\right|d\tau \tag{12}$$

The lift has been adjusted for the "leading edge force" in the classical manner, and the moment is about the semi-chord. If (10) and (11) are expanded, a few important points become evident:

1) Linear terms are recovered.
2) Between the prescribed modes of motion $h(t)$ and $\alpha(t)$ and their time derivatives, cross-coupling becomes very important.
3) No single term requires more than a double quadrature over the surface of the airfoil, and most integrations require only a single sweep.

Reference 8 gives a full explication of the terms.

Wagner's Nonlinear Integral Equation

Wagner's integral equation,[2,5] shown in equation (13), may be described as the relationship between the quasi-static circulation $\Gamma_0(t)$ bound to the airfoil and the strength of the trailing vorticity at a position ξ in the wake. The extension to the nonlinear regime effectively frees the wake to convect under local velocities by allowing the streaming variable s to integrate over complex space where the wake now resides. The resulting equation (14) is valid when we are careful not to integrate from one branch to another, as proven in appendix A of reference 8.

$$\Gamma_0(t) = \int_0^{\xi_{max}(t)} \gamma_w(\xi,t)\sqrt{\frac{\xi - x_{le}}{\xi - x_{te}}}\, d\xi \qquad (13)$$

$$\Gamma_0(t) = Re\left(\int_0^{s_{max}(t)} \gamma_w(s,t)\sqrt{\frac{e^{i\alpha(t)}\zeta_w(s,t) - x_{le}}{e^{i\alpha(t)}\zeta_w(s,t) - x_{te}}}\, ds \right) \qquad (14)$$

In equation (14), the wake vortex location $\zeta_w(s,t)$ is measured in the coordinate system fixed to the plate, and $s_{max}(t)$ is taken to be the end of the wake farthest from the trailing edge x_{te}. Equation (14) is written to take advantage of the discrete vortex method of modeling the wake, and the integration relies on the fact that the flow is assumed to be non-dissipative. This assumption assures that an effective "history" is maintained in the wake. It also guarantees that there are two unknowns at each time step: the strength and the position of the vortex formed closest to the trailing edge. As is also discussed by Scott,[8] an effective and useful solution to this problem is to use an offset or "threshold" distance that is small in relation to the chord length (typically $c/32$ to $c/4$). Such a preset position yields $\gamma_w(s,t)$ as the only unknown. $\Gamma_0(t)$ is a known quantity at each time step because it depends only on the velocity and position of the airfoil, which in the present case is a prescribed quantity.

Implementation and Results

The preceding analysis has been incorporated into a fast and efficient interactive computer program. Inputs to the program include the threshold vortex offset distance and the history of the motion of the airfoil. Analytic or continuous functions are not required as inputs, so the user may create effective histories for each of the independent and overlapping control variables $h(t)$ and $\alpha(t)$ by construction, using pieces of functions such as ramps, sinusoids, and steps as building blocks. Our experience shows that the only limiting parameter to this representation is the commonly seen breakdown of a wake formed of point vortices. Many models such as the Rankine vortex, the cloud-in-cell formulation,[11] and the scheme proposed by Mook et al.[12] have been offered as viable solutions to this inherent instability and will not be discussed here. Present coding allows considerable leeway in the choice of time increment and reduced frequency to obtain acceptable results.[3]

Typical results for the program are given in Figures 4 through 7. In Figure 4 we recreate Kármán's starting problem by imposing a step function of magnitude one degree in angle of attack at $t=5$ in order to apply instantaneously a constant bound circulation strength to the airfoil. Figure 4a is a trace of the input function, and Figure 4b is a picture of the airfoil and wake taken at $t=80$. The free stream velocity, which is the same for all cases presented in this section, is equal to $c/4$ per time step. Figure 4b shows the characteristic roll-up of the starting vortex as well as the bowing and overall downward displacement of the wake.

In Figure 4c, the lift coefficient asymptotes to its steady value as the starting vortex convects downstream. In addition, Kármán's starting value of the lift coefficient is recreated. Just as in the classical case, $C_L(t)$ attains half its steady magnitude immediately after the motion is completed. The nose-down pitching moment (Figure 4d) about the midchord shows initial overshoot of the steady value, but like the lift coefficient, the moment coefficient eventually decays toward the steady asymptotic solution. The overshoot gives insight for the case where the airfoil is unconstrained in motion, since the increased nose-up moment would tend to increase the angle of attack of an airfoil responding to induced forces.

Figure 5 shows the results of a large-amplitude oscillation of the height of the airfoil around the reference axis. The plunging airfoil experiences the motion shown in Figure 5a, and the resulting wake shows the large-scale roll-up patterns of Figure 5b. This wavy wake resembles an early stage in the development of the Kármán vortex street as exemplified in Van Dyke[13] or Mook et al.[12] Figures 5c and 5d detail the lead-lag characteristics of the motion, with Figure 5c showing that for a reduced frequency of 0.05 cycle based on the semi-chord, the unsteady total lift leads the quasi-static lift by approximately 29 degrees. The amount of lead or lag that is presently predicted by the program for a range of reduced frequencies from 0.005 cycle to 0.1 cycle shows divergence from the classical results for linearized small-amplitude unsteady motion derived by von Kármán and Sears.[3] However, the amount of phase divergence is fairly small, ranging from six degrees at low reduced frequencies to 30 degrees at the higher end, and is purely a numerical error. The present theory may be rewritten, as outlined by Scott[8] and McCune[9], so that this computational inaccuracy in calculating the normal force and moment on the airfoil is eliminated.

Figures 6 and 7 show two simple maneuvers and their effects on the loading of the airfoil. In the first maneuver, the airfoil undergoes a sinusoidal oscillation in angle of attack for one complete cycle, then stops its motion altogether, as shown in Figure 6a. Figure 6b shows the wake curling up downstream, while Figure 6c shows the effect of the maneuver on the total lift coefficient. The lift vector is shifted away from the forcing function $\alpha(t)$. In addition, both the lift and the moment (Figure 6d) show the residual effect of the wake's presence after the maneuver has stopped. The overshoot

in both cases is only 5 to 10 percent of the maximum values, and the sense of direction of the overshoot is that of the last completed maneuver. In other words, the motion of the airfoil is an upward pitch as it completes the sinusoid; this motion sheds counterclockwise vorticity into the wake, in turn creating a downwash on the airfoil. The downwash causes a decrease in the airfoil's lift as well as a sizable nose-up moment.

The controlling factor for the amount of overshoot appears to be the magnitude of the derivative of the forcing function. This is illustrated in Figures 7, where the input is a step function in angle of attack followed by the negative of this step 30 time increments later (Figure 7a). Figure 7b shows that the wake has a "square wave" appearance, and the lift augmentation (Figure 7c) is instantaneously on the order of 20 percent of the quasi-static value. Step changes cause the airfoil to move at high velocities (computationally finite but theoretically infinite). These velocities then introduce large amounts of vorticity into the wake. In the present study, instantaneous lift augmentation on the order of 50 percent has been seen. And, as shown in Figure 7d, the moment augmentation for the test case is substantially larger than that observed in the preceding C_L history.

Conclusion

The strong points of the present computational method are its speed and flexibility. Since we solve for only one unknown per time step, the results may be displayed interactively on a graphics screen. A typical run of 80 time steps, which may extend the wake 20 chord lengths or more downstream, takes only 5 to 10 minutes to generate when run on a DEC VAX 11-750 computer. In fact, the speed of the graphics plotting package is usually the limiting factor in such a calculation. In terms of flexibility, the program can accept any combination of sinusoids, pieces of sinusoids, step functions, or constant values in each of the input variables $h(t)$ and $\alpha(t)$. The user is free to "fly" a given maneuver on his own, having only to "construct" a realistic forcing function history with an interactive input. The advantages of the method are therefore threefold: the user input is flexible, the program is fast, and the results are completely nonlinear and exact.

Figure 4. The starting problem: Instantaneous loading of an airfoil.

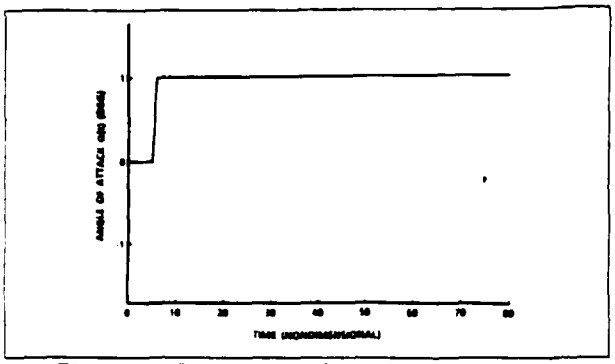

Figure 4a. Input angle of attack history ($\alpha(t)$).

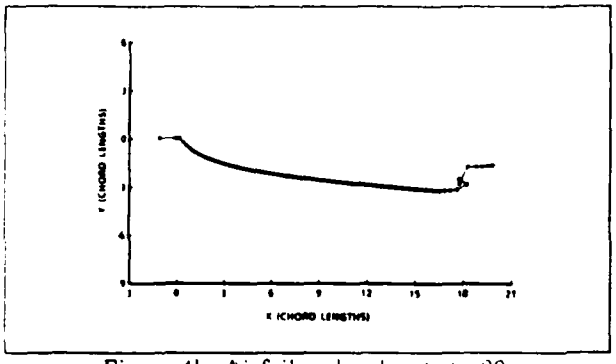

Figure 4b. Airfoil and wake at $t = 80$.

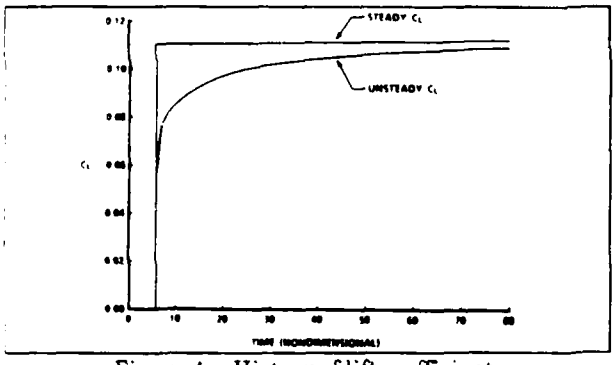

Figure 4c. History of lift coefficient.

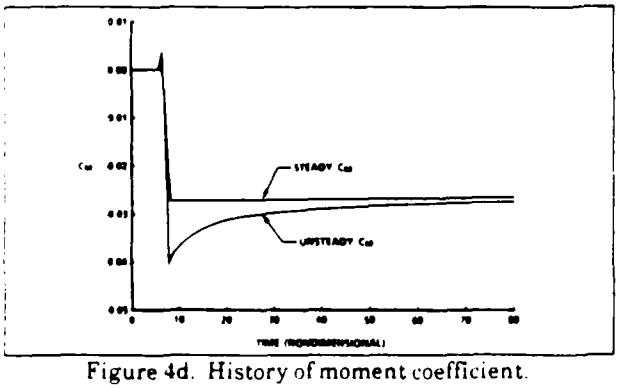

Figure 4d. History of moment coefficient.

Figure 5. Sinusoidal oscillation: Time variant loading of an airfoil.

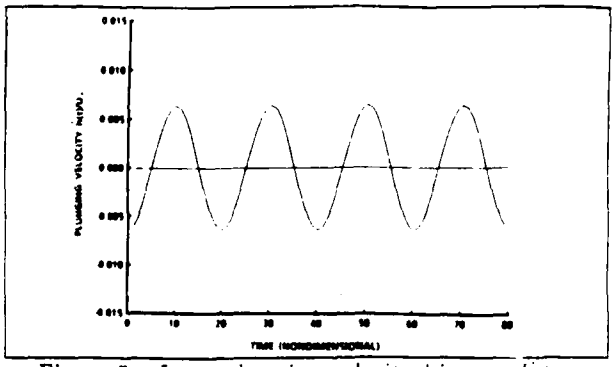

Figure 5a. Input plunging velocity history ($\dot{h}(t)$).

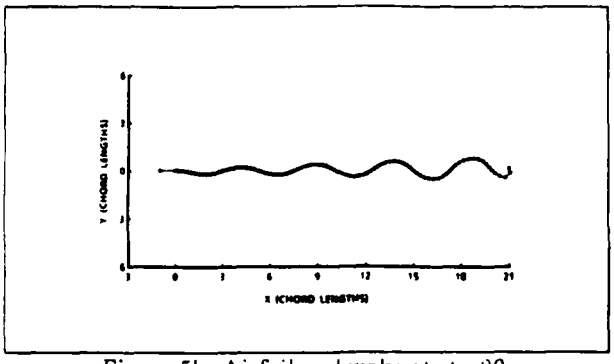

Figure 5b. Airfoil and wake at $t = 80$.

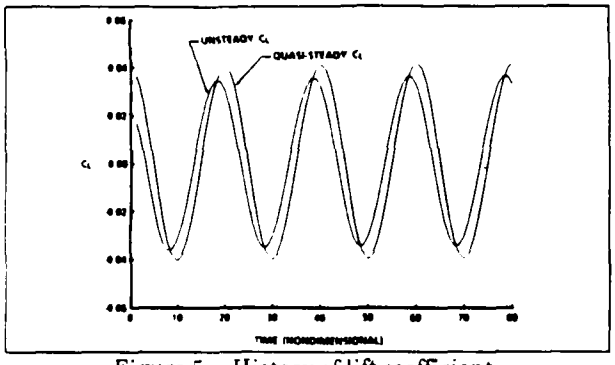

Figure 5c. History of lift coefficient.

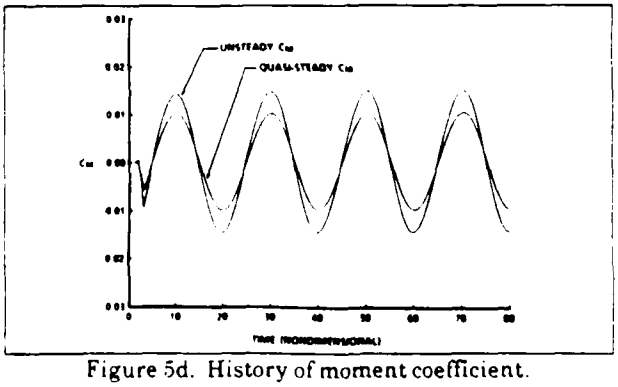

Figure 5d. History of moment coefficient.

Figure 6. Sinusoidal maneuver: Time variant loading and unloading of an airfoil.

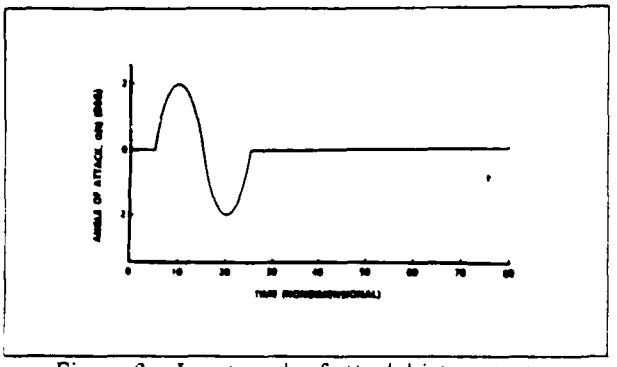

Figure 6a. Input angle of attack history ($\alpha(t)$).

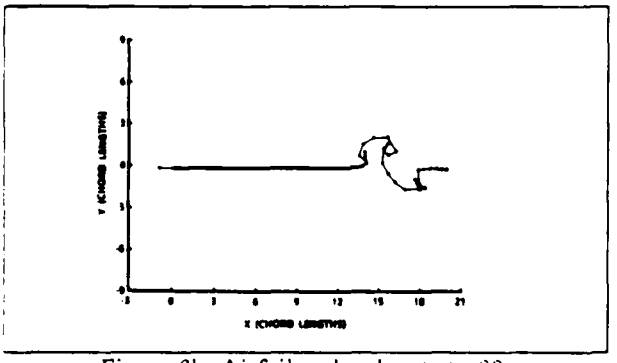

Figure 6b. Airfoil and wake at $t = 80$.

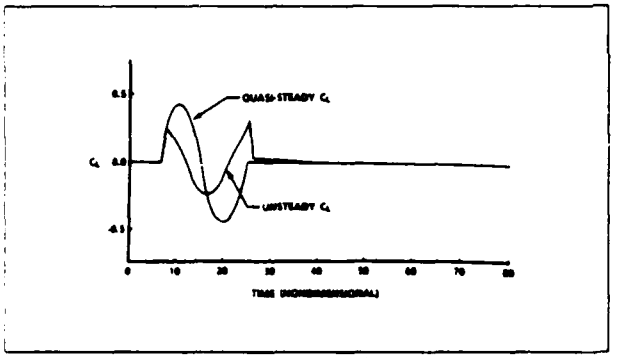

Figure 6c. History of lift coefficient.

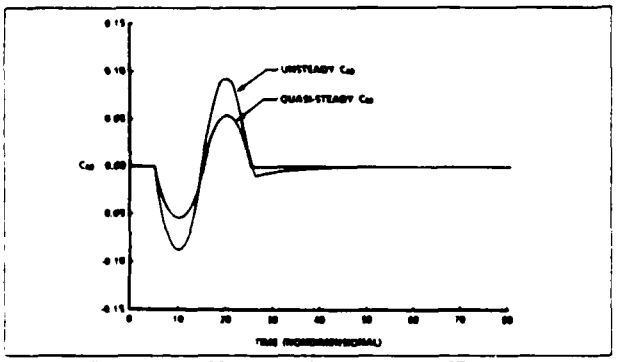

Figure 6d. History of moment coefficient.

Figure 7. Completed step function: Instantaneous loading and unloading of an airfoil.

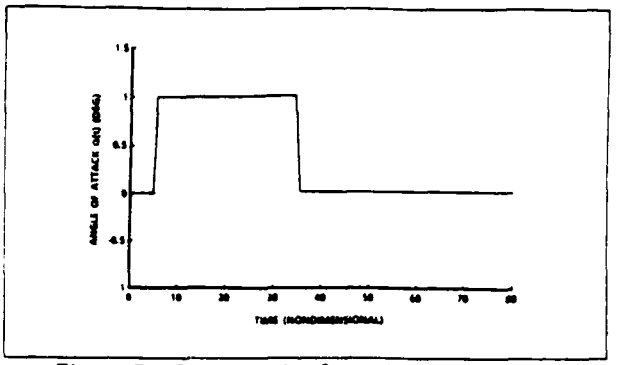

Figure 7a. Input angle of attack history ($\alpha(t)$).

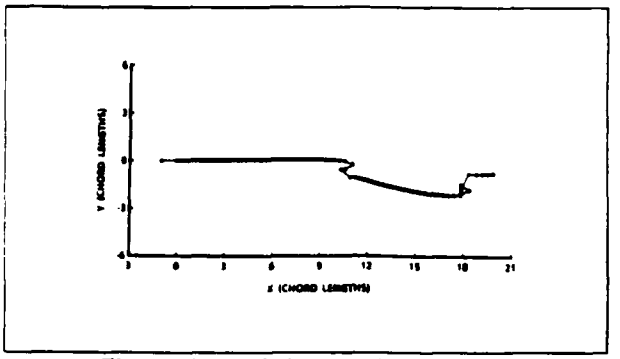

Figure 7b. Airfoil and wake at $t = 80$.

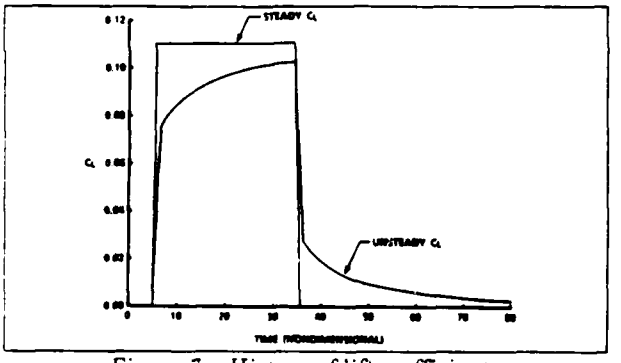

Figure 7c. History of lift coefficient.

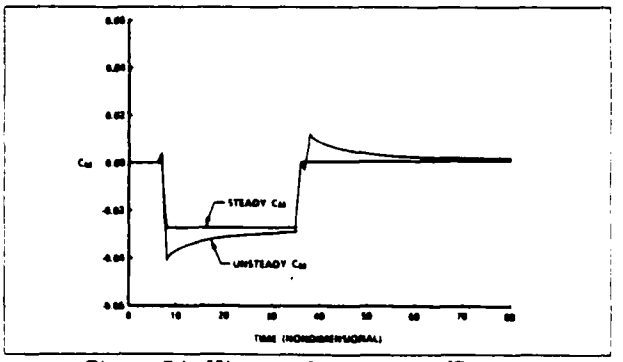

Figure 7d. History of moment coefficient.

References

1. Theodorsen, T., "General Theory of Aerodynamic Instability and the Mechanism of Flutter," NACA Rept. No. 496, 1935.

2. von Kármán, T., and Sears, W.R., "Airfoil Theory for Non-Uniform Motion," J. Aero. Sci., Aug. 1935, V. 5, No. 10.

3. Kussner, H.G., "Zusammenfassender Bericht uber den Instationaren Auftrieb von Flugeln," BD. 13, 1936, p. 410.

4. Sears, W.R., "Some Aspects of Non-Stationary Airfoil Theory and its Practical Application," J. Aero. Sci., Vol. 8, No.1, 1941, p. 104.

5. Wagner, H., "Dynamischer Auftrieb von Tragflugeln," Zeitscher. F. Agnew. Math. u. Mech., Bd. 5, 1925, p. 17.

6. Milne-Thomson, L.M., *Theoretical Aerodynamics*, Dover Publications Inc., New York, Fourth Edition, 1973.

7. Prandtl, L. and Tietjens, O.G., *Fundamentals of Hydro- and Aeromechanics*, Dover Publications, Inc., New York, First Edition, 1957.

8. Scott, M.T., "Nonlinear Airfoil-Wake Interaction in Large Amplitude Unsteady Flow," M.S. thesis, Dept. of Aeronautics and Astronautics, Massachusetts Institute of Technology, August, 1987.

9. McCune, J.E., "Non-Linear Unsteady Wing Theory Part I," Progress Report to NASA Langley Research Center, June, 1987.

10. McCune, J.E., "Interactive Aerodynamics of Wings in Severe Maneuver," presented at Workshop II on Unsteady Separated Flow, AFOSR, Air Force Academy, Colorado Springs, CO, July 1987.

11. Stremel, P.M., "A Method for Modeling Finite Core Vortices in Wake Flow Calculations," AIAA-84-0417, January, 1984.

12. Mook, D.T., et al., "On the Numerical Simulation of the Unsteady Wake Behind an Airfoil," AIAA-87-0190.

13. Van Dyke, M., *An Album of Fluid Motion*, The Parabolic Press, Stanford, CA, 1982.

INTERACTIVE AERODYNAMICS OF WINGS IN SEVERE MANEUVER*†

J.E. McCUNE

Massachusetts Institute of Technology, Cambridge, Massachusetts

ABSTRACT

This paper describes an interactive technique for the study and analysis of the aerodynamics of wings in severe maneuver. Both the 2D airfoil case and the cross-flow properties for slender 3D wings are addressed. To begin the study, the non-linear interaction of a 2D airfoil undergoing large-amplitude unsteady motion with its wake of shed vorticity was studied interactively on the computer using quick and efficient codes. The user can now input a "maneuver" and study and observe on-line the non-linear wake evolution and airfoil response. The allowable maneuvers for the airfoil presently include any combination of pitching and plunging, suddenly imposed. Also, airfoil response to sudden large-amplitude gusts of any shape and relative passage speed can be observed and analyzed. A detailed review of progress and results from this part of our work is provided by Scott.[1] In the present report we emphasize application of related techniques to 3D slender wings. We also provide information on improved methods of calculating lift and moment via wake integrals, emphasizing conservation of impulse, for the 2D as well as the 3D case.

1 Introduction

One important use of the non-linear 2D airfoil study is to provide a test of the exact wake evolution method, applied at low amplitudes, against classical linearized airfoil theory. This tests the accuracy and efficiency of the present approach, at least in the classical limit. But, in addition, the 2D work has set the stage for significant advances in the study of the 3D non-linear aerodynamic response of low-to-moderate $\mathcal{AR}$ wings (delta and other) to severe imposed maneuvers.

It has long been recognized that at large but finite Reynolds Nrs. the cross-flow at any chordwise station of a slender wing must include two "wakes" (actually, wake traces) representing concentrated vorticity, often partially rolled into "cores," convecting above the wing surface. The role of this vorticity, emanating via "leading-edge separation," is to maintain acceptably smooth flow at the wing edges. At sufficiently large Reynolds numbers, this smooth flow requirement is often called, even in this context, a "Kutta condition."

The present paper emphasizes recent progress in the development of a new method for studying on-line the dynamical effects of these two cross-flow wakes for the 3D wing. The method proceeds in analogy with, but also extends, techniques used in the 2D airfoil case. Additional ideas and theoretical framework needed for the 3D case are outlined. It is shown that the wake structures above a delta can be determined in a manner similar to the 2D airfoil problem, and that these structures have a history unique to any given maneuver.

As discussed in the body of the paper, the model of the wake structure used is somewhat idealized, in that the development during wake roll-up of vortex "cores" at finite Reynolds Numbers, with attendant regions of distributed total pressure loss, is not addressed. Similarly, the related occurrence of vortex breakup is not included in the present model. Our recent efforts to deal with these matters, as an elaboration of the technique described here, will be reported elsewhere.

2 Non-Linear Unsteady Wake Convection

2.1 2D Case

Any free vorticity associated with unsteady plane 2D fluid motion in the incompressible limit obeys the Helmholtz relation

$$\frac{D\Omega_z}{Dt} \equiv \frac{\partial \Omega_z}{\partial t} + \underset{\sim}{V} \cdot \nabla \Omega_z = 0 \qquad (2.1)$$

where $\underset{\sim}{V}$ is the planar fluid velocity, $\underset{\sim}{V} = (u, v, 0)$, and $\underset{\sim}{\Omega} = \text{curl } \underset{\sim}{V} = (0, 0, \Omega_z(x, y, t))$. Formally, therefore, if $A^{(1)} = \lambda(x, y, t)$ and $A^{(2)} = \eta(x, y, t)$ are two independent characteristic solutions of

$$\frac{DA^{(n)}}{Dt} = 0, \qquad (2.2)$$

*This work is dedicated to my teacher, Prof. Wm. R. Sears, in honor of his 75th birthday.

†This study was supported by the AFOSR under Grant Nr. AFOSR-86-157. Earlier phases of the research were also supported by NASA Langley under Grant Nr. NAG-1-658.

with appropriate boundary (/ initial) conditions, then $\Omega_s = \Omega_s(\eta, \lambda)$. Boundary conditions can be specified such that one of these characteristic variables, "η," say, is constant on streaklines drawn at fixed t. The remaining variable, λ, can be chosen to be

$$\lambda \equiv t - \tau \tag{2.3}$$

where

$$\frac{D\tau}{Dt} = 1. \tag{2.4}$$

"τ" is then the Eulerian "drift time" with the usual simple physical interpretation [2]. But if the velocity field is discontinuous as in the classical model of concentrated vortex sheets representing the wakes behind wings and airfoils, this formulation may not be convenient.

It turns out, however, that when a concentrated vortex sheet is embedded in the flow the variable η can be conveniently replaced by a continuous function, η_c, say, which instead of (2.2) satisfies

$$\left.\begin{aligned} \frac{\overline{D}\eta_c}{Dt} &\equiv \frac{\partial \eta_c}{\partial t} + \langle \underset{\sim}{V} \rangle \cdot \nabla \eta_c = 0 \\ \text{and} \qquad \Delta \underset{\sim}{V} \cdot \nabla \eta_c &= 0 \end{aligned}\right\} \tag{2.5}$$

i.e., η_c is constant on the sheet, and the sheet is a streak surface (streakline in 2D), whose deformation is controlled by convection at the mean velocity, $\langle \underset{\sim}{V} \rangle$:

$$\langle \underset{\sim}{V} \rangle \equiv \frac{1}{2}\left(\underset{\sim}{V}^+ + \underset{\sim}{V}^-\right) \tag{2.6}$$

As with a vortex sheet,

$$\Delta \underset{\sim}{V} \equiv \underset{\sim}{V}^+ - \underset{\sim}{V}^- \tag{2.7}$$

has no component perpendicular to the sheet at any time, as stated in (2.5(b)).

In a distance ds along the sheet at any fixed t the elemental change in circulation, $d\Gamma$, is determined by the local jump across the sheet of the velocity potential $\phi(x, y, t)$ such that

$$-d\Gamma = ds \Delta \frac{\partial \phi}{\partial s} = ds \frac{\partial}{\partial s} \Delta\phi = d\Delta\phi \qquad \text{(fixed } t\text{)}$$

In the 2D unsteady case the strength of this potential jump, $\Delta\phi$, occurring at the sheet specified by η_c = constant, is a function of both x and t which must be determined. But application of the Bernoulli equation on either side of the sheet, together with the requirement that there be no jump in static pressure across the sheet, yields the restriction

$$\frac{\partial \Delta\phi}{\partial t} + \langle \underset{\sim}{V} \rangle \cdot \nabla \Delta\phi = 0. \tag{2.8}$$

Thus, in the 2D case we can write $\Delta\phi = \Delta\phi(\bar{\lambda})$, and $d\Gamma = d\Gamma(\bar{\lambda}) = -\frac{d\Delta\phi}{d\lambda} d\bar{\lambda} \equiv \Gamma'(\bar{\lambda}) d\bar{\lambda}$ where

$$\bar{\lambda} \equiv t - \bar{\tau} \tag{2.9}$$

and

$$\frac{\overline{D}\bar{\tau}}{Dt} = \frac{\partial \bar{\tau}}{\partial t} + \langle \underset{\sim}{V} \rangle \cdot \nabla \bar{\tau} = 1 \tag{2.10}$$

Here, $\bar{\tau}$ is the "mean" drift time of fluid elements within the vortex sheet.

The variable η_c can be expressed in the form $\eta_c = y - Y_c(\bar{\tau}, t)$ where $\frac{\overline{D}Y_c}{Dt} = v$. With η_c=const. on the streakline, we have y = const.+ $Y_c(\bar{\tau}, t)$ on that line. When $\bar{\tau}$ is expressed in terms of x at any t we define a space curve, $y = y(x; t)$, giving the usual instantaneous picture of an airfoil wake. (See Figures 1 and 2.)

As noted above, condition (2.8) was derived by requiring that there be no net force anywhere on the free vortex sheet. For systems of conserved global circulation, this corresponds to guaranteeing conservation of impulse for the airfoil-plus-wake.

In the linear case, in which the wake is assumed simply to lie along the x-axis extending from the trailing edge with the vorticity within it convected at free-stream speed U_∞, the above exact results reduce to

$$\begin{aligned} \bar{\lambda} &\rightarrow t - \frac{x - x_0}{U_\infty} \\ \frac{d\bar{\lambda}}{dx} &\rightarrow -\frac{1}{U_\infty} \end{aligned}$$

so that, if $\gamma(x, t)$ is the wake vorticity in that limit,

$$d\Gamma(\bar{\lambda})^{(\text{linear})} \rightarrow \gamma(x, t) dx$$

and

$$\frac{d\Gamma^{(\text{lin})}}{d\bar{\lambda}} \frac{d\bar{\lambda}}{dx} \rightarrow -\frac{1}{U_\infty} \frac{d}{dt}\left(\Gamma^{(\text{lin})}\left(t - \frac{x - x_0}{U_\infty}\right)\right) = \gamma\left(t - \frac{x - x_0}{U_\infty}\right)$$

reproducing the classical result in the linear limit.

In the actual non-linear situation $\bar{\lambda}$ replaces x as the useful parameter along the vortex sheet representing the wake, whether the wake is distorting and rolling-up or not. Thus, for example, the total wake circulation at any given time t is

$$\Gamma_{\text{wake}}(t) = \int_0^t d\bar{\lambda} \Gamma'(\bar{\lambda}). \tag{2.11}$$

Further, the (plane, 2D) velocity induced by the wake can be written in complex-variable notation as

$$u_{wake}(x,y,t) - iv_{wake}(x,y,t) \equiv w_{wake}(x,t)$$
$$= \frac{1}{2\pi i}\int_0^t d\bar{\lambda}\Gamma'(\bar{\lambda})\frac{1}{z - z_v(\bar{\lambda},t)}. \qquad (2.12)$$

Here, $z \equiv x + iy$, and $z_v = x_v + iy_v$ is the complex location at t of the vortex element having circulation $d\Gamma(\bar{\lambda})$.

This formulation provides a powerful tool for writing down exactly all the various non-linear effects related to the wake in a manner which conveniently follows the contortions of the wake, including roll-up, as it evolves. Since $\bar{\lambda}$ is conserved during the history of each fluid element in the wake, it provides a convenient label for each such element. In the present example $\bar{\lambda}$ is the (earlier) time at which a given element entered the wake at the airfoil trailing edge. Figure 1 illustrates a portion of the evolution of a streakline constituting a vortex sheet, and Figure 2 shows a typical example of a computer-generated version of the wake behind an oscillating airfoil.

On the computer, of course, the above continuous vortex sheet model is replaced by an approximate discretized version. Individual discreet vortices of strength $\delta\Gamma(\bar{\lambda})$ replace the line elements of the sheet. Details of how to do this properly so as to maximize the effectiveness of the approximation have been discussed by Mook, et. al. [3] and more recently by Scott [1].

The computer screen provides an almost ideal tool for depicting and understanding wake evolution in this framework. At each time step each fluid element (and free circulation element) is advanced to its new location in x and y, moving in the field of all its neighbors. Since $\bar{\lambda}$ is constant for any fluid element and t is known, then $\bar{\tau}$ is determined at each new location at each t. In effect, the computer automatically maps the drift time field. When all the fluid elements in a given wake are shown in their new positions at each new time, t, for example, the line through them and the trailing edge at that moment is a streakline which depicts the momentary shape and location of the vortical wake. We discuss in Section 3 how the individual strengths, $d\Gamma$, of the circulation elements are determined (the Wagner equation).

2.2 3D Case

The classical picture of the 3D vortex-wake pattern above a delta wing in steady flow at large Reynolds Nr. and modest angle of attack is shown in Figures 3 and 4. At any chordwise station the trace of the double wake (somewhat idealized) is as illustrated in the inset of Figure 3. The necessity for a wake pattern resembling this structure, in order to provide acceptably smooth flow at the wing edges at large Re, has been recognized by many authors [4], [5], [6], [7], [8]. Even though the vorticity may roll up partially into two strong "cores," the strength of these cores must vary in the chordwise direction, which requires the existence of the joining umbilical vortical sheets from the edges to the cores, as illustrated.

Although this model is certainly oversimplified because of such effects as separation of the return boundary layers on the wing upper surface (leading to "secondary" and "tertiary" vortices [9], [10]), it offers an important improvement for real flows over the completely inviscid classical theory ($Re \equiv \infty$) with its singular flow at the edges [11]. This postulated wake pattern is often referred to as the result of "leading-edge separation" in the present context. The strength of the vorticity is presumed to be determined so as to provide Kutta conditions (smooth flow) at both wing edges. (Section 3.)

At higher angles of attack, even in steady flow, the model pattern in Figure 3 has a further defect. Vortex breakup [12], [13], [14] can be expected to occur at some conditions of interest with a consequent sudden and intense change at some chordwise location of the vorticity pattern above the wing. This paper does not attempt to deal with vortex breakup phenomena.

In the unsteady case, especially for 3D wings in severe maneuver, the classical wake pattern also has other defects. Clearly, for example, a pilot could well be able to roll or pitch so rapidly as to catch and move through his own wake pattern. Understanding wing response to that sort of condition will require improved understanding of the vorticity distribution within the cores themselves and any associated total head loss within the wake system. [15], [16] For that matter, the same improved understanding of the cores and total pressure defects appears to be required to interpret vortex breakup [12]. In the following discussions we largely ignore such defects, leaving their treatment for future elaborations of the technique we wish to describe here.

The evolution of the free 3D wake pattern over the wing proceeds in a manner analogous to the 2D case, complicated only by the need for an additional characteristic variable in the chordwise direction. To maintain zero net force on the free wake system each circulation element, $-\Delta\phi(x,z,t)$, once it enters the wake pattern at a wing edge location, is convected unchanged at the speed determined by the mean velocity at the sheet, including the motion "induced" by all its neighboring vortex elements. Thus, again,

$$\frac{\partial\Delta\phi}{\partial t} + \langle \underset{\sim}{V} \rangle \cdot \nabla\Delta\phi = 0 \qquad (2.13)$$

where $\underset{\sim}{V} = (u,v,w)$ and

$$\langle \underset{\sim}{V} \rangle \equiv \frac{1}{2}(\underset{\sim}{V}^+ + \underset{\sim}{V}^-) \qquad (2.14)$$

Once more we define the mean drift time, $\bar{\tau}$, now in the 3D field, such that

$$\frac{\partial\bar{\tau}}{\partial t} + \langle \underset{\sim}{V} \rangle \cdot \nabla\bar{\tau} = 1 \qquad (2.15)$$

and reintroduce the characteristic variable (now 3D)

$$\bar{\lambda} \equiv t - \bar{\tau} \qquad (2.16)$$

which is constant, as before, for each fluid element moving in the vortex wake system.

What emerges is the description of the overall 3D wake pattern, however contorted, made up of twisted streaklines of vorticity extending at any instant from the plane of observation at a given chordwise location to the upstream wing edge location at which the corresponding vortex elements have entered or are entering the wake system. To describe the shape and location of these streaklines we again need the characteristic, η_e, as defined in (2.5), and one additional characteristic

$$\varsigma_e \equiv x - Z_e(x, y, z, t) \tag{2.17}$$

where

$$\frac{\overline{D} Z_e}{Dt} \equiv \frac{\partial Z_e}{\partial t} + < \underset{\sim}{V} > \cdot \nabla Z_e = w. \tag{2.18}$$

For the latter we can choose the boundary condition $Z_e = 0$ at or along any wing edge so that Z_e is just the chordwise distance at any t and x a given element of the wake has travelled since entering the system at the upstream chordwise location ς_e, and at a corresponding earlier time $\overline{\lambda}$. Thus, $\varsigma_e = 0$ for any wake element entering the pattern at the wing vertex, and $\varsigma_e = x$ for any element just entering at the plane of observation at x. The η_e and ς_e variables define instantaneous surfaces in the 3D case, and their intersections are the streaklines making up the wake pattern at any given moment.

In analogy with the 2D case one can express the variables η_e and ς_e in the forms

$$\eta_e = y - Y_e(\overline{\tau}, \varsigma_e, t)$$
$$\varsigma_e = x - Z_e(\overline{\tau}, \eta_e, t)$$

$\overline{\tau}$, in turn, is a function at each x and t of x, the height of the wake element above the wing surface. For example, in the linear model of a wake, with wake elements convected on straight lines at speed U_∞ as depicted in Figure 4(b), we have

$$\begin{aligned} \overline{\tau} &= \frac{h}{U_\infty \sin\overline{\alpha}} \; ; \; \varsigma_e = Z_{\text{edge}} \; ; \; \eta_e = Y_{\text{edge}} \\ y &= Y_{\text{edge}}(Z_{\text{edge}}) + f U_\infty \overline{\tau} \cos\overline{\alpha} \\ x &= Z_{\text{edge}} + U_\infty \cos\overline{\alpha}\, \overline{\tau} \end{aligned}$$

so that the simple surfaces

$$\begin{aligned} x - Z_{\text{edge}} &= \frac{h}{\tan\overline{\alpha}} \\ y - Y_{\text{edge}} &= \frac{f h}{\tan\overline{\alpha}} \end{aligned}$$

are formed. The more realistic non-linear case follows similar rules and is depicted in Figure 4(a).

When observed at a given chordwise location, x, in the corresponding cross-flow plane including the wing trace, the vortex pattern over the wing creates a trace (actually, a pair of traces) of the wake as it passes through the observation plane. In the unsteady case, these traces will deform, contort, and appear to roll-up, much as if we were observing a 2D airfoil with <u>two</u> wakes rather than one.

In Figure 5 we illustrate the sort of wake surfaces, and their traces, to be expected above a delta wing undergoing yaw and roll. Simultaneous observation of the wake trace behavior at several cross-flow planes can provide significant insight as to the interactive aerodynamics associated with violent maneuvers. On-line use of computer graphics, including split screen capabilities, promises to be very helpful in understanding the large-scale unsteady behavior of the wing and its wake.

On taking account of the right hand rule in the definition of circulation, each circulation element in each trace at fixed x and t can now be described in terms of the above variables as

$$\begin{aligned} d\Gamma^{STBD} &= -d\Delta\phi(\varsigma_e, \overline{\lambda})^{STBD} \\ d\Gamma^{PORT} &= +d\Delta\phi(\varsigma_e, \overline{\lambda})^{PORT} \end{aligned} \tag{2.19}$$

in view of (2.13). (In the steady case, with nothing changing in time at a given x, only the first variable need appear and $d\Gamma = d\Gamma(x - Z_e(x, y, z)) = \Gamma'(\varsigma_e) d\varsigma_e$) in each wake.

The drift time $\overline{\tau}$ observed at x and t for any element in either of the two wake traces is related to ς_e, so that we can find $\overline{\lambda}(\varsigma_e, x, x, t)$, and/or the inverse. Then, the total circulation at fixed x and t in either trace (starboard or port) can be written

$$\begin{aligned} \Gamma_{\text{wake}}^{STBD.PORT}(x,t) &= \int_{(\text{fixed}_{x,t})} d\Gamma(\varsigma_e, \overline{\lambda})\,(\varsigma_e) \\ &\qquad (STBD.PORT) \\ &= \int_0^x d\varsigma_e \frac{d\Gamma^{STBD.PORT}}{d\varsigma_e} \\ &= \mp \int_x^0 d\varsigma_e \left(\frac{\partial \Delta\phi}{\partial x} + \frac{\partial \Delta\phi}{\partial t} \frac{d\overline{\lambda}}{d\varsigma_e} \right)^{STBD.PORT} \end{aligned} \tag{2.20}$$

Note that in the linear case or for slender wings at mean angle of attack $\overline{\alpha}$, $\frac{d\overline{\lambda}}{d\varsigma_e} = \frac{1}{(U_\infty \cos\overline{\alpha})}$.

As discussed in Section 3.2, the incremental circulation associated with each vortex element is determined just as it enters the wake pattern so as to always maintain the postulated smooth flow at the edges. After that, each element is simply convected, at fixed elemental circulation, to new locations in the wake pattern.

3 Determining the Vortex Strength Distribution in the Wakes

3.1 2D Airfoil Case

In our treatment of this case we assume the Kutta condition to hold at the airfoil trailing edge at any instant. The airfoil itself is assumed to be a flat plate[1] in arbitrary

[1] A general 2D airfoil profile can be treated in the same manner, with only a minor elaboration of the technique used here.

plunging and/or pitching motion.

As already discussed, the unsteady airfoil motion requires the existence of a wake such as illustrated in Figure 2, so that the net circulation of the wake-plus-airfoil is constant. No linearisations of the airfoil motion of wake contortions are admitted in the present treatment.

The airfoil circulation can be described conveniently in two parts. The first, $\Gamma_0(t)$, is the "quasi-steady" Kutta value associated with the airfoil motion itself and calculated as if no wake were present. Thus, $\Gamma_0(t)$ is known for any specified airfoil motion. The general expression is

$$\Gamma_0 = -\pi c U_\infty \sin\alpha(t) + 2\int_{-\frac{c}{2}}^{\frac{c}{2}} d\hat{x}\,\hat{v}_0(\hat{x},t)\sqrt{\frac{\frac{c}{2}+\hat{x}}{\frac{c}{2}-\hat{x}}} \qquad (3.1)$$

where "c" is the airfoil chord, $\alpha(t)$ is the angle of attack, $\hat{x}$ is the instantaneous chordwise coordinate along the airfoil, and $\hat{v}_0(\hat{x},t)$ is the actual normal component of fluid velocity at the oscillating and plunging plate necessary to accommodate its unsteady motion. (See Figure 6). Then, without approximation, (see Ref. [1] for more details)

$$\hat{v}_0 = \dot{h}\cos\alpha(t) - \hat{x}\dot{\alpha} \qquad (3.2)$$

and

$$\Gamma_0(t) = -\pi c\left(U_\infty \sin\alpha - \dot{h}\cos\alpha\right) - \frac{\pi c^2}{4}\dot{\alpha}. \qquad (3.3)$$

The bound vorticity associated with Γ_0 and $\hat{v}_0$ is called $\gamma_0(\hat{x},t)$ and

$$\Gamma_0(t) = \int_{-\frac{c}{2}}^{\frac{c}{2}} \gamma_0(\hat{x},t)\,d\hat{x}. \qquad (3.4)$$

Defining the angle variable β such that $\hat{x} \equiv \frac{c}{2}\cos\beta$, we can write

$$\gamma_0(\hat{x},t) = -2\left(U_\infty\sin\alpha - \dot{h}\cos\alpha\right)\frac{1-\cos\beta}{\sin\beta} - c\dot{\alpha}\sin\beta \qquad (3.5)$$

This "quasi-steady" bound vorticity would be all that is present if it weren't for the wake. But, as illustrated in Figure 6, and calculated in Eq. (2.12), the wake causes an apparent upwash at the airfoil which must be cancelled out by the action of additional bound vorticity on the airfoil, $\gamma_1(\hat{x},t)$. The amount needed is given by the theory of conjugate functions in the form

$$\gamma_1(\hat{x},t) = \frac{1-\cos\beta}{\pi\sin\beta}\int_0^\pi \frac{d\tau\left(-2\hat{v}_{\text{wake}}\right)(1+\cos\tau)}{\cos\tau-\cos\beta} \qquad (3.6)$$

where, as in (3.5), the Kutta condition has been applied at the trailing edge. Correspondingly, the additional circulation on the airfoil, $\Gamma_1(t)$, is given by

$$\Gamma_1(t) \equiv \int_{-\frac{c}{2}}^{\frac{c}{2}} \gamma_1(\hat{x},t)\,d\hat{x} = 2\int_{-\frac{c}{2}}^{\frac{c}{2}} d\hat{x}\left(-\hat{v}_{\text{wake}}(\hat{x},t)\right)\sqrt{\frac{\frac{c}{2}+\hat{x}}{\frac{c}{2}-\hat{x}}} \qquad (3.7)$$

The quantity $\hat{v}_{\text{wake}}(\hat{x},t)$ can be obtained readily from (2.12). Using a system $\hat{z} \equiv e^{-i\alpha(t)}(z - ih(t)) = \hat{x} + i\hat{y}$ rotating and plunging with the airfoil, the normal component of the apparent wake velocity at the airfoil is determined. Inserting the result in (3.7) yields an expression for $\Gamma_1(t)$ in terms of an integral over the wake vorticity. Details of this calculation are available in Ref. [1].

The next step is to apply the Kelvin Theorem in the form

$$\Gamma_{\text{airfoil}}(t) + \Gamma_{\text{wake}}(t) = \text{constant} = \Gamma(0) \qquad (3.8)$$

where $\Gamma(0)$ is any existing initial or steady-state airfoil circulation. For example, if the airfoil maneuver begins from steady flight at angle of attack α_0,

$$\Gamma(0) = -\pi c\sin\alpha_0.$$

But we have

$$\Gamma_{\text{airfoil}} = \Gamma_0(t) + \Gamma_1(t)$$

and $\Gamma_{\text{wake}}(t)$ is written out in Eq. (2.11), also in terms of an integral over the wake circulation elements. Cancellations occur, and the final result is, in complex-variable notation,

$$\Gamma_0(t) - \Gamma(0) = Re\int_0^t d\bar{\lambda}\,\Gamma'(\bar{\lambda})\sqrt{\frac{\hat{z}_*(\bar{\lambda},t)+\frac{c}{2}}{\hat{z}_*(\bar{\lambda},t)-\frac{c}{2}}} \qquad (3.9)$$

where "Re" means real part implied and

$$\hat{z}_* \equiv e^{i\alpha}(z_* - ih(t))$$

with z_* as defined below (2.12).

Equation (3.9) was first derived by Wagner [17], in the linearized limit, and used by many authors to understand airfoil response to sudden starts, sudden (but small) changes in angle of attack, and flying through gusts. [18], [19] It seems remarkable that the non-linear version (3.9) of Wagner's equation is essentially the same as his original except that $\hat{z}_*(\bar{\lambda},t)$ is complex, reflecting the distortion and roll-up of the wake. The principal mathematical nicety in the non-linear case is the need to determine the correct branch of the complex square root occurring in the integral.

The left-hand side of (3.9) is known as a function of t for any given imposed airfoil motion (see Eqn. (3.3), for example), so Eqn. (3.9) is an integral equation for the strengths, $d\Gamma(\bar{\lambda})$, of the circulation elements in the wake.

Operationally, on the computer, use of Eqn. (3.9) to determine the wake vorticity is relatively straightforward, except for finding the initial incremental vortex element at the very start of a maneuver. Difficulties arise there because the kernel on the *rhs* of (3.9) is singular. An effective method for treating this crucial first moment of the "starting problem" is described in Ref. [1]. After the procedure has been properly started, however, it runs easily because once the strength of a vortex element has been determined by (3.9), at the instant it enters the wake, that strength, as measured by its incremental circulation, remains unchanged as the element convects to its subsequent positions in the wake.

3.2 3-D Case. Smooth Flow at Both Edges

From Kelvin's theorem we know the net circulation in each cross-flow plane is zero:

$$\Gamma_{STBD} + \Gamma_{PORT} + \Gamma_{TRACE} = 0 \qquad (3.10)$$

We treat the 3D case in this paper in the slender-wing (low $\mathcal{AR}$) limit, determining the velocity and potential field in each cross-flow plane on a quasi-two-dimensional basis in the spirit of Ref. [11]. In that limit we must determine the 2D potential solution in each observation plane corresponding to the concentrated vorticity on the wing trace and in the traces of the two wakes (Figure 7).[2]

In order to treat a general large-amplitude maneuver and still maintain an inertial frame "almost" moving with the wing, we specify a system moving with the mean or initial steady flight condition, as sketched in the figure. This initial or mean forward speed is U_∞, with angle of attack $\bar{\alpha}$. A cross-flow observation plane at any fixed x (analogous to the computer screen) is oriented normal to the wing surface in its initial or mean configuration. The observer in this plane sees an incoming steady free stream of speed U_∞ at angle $\bar{\alpha}$ to the x axis. Additional pitch, yaw, or roll of the wing, as well as plunging or sideslip of the wing vertex, are perceived in each observation plane as vertical or sideways displacements, $X_0(x,t)$ and $Y_0(x,t)$. Acceleration or deceleration of the vertex in the x-direction is seen as a growth or shrinking of the wing trace at any x. For maneuvers with very rapid forward acceleration or complete changes in flight direction, a frame fixed in the atmosphere may be preferable, with the wing flying "through" the observation plane or planes. Of course, one could also choose an observation system fixed in the wing, with attendant complications associated with non-inertial frames of reference. For our present purposes, we adopt the scheme shown in Figure 7.

In complex-variable notation the quasi-2D cross-flow velocity field associated with the wakes is, with $Z = X + iY$,

$$U_{\text{wake}} - iV_{\text{wake}} = W_{\text{wake}}(Z)$$
$$= \frac{1}{2\pi i}\left\{\int_0^x d\zeta_e \frac{d\Gamma^{STBD}(\zeta_e,\bar{\lambda})}{d\zeta_e}\frac{1}{Z - Z_v^{STBD}} \right. \qquad (3.11)$$
$$\left. + \int_0^x d\zeta_e \frac{d\Gamma^{PORT}(\zeta_e,\bar{\lambda})}{d\zeta_e}\frac{1}{Z - Z_v^{PORT}}\right\}$$

in analogy with (2.12). Here, we have used (2.19) and $Z_v^{STBD}(\zeta_e,t,x)$ and $Z_v^{PORT}(\zeta_e,t,x)$ are the instantaneous complex locations in any given cross-flow plane (x,y) of the vorticity elements in the starboard and port wake traces respectively. In the following we also have use for

$$\begin{aligned} \hat{W}_{\text{wake}}(x) &\equiv e^{-iK} W_{\text{wake}} \\ &= \hat{U}_{\text{wake}} - i\hat{V}_{\text{wake}}. \end{aligned}$$

The boundary condition at the wing trace as viewed in each cross-flow plane can be written in a form somewhat similar to that in (3.2) for the 2D airfoil. Using the coordinates suggested in Figure 7 the actual component of velocity in the (x,y) plane normal to the instantaneous wing trace can be written

$$\hat{U}_0(\hat{y},x,t) = \frac{D_x X_0(x,t)}{Dt}\cos K + \frac{D_x Y_0(x,t)}{Dt}\sin K - \hat{y}\frac{D_x K(x,t)}{Dt} \qquad (3.12)$$

where $\frac{D_x}{Dt} \equiv \frac{\partial}{\partial t} + \overline{W}\frac{\partial}{\partial x}$. For a low $\mathcal{AR}$ wing in steady forward flight without pitch or yaw, for example, $\overline{W} = U_\infty \cos\bar{\alpha}$, since the additional fluid speed in the chordwise direction is neglible because of the wing slenderness. During pitch and yaw, however, $\overline{W}$ requires adjustment to allow for the instantaneous flight angles and the fact that the chordwise (or "slenderness") direction is then misaligned with the x-axis chosen in Figure 7.

Starting from the mean or initial steady flight condition described above, an observer on the wing sees an effective cross-flow from below of $U_\infty \sin\bar{\alpha}$, the normal component of which is $U_\infty \sin\bar{\alpha}\cos K$. Eqn. (3.12) then allows for any additional unsteady wing motion, including any acceleration of the wing vertex as well as pitch, yaw and roll about specified axes. Any built-in camber of the wing can also be included in the form (3.12). The angle "K" is an apparent

[2] For 3D wings and their wakes during sudden and violent maneuver the "slenderness direction" becomes somewhat ambiguous. Near and on the low $\mathcal{AR}$ wing, for example, quantities may vary slowly in space only in the instantaneous chordwise direction, whereas this is generally misaligned with the original x-axis of Figure 7. The main wake structure, on the other hand, may still tend to be "slender" with respect to the original flight alignments. Ultimately, of course, use of the full 3D relations is required. We are suggesting here, however, that this be done after fully exploiting the additional insights to be gained in the Jones-Munk tradition.

"roll" angle, observed at fixed z, which is actually a composite of the usual Euler angles. For this reason X_0, Y_0 and K can depend on z as well as t. For simplicity we assume the wing trace to be flat, although the method used here can be generalised to include any moderately thin cross section as well as control surface deflections. Note that $\hat{y}$, in this case, is the instantaneous spanwise coordinate as shown in Figure 7, and $\frac{\hat{b}}{2}$ is the effective semispan at that instant at the specified z. Thus, $X_0(z,t)$, $Y_0(z,t)$ give the instantaneous position of the mid-effective span which is not on the wing center line during yaw.

If there were no wake the discontinuous part of the velocity at the wing trace, $\Delta\hat{V}_0$, would be

$$\Delta\hat{V}_0|_{\text{trace}} = -\frac{2\hat{y}}{\sqrt{\frac{\hat{b}^2}{4}-\hat{y}^2}}\left[\left(U_\infty \sin\bar{\alpha} - \frac{DX_0}{Dt}\right)\cos K - \sin K\frac{D_sY_0}{Dt}\right] + 2\frac{D_sK}{Dt}\left(\sqrt{\frac{\hat{b}^2}{4}-\hat{y}^2} - \frac{\left(\frac{\hat{b}^2}{8}\right)}{\sqrt{\frac{\hat{b}^2}{4}-\hat{y}^2}}\right) \tag{3.13}$$

since in that case, according to (3.10), we would have $\Gamma_{TRACE} = 0$. For example, in the limit of steady motion at small $\bar{\alpha}$ and with no yaw, pitch or roll, (3.13) reduces to

$$\Delta\hat{V}_0|_{\text{trace}} = -\frac{2y}{\sqrt{\frac{b^2}{4}-y^2}}U_\infty\bar{\alpha} \tag{3.13a}$$

corresponding to Jones' classical result [11]. Note that in either (3.13) or (3.13a) the flow predicted in this way (without vortical wakes above the wing) is singular at the wing edges. The next step is to add the wakes and to determine their vorticity distributions so as to "smooth" the flow at the edges.

In a manner similar to that used for the 2D airfoil, we introduce an "angle variable" such that

$$\hat{y} = \frac{\hat{b}}{2}\sin\beta \tag{3.14}$$

and use the theory of conjugate functions to write down the additional vorticity (or jump in $\hat{V}$) required at the wing trace in order to continue to satisfy the boundary condition (3.12) despite the velocity field (3.11) induced by the wakes. The result is

$$\Delta\hat{V}|_{\text{trace}} \equiv \Delta\hat{V}_0|_{\text{trace}} + \Delta\hat{V}_1|_{\text{trace}}$$

where

$$\Delta\hat{V}_1|_{\text{trace}} = +\frac{2\Gamma_{TRACE}(z,t)}{\pi\hat{b}\cos\beta} + \frac{2\tan\beta}{\pi}\oint_{-\frac{\pi}{2}}^{\frac{\pi}{2}}\frac{d\tau\left(-\hat{U}_{\text{wake}}\cos\tau\right)}{\cos\tau-\cos\beta} \tag{3.15}$$

The wing-edge singularities in these additional "wake-induced" terms must exactly cancel the singularities in $\Delta\hat{V}_0|_{\text{trace}}$ at both edges of the wing if our Kutta-condition postulate is to be satisfied. Note that at this point we can no longer simply assume $\Gamma_{TRACE} = 0$, but must apply (3.10) in order to try to determine it.

In Eqn. (3.15) $\hat{U}_{\text{wake}}(\hat{y},t)$ can be written down in terms of the wake integrals in (3.11). Cancellation of the singularities at both wing edges then requires

for $\hat{y} = +\frac{\hat{b}}{2}$:

$$2\left[\left(U_\infty\sin\bar{\alpha} - \frac{DX_0}{Dt}\right)\cos K - \sin K\frac{D_sY_0}{Dt}\right] + \hat{b}\frac{D_sK}{Dt} = \frac{2\Gamma_{TRACE}(z,t)}{\pi\hat{b}} + Re\frac{i}{\pi}\int_0^s d\zeta_c\left\{\frac{\frac{d\Gamma^{PORT}}{d\zeta_c}}{\sqrt{\left(\hat{Z}_*^{PORT}\right)^2+\frac{\hat{b}^2}{4}}} + \frac{\frac{d\Gamma^{STBD}}{d\zeta_c}}{\sqrt{\left(\hat{Z}_*^{STBD}\right)^2+\frac{\hat{b}^2}{4}}}\right\}$$

for $\hat{y} = -\frac{\hat{b}}{2}$:

$$2\left[\left(U_\infty\sin\bar{\alpha} - \frac{DX_0}{Dt}\right)\cos K - \sin K\frac{D_sY_0}{Dt}\right] - \hat{b}\frac{D_sK}{Dt} = -\frac{2\Gamma_{TRACE}(z,t)}{\pi\hat{b}} + Re\frac{i}{\pi}\int_0^s d\zeta_c\left\{\frac{\frac{d\Gamma^{PORT}}{d\zeta_c}}{\sqrt{\left(\hat{Z}_*^{PORT}\right)^2+\frac{\hat{b}^2}{4}}} + \frac{\frac{d\Gamma^{STBD}}{d\zeta_c}}{\sqrt{\left(\hat{Z}_*^{STBD}\right)^2+\frac{\hat{b}^2}{4}}}\right\}$$

In the above relations

$$\hat{Z}_*^{PORT} \equiv e^{-iK(s,t)}\left(Z_*^{PORT}(\zeta_c,t,z) - (X_0+iY_0)\right)$$

and

$$\hat{Z}_*^{STBD} \equiv e^{-iK(s,t)}\left(Z_*^{STBD}(\zeta_c,t,z) - (X_0+iY_0)\right)$$

with the Z_* as defined below (3.11).

Taking the difference of the two equations involving Γ_{TRACE} yields $\Gamma_{TRACE} = \left(\frac{\pi\hat{b}^2}{2}\right)\frac{D_sK}{Dt}$, so that we obtain the constraint

$$\Gamma_{PORT}(z,t) + \Gamma_{STBD}(z,t) = -\frac{\pi\hat{b}^2}{2}\frac{D_sK}{Dt} \tag{3.16}$$

The sum of the two relations then yields an equation for the vorticity strengths (circulation elements) in the wake traces which is analogous to the Wagner integral equation (3.9). The result is

$$\left(U_\infty\sin\bar{\alpha} - \frac{DX_0}{Dt}\right)\cos K - \sin K\frac{D_sY_0}{Dt} = Re\frac{i}{2\pi}\int_0^s d\zeta_c\left\{\frac{\frac{d\Gamma^{PORT}(\zeta_c,\bar{\lambda})}{d\zeta_c}}{\sqrt{\left(\hat{Z}_*^{PORT}\right)^2+\frac{\hat{b}^2}{4}}} + \frac{\frac{d\Gamma^{STBD}(\zeta_c,\bar{\lambda})}{d\zeta_c}}{\sqrt{\left(\hat{Z}_*^{STBD}\right)^2+\frac{\hat{b}^2}{4}}}\right\} \tag{3.17}$$

The left-hand-side of (3.17) is known at each z and t for any given imposed wing motion. Thus, (3.17), together with (3.16) and (2.20), determines the circulation elements throughout the wake system within the present model. Solution proceeds in a manner mathematically quite similar to the 2D airfoil case.

4 Loads, Forces and Moments

4.1 2D Airfoil Case. Large-Amplitude Unsteady Response

In Ref. [1] the forces and moments occurring on 2D airfoils in large-amplitude unsteady motion were calculated using the pressures over the airfoil surface as predicted by the Bernoulli equation for unsteady potential flow. In reckoning the lift, a "leading-edge force" was included in the classical manner, except that no linearizations were admitted. This procedure was built into the "NLWAKE" code reported in [1].

More recently, we have reformulated the lift and moment expressions by taking advantage of the possibility of expressing all or most wake-related terms (without linearizing) in terms of the corresponding "wake integrals" - integrals over the (known) wake vorticity. This step mimics classical procedures in the linear theory [18] and establishes the equivalence of the original formulation in Ref. [1] with the application of the principle of conservation of impulse. Most importantly, the reformulation greatly improves the numerical accuracy achievable in the codes. The reason is that several large contributing terms in C_ℓ and C_{m_0} in NLWAKE almost exactly cancel, leaving crucial small differences which can be difficult to calculate with sufficient accuracy. In the extension of NLWAKE to include the new formulation, these partial cancellations are explicit and the remainders are written in a manner more suited to precise numerical evaluation.

The (non-linear) expressions for lift and moment including the appropriate wake integrals in this way are written out here both for completeness and for comparison with their classical linear versions. For the lift coefficient, using the notation of Eqn. (2.11), (3.3) and (3.5), we find

$$
\begin{aligned}
C_\ell(t) = &-\frac{2\Gamma_0}{U_\infty c}\left(\frac{\overline{U}}{U_\infty}\right) + \frac{2c}{U_\infty \cos\alpha}\,\frac{d}{dt}\int_{-\hat{s}}^{\hat{s}} \frac{d\hat{z}\,\hat{z}\,\gamma_0(\hat{z},t)}{c^2 U_\infty} \\
&- \frac{2}{c\cos\alpha} Re \int_0^t \frac{d\lambda\Gamma'(\lambda)}{U_\infty^2}\left(\frac{c}{2}\,\frac{da}{dt}\right)\frac{1}{\sqrt{a^2-1}} \qquad (4.1)\\
&- \frac{2}{c\cos\alpha} Re \int_0^t \frac{d\lambda\Gamma'(\lambda)}{U_\infty^2}\left[\left(\frac{c}{2}\,\frac{da}{dt}\right) - \overline{U}\cos\alpha\right]\left\{\sqrt{\frac{a+1}{a-1}} - 1\right\} \\
&- \tilde{C}_{\ell\,\text{wake}}(t)
\end{aligned}
$$

where $a \equiv 2\hat{z}_*/c$ with $\hat{z}_*$ defined as below (3.9), and $\overline{U} \equiv U_\infty + h\tan\alpha$. The small non-linear term $\tilde{C}_{\ell\,\text{wake}}(t)$ is

$$
\tilde{C}_{\ell\,\text{wake}}(t) \equiv -\frac{2}{cU_\infty^2\cos\alpha}\int_{-\hat{s}}^{\hat{s}} d\hat{z}\;\hat{u}_{\text{wake}}(\hat{z},t)\left(\gamma_0(\hat{z},t) + \gamma_1(z,t)\right), \qquad (4.1a)
$$

and can also be written out in terms of wake integrals. The resulting expression is cumbersome, however. It is perhaps more useful here simply to note that $\tilde{C}_{\ell\,\text{wake}}$ vanishes identically in the linear limits of a wake extending straight behind the airfoil since it involves $\hat{u}_{\text{wake}}$. Also, we have not yet encountered a case, even in the non-linear treatment, for which $\tilde{C}_{\ell\,\text{wake}}$ has been important, even though it clearly can be significant or even crucial, for a maneuver in which the airfoil flies "through," or just above or below, its own wake.

The fourth term on the *rhs* of (4.1) also vanishes in the linear limit, since in that case both $\frac{c}{2}\left(\frac{da}{dt}\right)$ and $\overline{U}\cos\alpha$ approach U_∞. This term in fact illustrates the numerical advantage of the wake-integral formulation, since it represents explicitly the partial cancellation between two otherwise quite large terms.

The first three terms on the *rhs* of (4.1), on the other hand, approach their classical linear counterparts exactly in the limit of small amplitude motion. The 2nd term is often called the "apparent mass" term, and the 3rd the "wake effect." Thus, on using (4.1), we know that the non-linear theory appropriately reproduces the linear version, and includes it.

The corresponding moment coefficient, C_{m_0}, about mid-chord is given in similar fashion by

$$
\begin{aligned}
C_{m_0}(t) = &-2\frac{\overline{U}\cos\alpha}{U_\infty}\int_{-\hat{s}}^{\hat{s}} \frac{d\hat{z}\,\hat{z}\,\gamma_0(\hat{z},t)}{c^2 U_\infty} \\
&+ \frac{c}{U_\infty}\,\frac{d}{dt}\int_{-\hat{s}}^{\hat{s}} \frac{d\hat{z}\,\gamma_0(\hat{z},t)\left(\hat{z}^2 - \frac{c^2}{8}\right)}{c^3 U_\infty} \qquad (4.2)\\
&+ \frac{1}{2c} Re \int_0^t \frac{d\lambda\Gamma'(\lambda)}{U_\infty^2}\left(\frac{c}{2}\,\frac{da}{dt}\right)\frac{1}{\sqrt{a^2-1}} \\
&- \frac{1}{c} Re \int_0^t \frac{d\lambda\Gamma'(\lambda)}{U_\infty^2}\left[\left(\frac{c}{2}\,\frac{da}{dt}\right) - \overline{U}\cos\alpha\right]\left\{\sqrt{a^2-1} - a\right\} \\
&- \tilde{C}_{m_{\text{wake}}}(t)
\end{aligned}
$$

where

$$
\tilde{C}_{m_{\text{wake}}}(t) \equiv -\frac{2}{c^2 U_\infty^2}\int_{-\hat{s}}^{\hat{s}} \hat{z}\,d\hat{z}\;\hat{u}_{\text{wake}}(\hat{z},t)\left(\gamma_0(\hat{z},t) + \gamma_1(\hat{z},t)\right). \qquad (4.2a)
$$

Once again, the final two terms on the *rhs* of (4.2) vanish at small amplitudes, and the first three terms reduce precisely to their classical counterparts in the linear limit.

Computer-generated results corresponding to Eqns. (4.1) and (4.2) are illustrated in Section 5 in terms of 2D airfoil response to large-amplitude imposed motions.

4.2 3D Case. Loads and Normal-Force Distribution on Slender Wings

The pressure difference, or loading, across the wing for the 3D case can again be calculated using the Bernoulli equation for unsteady potential flow on either side of the

wing. As before, the wake-related terms are two-fold. First, the associated velocity field of the wake, as given by Eqn. (3.11), contributes directly to the pressure variations. Secondly, the apparent upwash caused by the wake must be cancelled out by the effects of an addition wing-trace vorticity, $\Delta V_1(\hat{y},t)$, as given in (3.15), thus implying an additional jump in the $\frac{\partial\phi}{\partial t}$ term in the Bernoulli relation. In calculating the latter we take advantage of the possibility of writing $\phi(x,y,t)$ on the wing on either side $(+,-)$ as

$$\phi^{\pm}(x,y,z,t) \equiv \Phi(z,t;\hat{y},\hat{z}=0^{\pm})$$

where the coordinates $(\hat{z},\hat{y})$ are as illustrated in Figure 7. We find, for slender wings, with $\underset{\sim}{V} = (\hat{u},\hat{v},\hat{w})$

$$\begin{aligned} -\frac{1}{\rho_\infty}\Delta p &\equiv \frac{1}{\rho}p\Big]_{\text{bottom}}^{\text{top}} \equiv p^-(x,t;\hat{y},0^-) - p^+(x,t;\hat{y},0^+) \\ &= <\underset{\sim}{V}>\cdot\Delta\underset{\sim}{V} + \Delta\left(\frac{\partial\phi}{\partial t} + w\frac{\partial\phi}{\partial z}\right) \qquad (4.3) \\ &\cong <\hat{V}>\Delta\hat{V} \\ &\quad + \frac{D_s}{Dt}\Delta\Phi(x,t;\hat{y}) + \Delta\hat{V}\left(\frac{D_sX_0}{Dt}\sin K - \frac{D_sY_0}{Dt}\cos K\right) \end{aligned}$$

where $\frac{D_s}{Dt} \equiv \frac{\partial}{\partial t} + \overline{W}\frac{\partial}{\partial z}$ as before. In writing (4.3) we have also used the notation defined in (2.6) and (2.7) and below (3.12), as well as in Figure 7.

As mentioned in Section (3.2) proper use of the slender-wing concept allows us to repace $\hat{W}$ with $\overline{W}$, provided we recall that the low $\mathcal{AR}$ wing is "slender" along the chordwise direction and not necessarily along the z-direction during violent pitch and yaw.

The $\Delta\Phi$ occurring in (4.3) can be written

$$\begin{aligned} \Delta\Phi(\hat{y},z,t) &= \Gamma_{STBD}(z,t) \\ &\quad + \int_{-\frac{\hat{b}}{2}}^{\hat{y}} d\hat{y}\;\Delta\hat{V}(\hat{y},z,t) \qquad (4.4) \end{aligned}$$

where $\Delta\hat{V}$ is given in (3.13) and (3.15). Further, $<\hat{V}> = -U_\infty\sin\bar{\alpha}\sin K + \hat{V}_{\text{wake}}$.

Expression (4.3), with (4.4), lends itself to relatively straightforward calculation of the normal force distribution $C_n(z,t)$. Spanwise integration with respect to $\hat{y}$ proceeds in a manner mathematically the same as for the 2D airfoil case, except that in the present model no edge forces are included. The lift and drag and also the roll, pitch, and yaw moments of a given wing can be reckoned in a similar manner, on including subsequent weighted integrations over z. We find

$$\begin{aligned} C_n(z,t) &\equiv \frac{2}{\rho U_\infty^2\hat{b}(z,t)}\int_{-\frac{\hat{b}}{2}}^{\frac{\hat{b}}{2}} d\hat{y}\;\; p](\hat{y},z,t) \\ &= \frac{1}{U_\infty^2}\frac{D_s}{Dt}\left\{\frac{\pi\hat{b}}{2}U_\infty\sin\bar{\alpha}\cos K\right. \\ &\quad \left. -\frac{\pi\hat{b}}{2}\left(\frac{D_sX_0}{Dt}\cos K + \frac{D_tY_0}{Dt}\sin K\right)\right\} \\ &\quad -\left(\frac{\pi\hat{b}}{U_\infty^2}\frac{D_sK}{Dt}\right)\left\{U_\infty\sin\bar{\alpha}\sin K\right. \\ &\quad \left. -\frac{D_sX_0}{Dt}\sin K + \frac{D_sY_0}{Dt}\cos K\right\} \qquad (4.5) \\ &\quad + C_{n_{\text{wake}}} + \tilde{C}_n \end{aligned}$$

where

$$C_{n_{\text{wake}}}(z,t) \equiv \frac{1}{U_\infty^2}\frac{D_s}{Dt}\left\{\hat{b}\int_{-\frac{\pi}{2}}^{\frac{\pi}{2}} d\beta\left(\cos^2\beta\right)\hat{U}_{\text{wake}} + \frac{\Gamma^{STBD} - \Gamma^{PORT}}{2}\right\} \qquad (4.5a)$$

and

$$\tilde{C}_n(z,t) \equiv \frac{1}{U_\infty^2}\int_{-\frac{\pi}{2}}^{\frac{\pi}{2}} d\beta\cos\beta\hat{V}_{\text{wake}}\left(\Delta\hat{V}_0 + \Delta\hat{V}_1\right) \qquad (4.5b)$$

Using (3.11) we can express $C_{n\text{wake}}(z,t)$ in terms of a wake integral analogous to the 2D airfoil case. The result is

$$\begin{aligned} &C_{n_{\text{wake}}}(z,t) \\ &\quad = \frac{1}{U_\infty^2}\frac{D_s}{Dt}Re\int_0^s d\zeta_c\left\{\frac{d\Gamma^{STBD}}{d\zeta_c}\left(\frac{1}{2} - ia_s - i\sqrt{a_s^2+1}\right)\right. \\ &\quad \left. + \frac{d\Gamma^{PORT}}{d\zeta_c}\left(-\frac{1}{2} - ia_p - i\sqrt{a_p^2+1}\right)\right\} \qquad (4.6) \end{aligned}$$

where

$$a_s \equiv 2Z_s^{STBD}/\hat{b}\;;\quad a_p \equiv 2Z_s^{PORT}/\hat{b}$$

and we note $a_s = -1$ at the starboard edge and $a_p = +1$ at the port edge.

In the interactive method for the slender wing case this latter "wake-integral" is easy to calculate on the computer, since the necessary information becomes available automatically at the same time the wake structure itself is being generated using the method described in Section (3).

The $\tilde{C}_n(z,t)$ term can also be calculated in terms of wake integrals, and that approach appears to be the most convenient and numerically accurate method to determine its value. We note here only that $\tilde{C}_n$ has no linear counterpart (and vanishes by symmetry in certain simple flight configurations), yet its effect appears to be potentially of great importance in certain maneuvers involving intimate interaction between the wing and its wakes.

The first term on the rhs of (4.5) corresponds for small $\bar{\alpha}$ to the linear theory result of Ref. [11]. In fact, for pointed slender wings in steady flight at small $\bar{\alpha}$, this term integrates chordwise to yield

$$C_L \doteq \frac{\pi\mathcal{AR}}{2}\bar{\alpha}, \qquad (4.7)$$

the classical Jones result. The additional terms in the corresponding curly brackets represent the local, instantaneous

normal-force effects of plunge, pitch, etc., that would arise if there were no wakes.

The wake-integral terms, $C_{n_{wake}}(s,t)$ and $\dot{C}_n(s,t)$, represent "history effects" in the relationship between wing motion and wing loading or response. As we have seen, the various vorticity elements in each wake reflect conditions imposed at upstream wing edges, each at an earlier time. Thus, for example, in the event of a sudden maneuver of short duration, the outer parts of the wake affecting $C_n(s,t)$ will often represent wing attitude and other conditions in effect before the maneuver began. Conversely, after a given maneuver is "over", many outer wake elements will still reflect the actions taken during the maneuver, so that wing loading will take time to adjust and/or return to "normal." Naturally, any occurrence of vortex breakup can have a drastic effect on this history-related part of the wing response, although it may not always be unfavorable. Of course, before we can regard wing response as "deterministic" we must learn how to predict both the occurrence and specific nature of such vortex bursting. [12]-[14]

5 Typical On-Line Results: Non-Linear 2D Airfoil Response

A critical part of studying the behavior of wings in maneuver is the understanding of the wing's aerodynamic response to new conditions suddenly imposed. Representative of such response are, for the 2D case, the results of the classical Wagner problem, illustrated for the low-amplitude (linear) case in Figure 8(a). The net bound circulation on the airfoil, $\Gamma_0 + \Gamma_1$, adjusts only gradually to the suddenly imposed change in angle-of-attack as represented by the jump in Γ_0. The lift coefficient jumps to $\frac{1}{2}$ its eventual value and gradually adjusts. Note that the relaxation to the quasi-steady result, is very slow. On the Figures, time is normalized to $\left(\frac{1}{4}\right)(c/U_\infty)$.

The corresponding nonlinear (large-amplitude) case is illustrated in Figure 9(a). Note that the response is very similar to the linearized result, despite the relatively severe deformation of the wake as illustrated in Figure 9(b). This appears to be a result of the fact that the wing in each case is adjusting to shed vorticity which is rather strongly concentrated toward the far reaches of the wake, ultimately several chord lengths downstream.

Illustration of the airfoil's aerodynamic response to a rudimentary but severe maneuver is illustrated in Figure 10. There, a sudden single-cycle sinusoidal angle of attack variation of large amplitude is imposed and just as suddenly stopped. The wake vorticity coagulates and begins roll-up without significant net displacement from the plane of the airfoil (Figure 10(a)). The lift jumps quickly, and then leads the quasi-steady value into the negative lift region (Figure 10(b)). It then overshoots the recovery, plunges again, and only very slowly recovers to the state before the maneuvers, illustrating a "history effect" for the 2D case suggestive of the phenomena discussed at the end of Section 4. During the maneuver, from start to finish, the airfoil advances 5 chord lengths in this example. Both "apparent mass" effects and upwash associated with the developing wake play vital roles in the net result.

The pitching moment for this example, though large in amplitude, is essentially classical in response, except for the relatively pronounced history effect after the maneuver is complete (Figure 10(c)).

A number of additional examples of airfoil response to imposed large-amplitude motions of various types are reported in Ref. [1]. It is especially instructive, in addition to the figures, to actually run the codes of [1] on-line, taking advantage of the almost instantaneous wake displays to develop a sense of airfoil response and the reasons for it. Several of these "flight" sessions have been taped recently. In the 3D case one can carry out similar on-line runs with split-screen displays of the wing configuration, wake deformations at various locations, and wing loading response.

References

1. Scott, Matthew T., "Nonlinear Airfoil-Wake Interactions in Large Amplitude Unsteady Flow," M.I.T. Master's Thesis, June, 1987. See also: Scott, M. and McCune, J.E. AIAA paper Nr. 88-0129, AIAA 26th Aerospace Science Meeting, Reno NV, Jan., 1988.

2. Lamb, Sir Horace, *Hydrodynamics*, 6th edition, Dover Publ., N.Y., 1945.

3. Mook, D.T., et.al., "On the Numerical Simulation of the Unsteady Wake Behind an Airfoil," AIAA-87-0190, Jan., 1987.

4. Adams, Mac, "Leading Edge Separation from Delta Wings at Supersonic Speeds," J. Aeron. Sci., 21, Readers Forum, June, 1953.

5. Edwards, R.H. "Leading Edge Separation from Delta Wings," J. Aeron. Sci., 21, Readers Forum, Nov., 1953.

6. Cheng, H.K., "Remarks on Non-Linear Lift and Vortex Separation," J. Aeron. Sci., 21, Readers Forum, Dec., 1953.

7. Brown, C.E., and Michael, W.H., Jr., "Effects of Leading Edge Separation on the Lift of a Delta Wing," J. Aeron. Sci., 22, 1954.

8. Mangler, K.W., and Smith, J.H.B., "A Theory of the Flow Past a Slender Delta Wing with Leading Edge Separation," Proc-Roy Soc. 251, 200-217, 1959.

9. Powell, Kenneth G., "Vortical Solutions of the Conical Euler Equations," M.I.T. Ph.D. Thesis, June, 1987.

10. Müller, Berndhard, and Rizzi, Arthur, "Navier-Stokes Computation of Transonic Vortices Over a Round Leading Edge Delta Wing," AIAA Paper Nr. 87-1227, AIAA 19th Fluid Dyn., Plas. Dyn., and Laser Conf., Honolulu, June, 1987.

11. Jones, R.T., "Properties of Low-Aspect-Ratio Pointed Wings at Speeds Below and Above the Speed of Sound," NACA TR 835, 1946.

12. Hall, M.G., "Vortex Breakdown," Annual Review of Fluid Mechanics, Vol. 4, 1972, pp. 195-218.

13. Lambourne, N.C. and Bryer, D.W., "The Bursting of Leading Edge Vortices; Some Observation and Discussion of the Phenomenon," Aeronautical Research Council, R and M 3282, 1961.

14. Reynolds, G.A. and Abtahi, Ali, "Vortex Dynamics for Transient Flight Conditions," Lockheed-Georgia Company, Presented at AFOSR Workshop on Unsteady Separated Flows, Air Force Academy, 28-30, July, 1987.

15. Murman, E.M., Powell, K.G., Goodsell, A.M., and Landahl, M.T., "Leading Edge Vortex Solutions with Large Total Pressure Losses," AIAA Paper Nr. 87-0039, AIAA 25th Aerospace Sciences Meeting, Reno, NV, Jan., 1987.

16. McCune, J.E., Tavares, T. Sean, Lee, Norman, and Weissbein, David, "Slender Wing Theory Including Regions of Embedded Total Pressure Loss," AIAA Paper Nr. 88-0320, AIAA 26th Aerospace Sciences Meeting, Reno, NV, Jan. 1988.

17. Wagner, H., "Dynamischer Auftrieb von Tragflügeln," Zeitschr. f. Angew. Math. u. Mech. (ZAMN), 5, 17, 1925.

18. von Karman, T., and Sears, W.R., "Airfoil Theory for Non-Uniform Motion," J. Aeron. Sci., 5, 10, 1935.

19. Küssner, H.G., "Zusammenfassender Bericht über den instationären Auftrieb von Flügeln," Luftfahrtforschung, Bd. 13, page 410, 1936.

20. Ashley, H. and Landahl, M., *Aerodynamics of Wings and Bodies*, Dover edition, Dover Publ., N.Y., 1985.

Figure Captions

1. Particle Paths vs. Streakline. Formation of a Vortex Sheet.
2. Wake Behind an Oscillating Airfoil.
3. Sketch of Wakes from a Delta Wing.
4. Typical Wake Traces. a) Non-Linear. b) Linear, Idealized
5. Wing in Maneuver. a) Wing and Wake Traces at Various Chordwise Locations. b) A Streak Surface, Starboard Side, for given t.
6. Superposition Algorithm for Determining Bound Vorticity Necessary to Cancel Upwash at the Plate.
7. Choice of Cross-Flow Observation Planes. a) $x - z$ Projection. b) $x - y$ Projections and "Roll".
8. Airfoil Response to Low-amplitude Step Change in Attitude. a) Circulation and C_ℓ *vs.* Time. b) Wake Display.
9. Airfoil Response to Large Amplitude Step Change in Attitude. a) Circulation and C_ℓ *vs.* Time. b) Wake Display.
10. Airfoil Response to a Single Full-cycle Completed Imposed Oscillation. a) Wake Display. b) Lift and Circulation *vs.* Quasi-steady Values. c) Moment Coefficient, with History Effect.

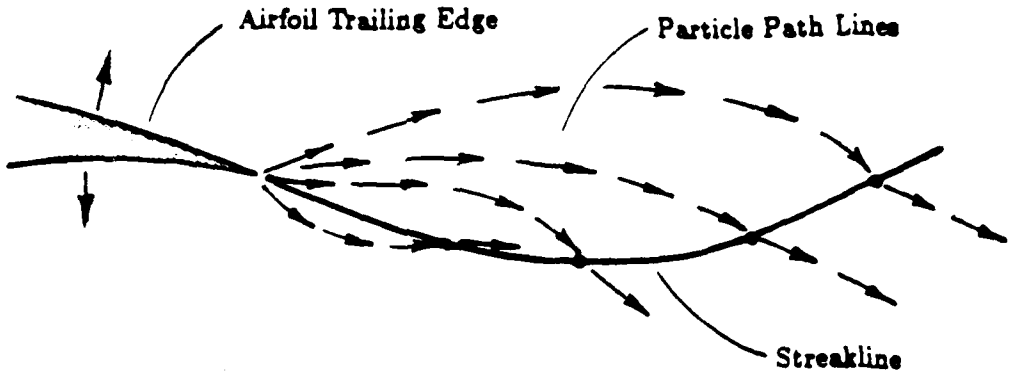

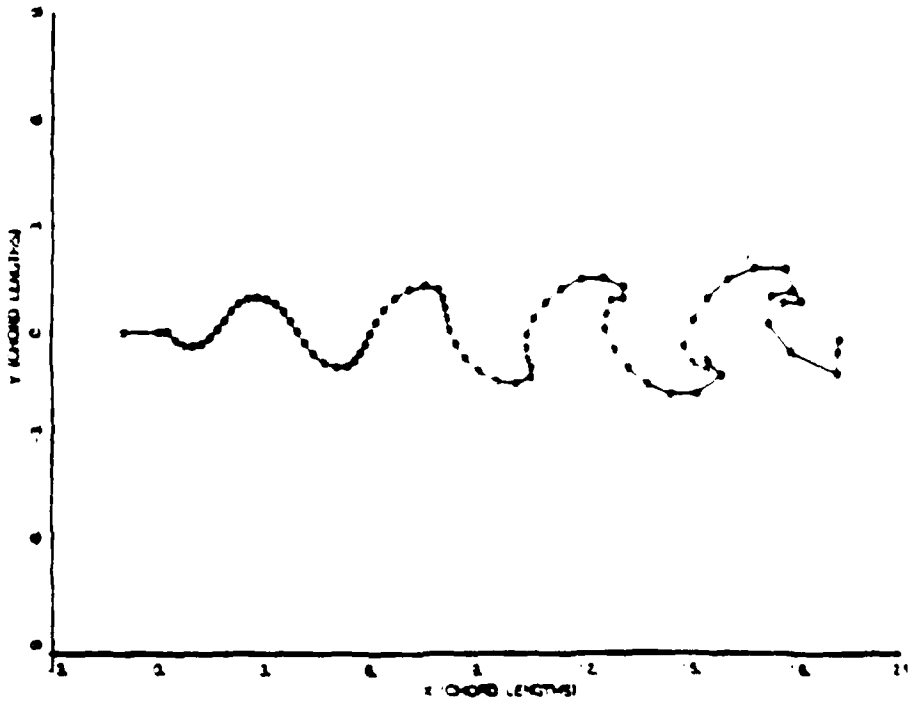

Figure 2 Wake behind an oscillating airfoil.

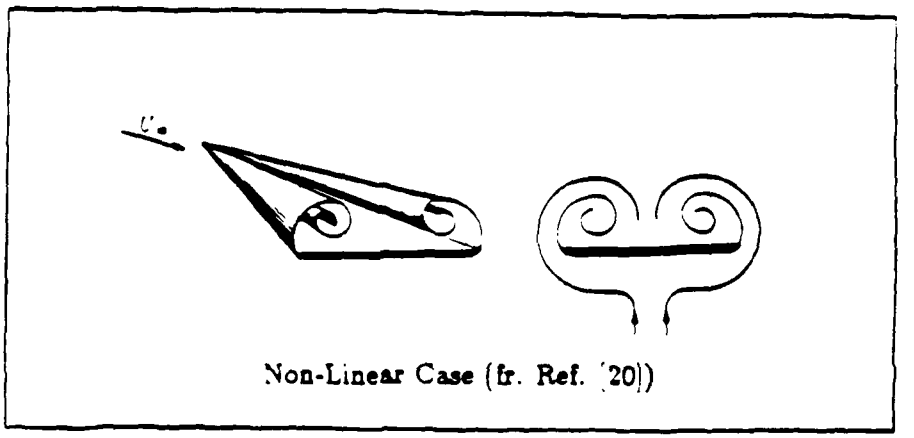

Figure 3 Sketch of Wakes From a Delta Wing

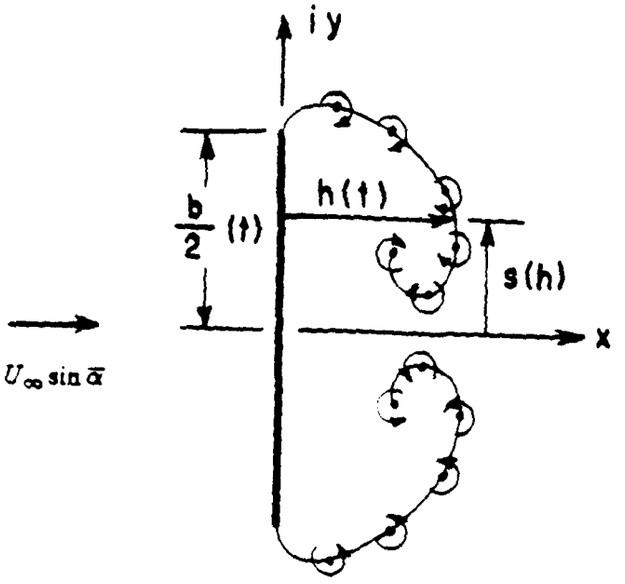

a) Non-Linear Representation Of Wakes

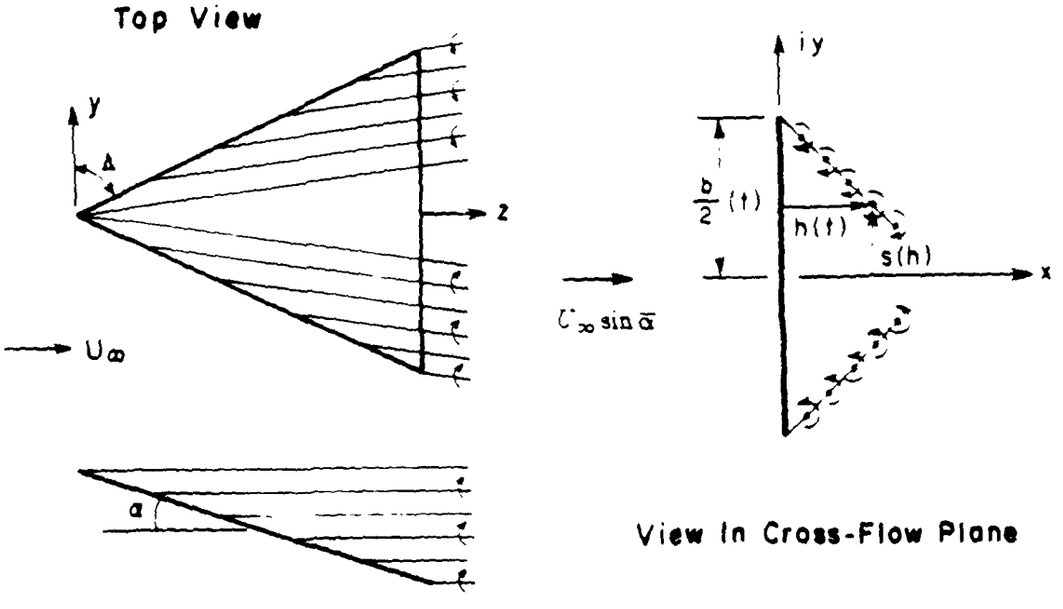

b) Linear Representation Of Wakes

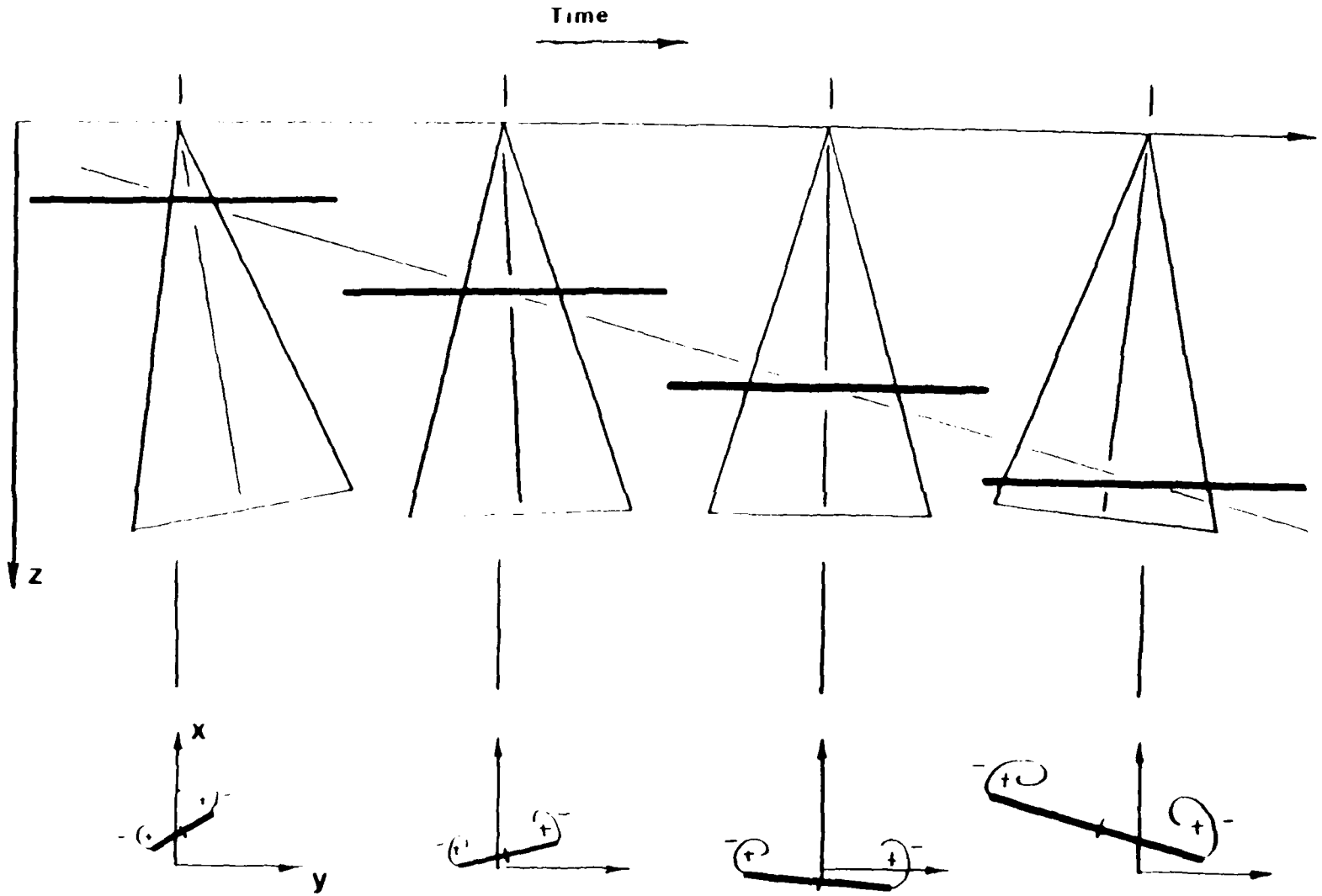
Time
z
x
y

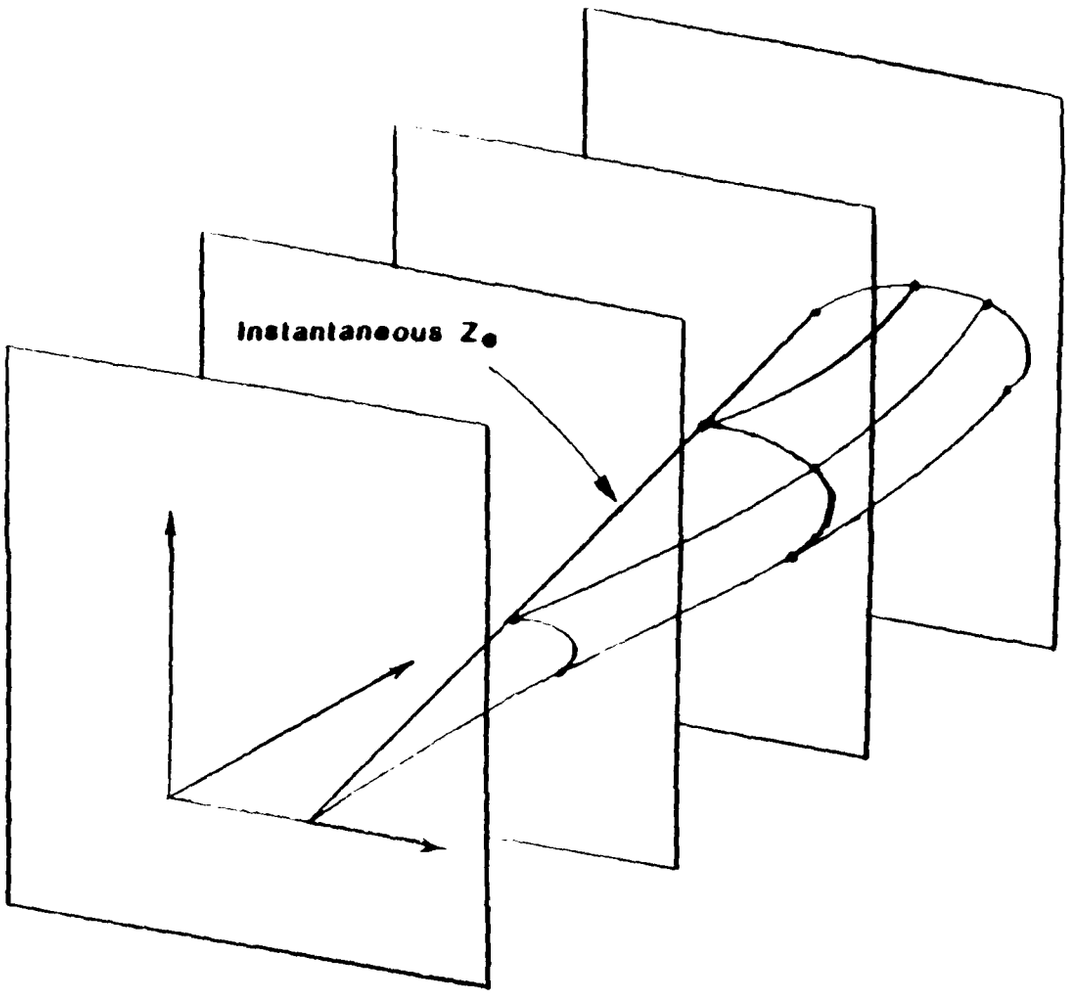

Streak Surface

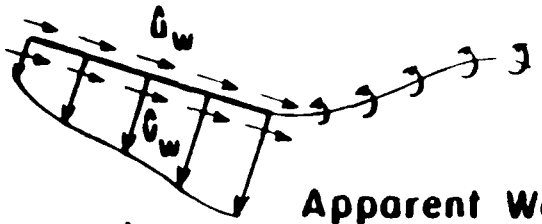

Apparent Wake Induced Velocity

+

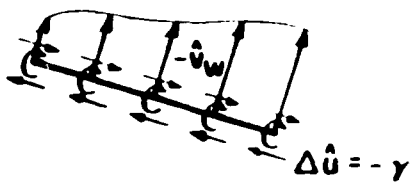

= Velocity Due To Additional Bound Vorticity

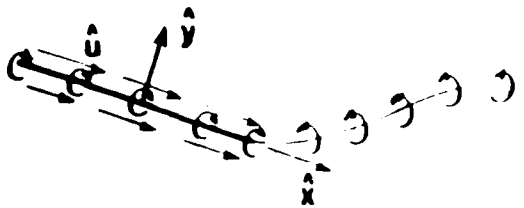

Net Flow With Normal Velocity Cancelled At Airfoil Surface

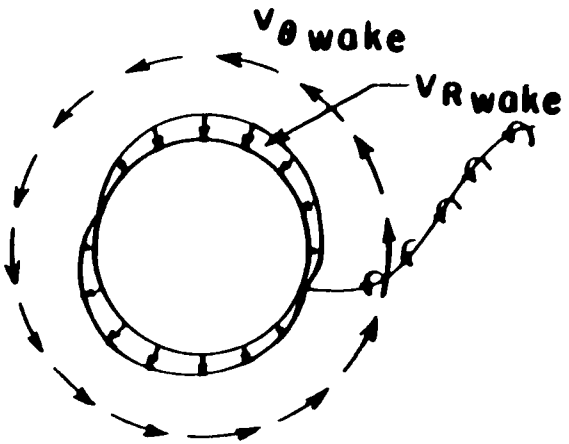

Radial And Tangential Components Of Wake Induced Velocity As Viewed In The Circle Plane

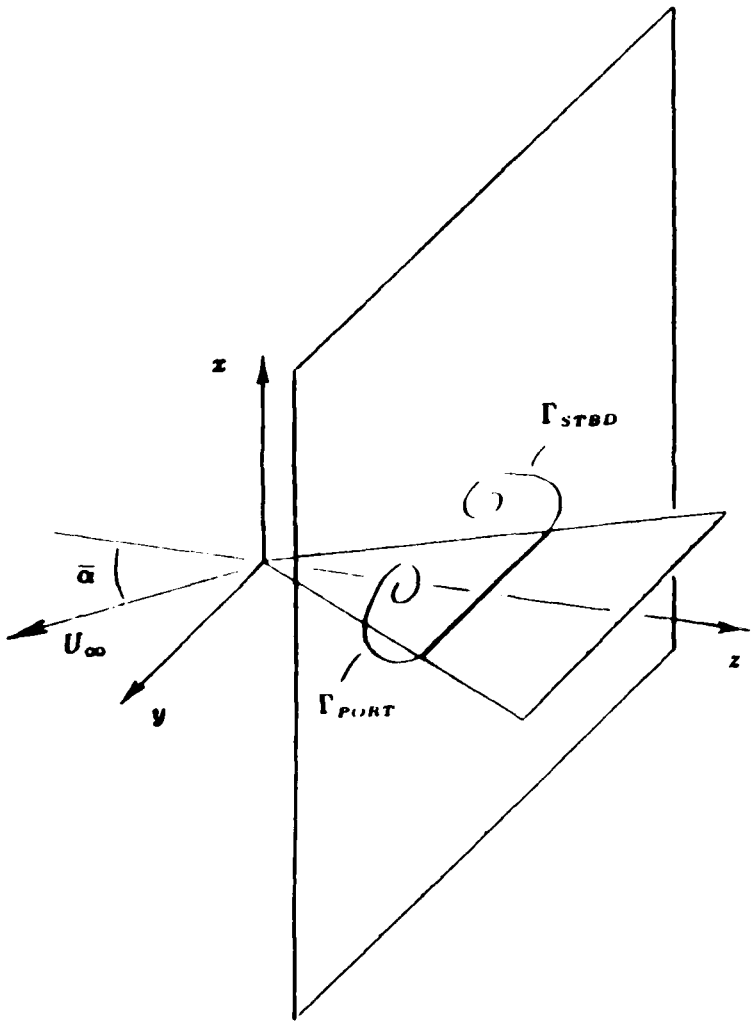

Wing in Steady Motion at Constant Angle of Attack

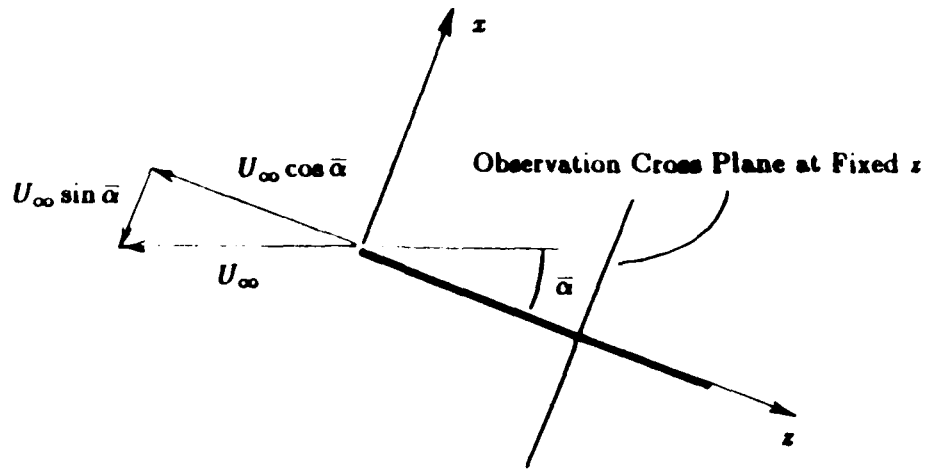

Mean Location of Projection of Wing Trace in (x, z) Plane

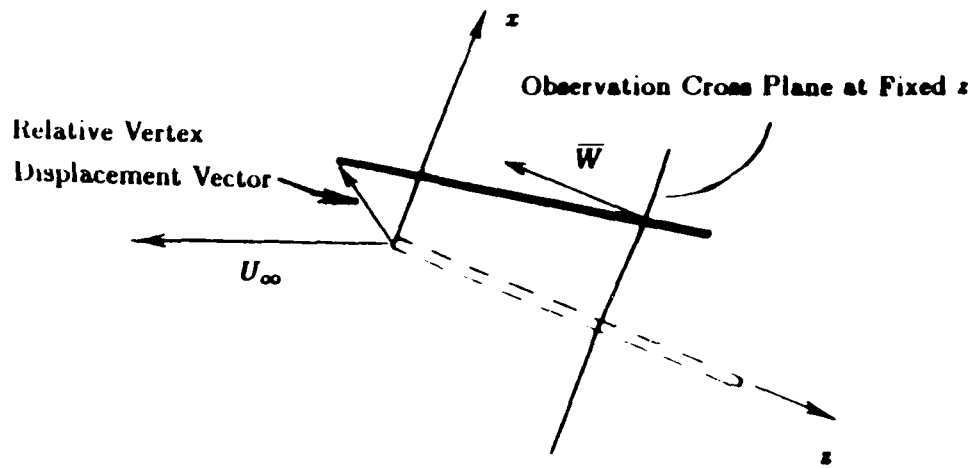

Instantaneous Projection of Wing Trace in (x, z) Plane

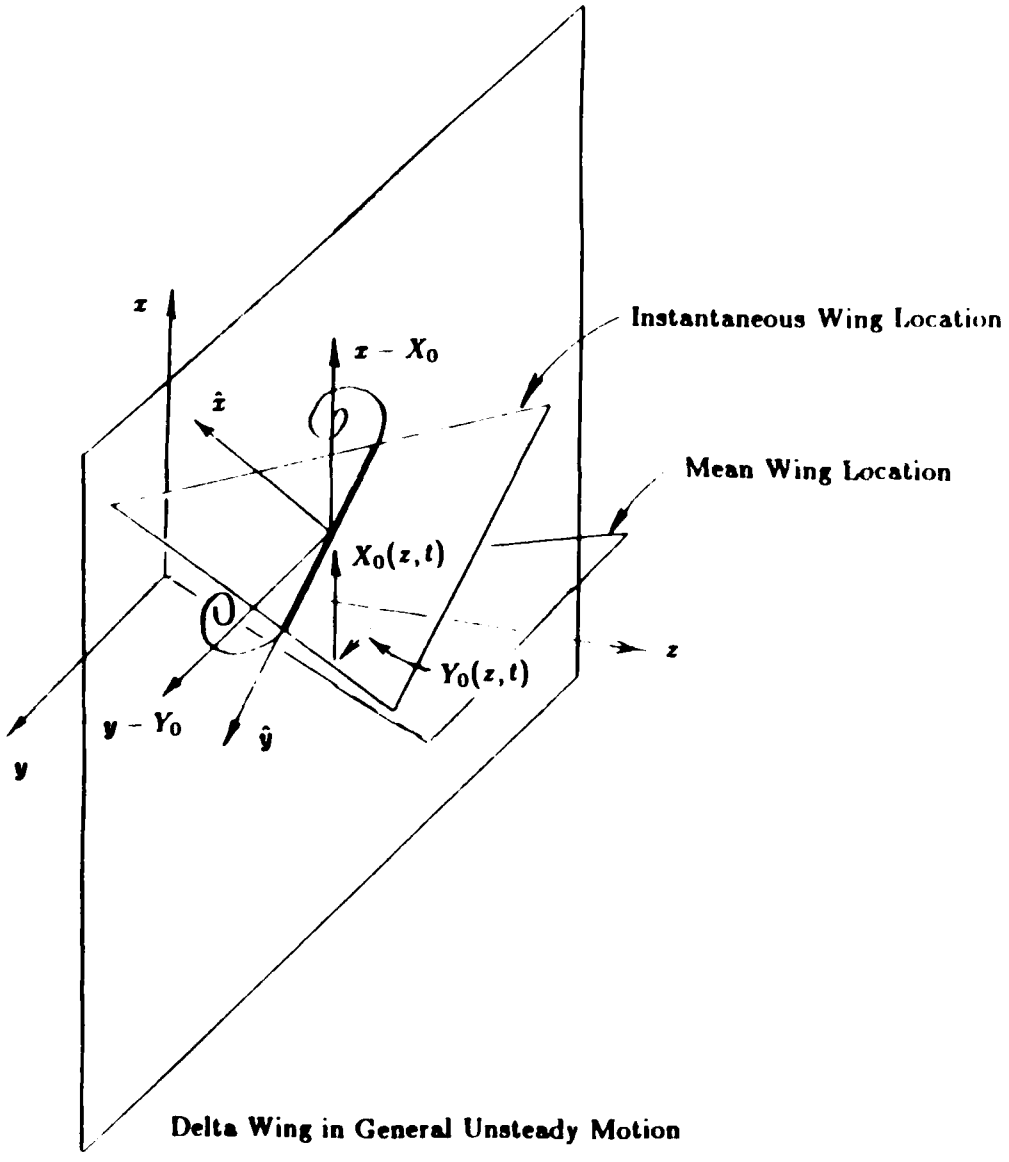

Delta Wing in General Unsteady Motion

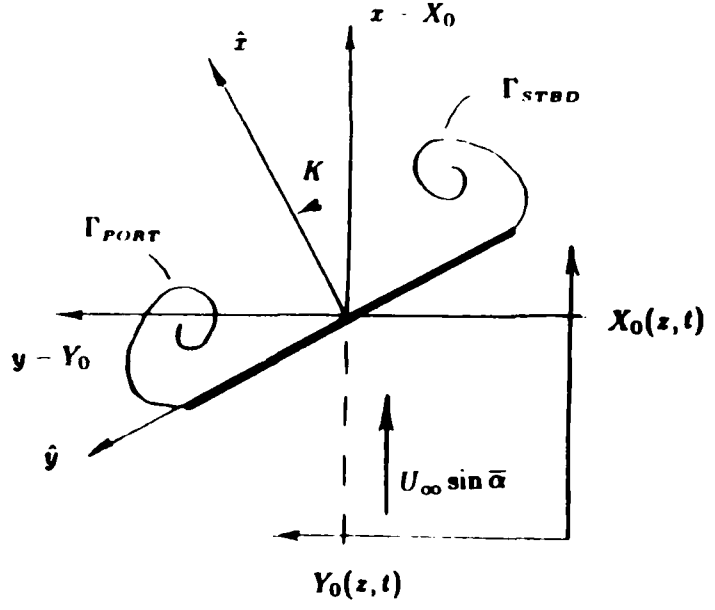

Projection of Wing Trace in (x, y) Plane

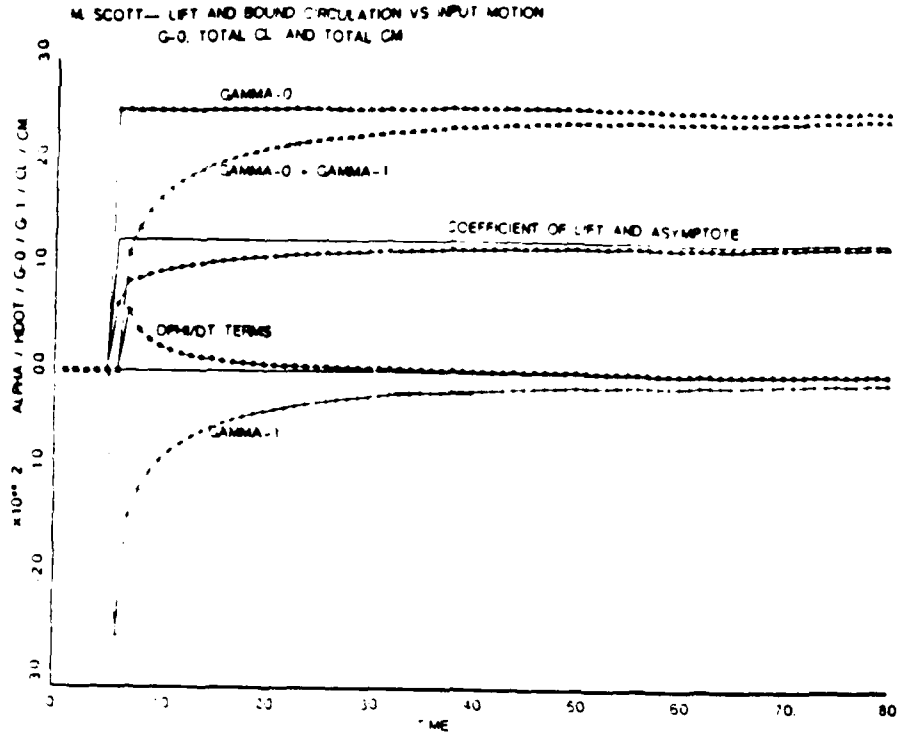
M. SCOTT— LIFT AND BOUND CIRCULATION VS INPUT MOTION
G-0, TOTAL CL AND TOTAL CM
GAMMA-0
GAMMA-0 + GAMMA-1
COEFFICIENT OF LIFT AND ASYMPTOTE
DPHI/DT TERMS
GAMMA-1
ALPHA / HDOT / G-0 / G-1 / CL / CM
x10** 2
TIME

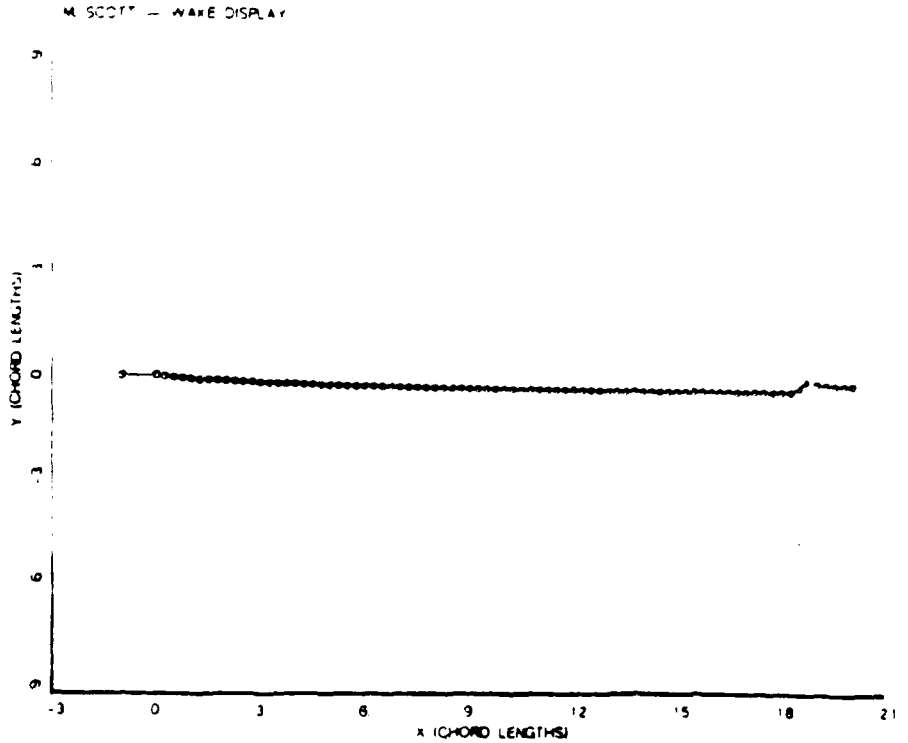
M. SCOTT — WAKE DISPLAY
Y (CHORD LENGTHS)
X (CHORD LENGTHS)

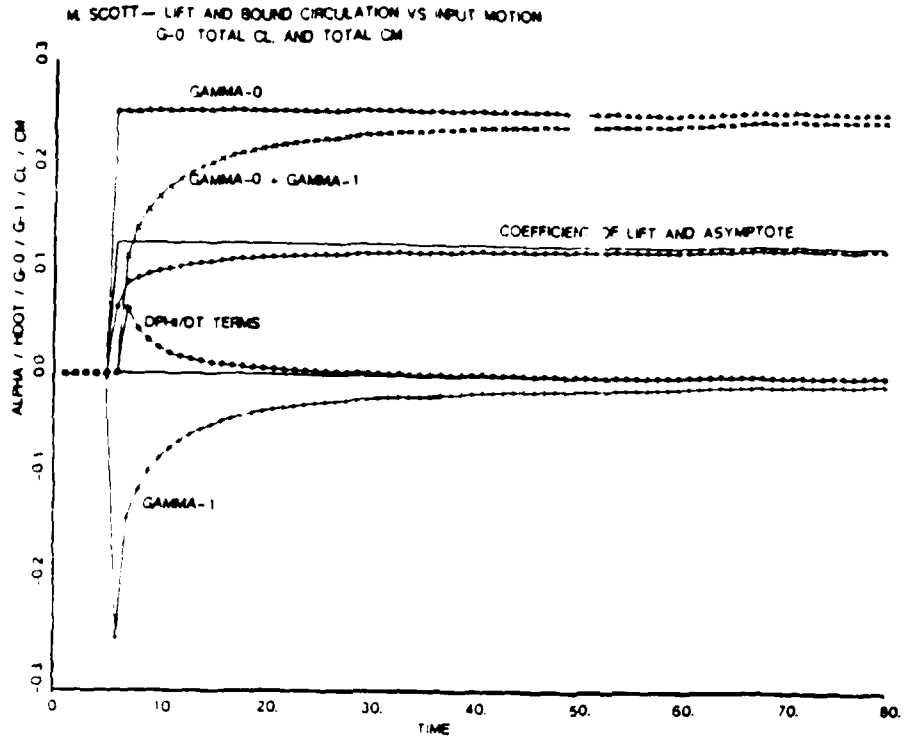
M. SCOTT— LIFT AND BOUND CIRCULATION VS INPUT MOTION
G-0 TOTAL CL AND TOTAL CM
GAMMA-0
GAMMA-0 + GAMMA-1
COEFFICIENT OF LIFT AND ASYMPTOTE
DPHI/DT TERMS
GAMMA-1
ALPHA / HDOT / G-0 / G-1 / CL / CM
TIME

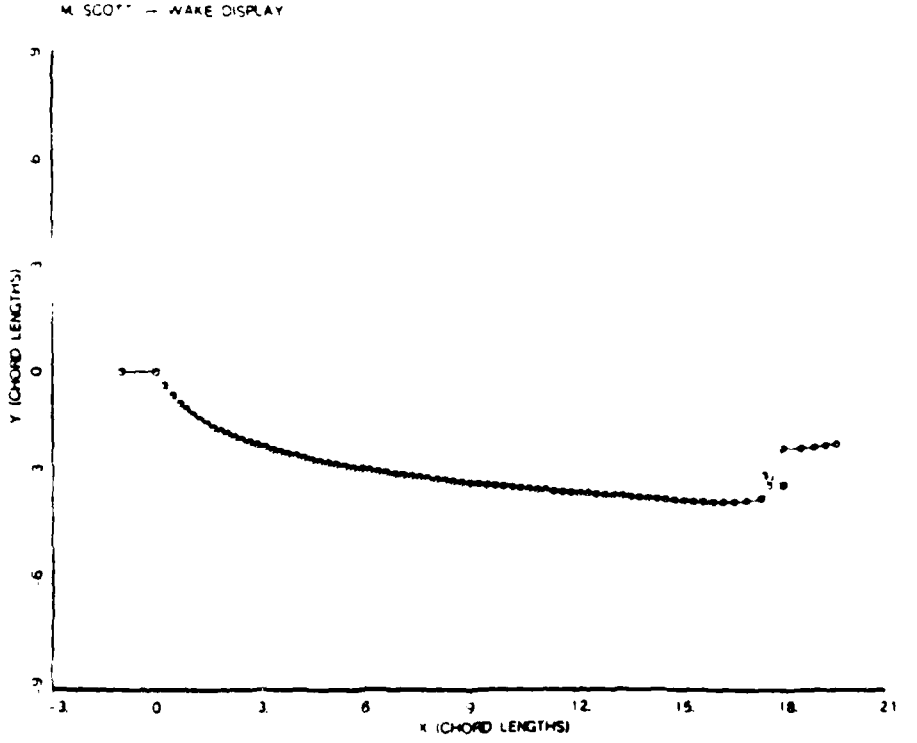
M. SCOTT — WAKE DISPLAY
Y (CHORD LENGTHS)
X (CHORD LENGTHS)

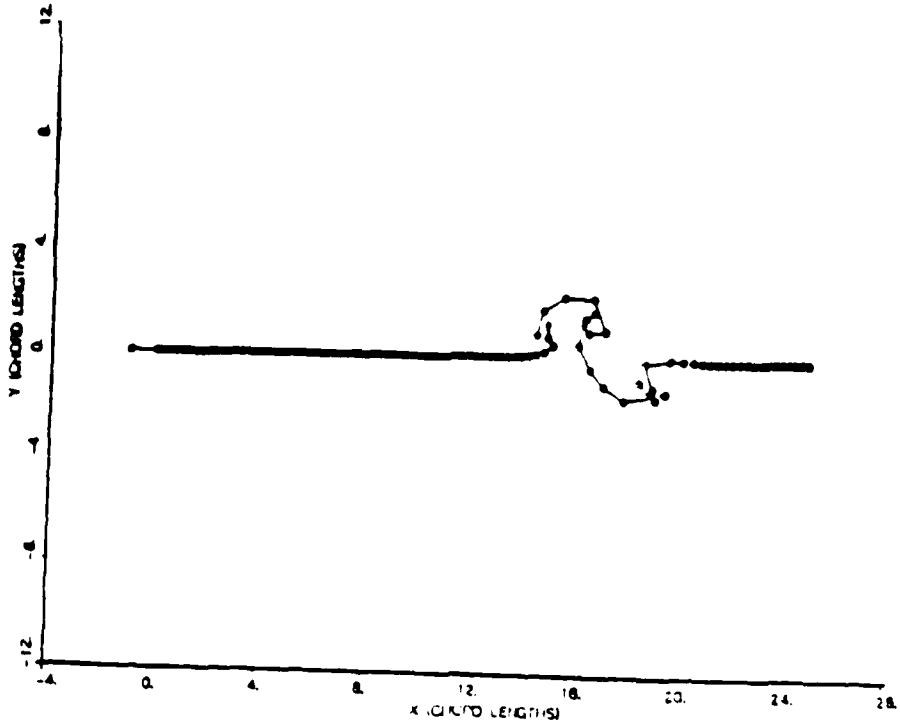
12.
8.
4.
0.
-4.
-8.
-12.
-4.
0.
4.
8.
12.
16.
20.
24.
28.

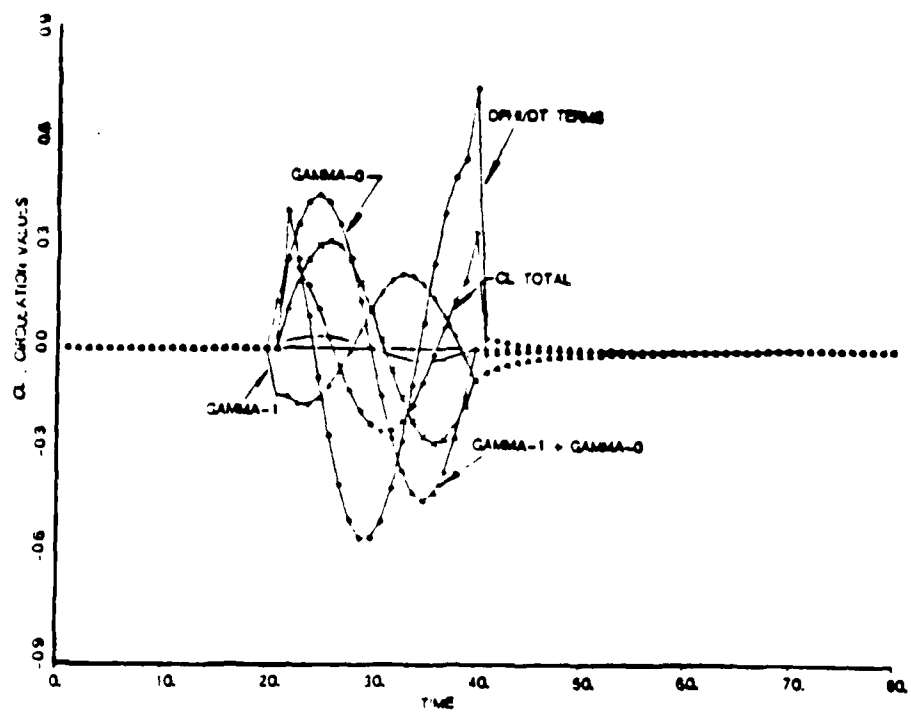
DP/DT TERMS
GAMMA-0
CL TOTAL
GAMMA-1
GAMMA-1 + GAMMA-0
0.9
0.6
0.3
0.0
-0.3
-0.6
-0.9
0.
10.
20.
30.
40.
50.
60.
70.
80.

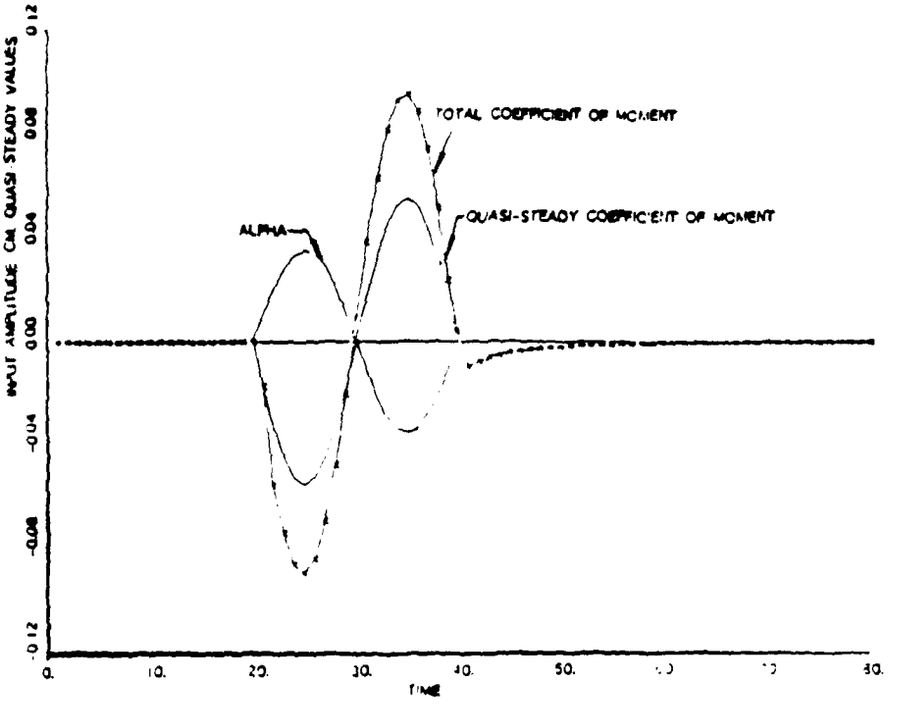
INPUT AMPLITUDE CM QUASI STEADY VALUES
0.12
0.08
0.04
0.00
-0.04
-0.08
-0.12
ALPHA
TOTAL COEFFICIENT OF MOMENT
QUASI-STEADY COEFFICIENT OF MOMENT
0.
10.
20.
30.
40.
50.
60.
TIME

Slender Wing Theory Including Regions of Embedded Total Pressure Loss*

James E. McCune,† T. Sean Tavares,‡ Norman K.W. Lee,‖ and David Weissbein¶

Department of Aeronautics and Astronautics
Massachusetts Institute of Technology, Cambridge, Massachusetts

Abstract

An aerodynamic theory of the flow about slender delta wings is described. The theory includes a treatment of the self-consistent development of the vortex wake patterns above the wing necessary to maintain smooth flow at the wing edges. The paper focuses especially on the formation within the wake of vortex "cores" as embedded regions of total pressure loss, fed and maintained by umbilical vortex sheets emanating from the wing edges. Criteria are developed for determining the growing size and location of these cores, as well as the distribution and strength of the vorticity within them. In this paper, however, the possibility of vortex breakup is omitted. The aerodynamic consequences of the presence and evolution of the cores and the associated wake structure are illustrated and discussed. It is noted that wake history effects can have substantial influence on the distribution of normal force on the wing as well as on its magnitude.

1 Introduction

The underlying assumption adopted in this work is that at the Reynolds numbers of full-scale flight it should be possible to advance our understanding of the aerodynamic behavior of wings, even in severe maneuver, without necessarily resorting to the full Navier-Stokes equations. This classical notion envisions the flow past the wing as consisting of large surrounding "outer" regions of essentially inviscid flow in which are embedded "inner" flows, many key features of which are viscous or viscous-related. These embedded flows may include not only the usual boundary layers and viscous wakes but also larger recirculating regions (such as separation bubbles) as well as shed vortices and vortex "streets" complete with their own inner "cores". The location, size, and shape of the inner embedded flow regions is determined interactively with the larger-scale inviscid flow, but their very existence depends on the presence of viscous action occurring somewhere, especially at the various interfaces with the outer flow.

To the extent that such an hypothesis is viable one can contemplate an analytic approach, albeit computer-assisted, to the study of non-linear, unsteady wing aerodynamics. In many situations the outer flow will be potential; even the embedded flow regions, when of large enough scale, may be essentially inviscid within, although they must then be surrounded by viscous layers or "sheaths" separating them from the outer (potential) flow. A common feature shared among the embedded flow regions, however, is that they will not be irrotational; reduced total pressure, distributed variously over the inner regions, will be present. In addition, when any of the embedded flows detach from the wing surface a key part of the aerodynamic problem is to determine their evolution, in size, shape and location, as affected both by convection in and viscous interaction with the surrounding flows. When compressibility is important, the possible formation of shocks as well as the propagation of acoustic disturbances can also affect the interplay of the inner and outer flows. In this paper, however, we limit ourselves to the incompressible case.

If flow models of wing aerodynamics are constructed along these lines, fully three-dimensional analytic studies of the problem can be carried out and the procedure is essentially classical. Given a wing's geometry and attitude and its flight status or sequence, the precise boundary conditions needed to determine the flow can be written down and classical potential flow techniques applied. The inner flows can be treated using a variety of approximate treatments. The algebraic complexities in the 3D case are formidable, however, and (at least at the outset) may serve only to obscure the progress we wish to make with an analytic or quasi-analytic approach. In this paper, therefore, we adopt the ideas of the slender wing theory of R.T. Jones [1] as a means of illustrating the proposed techniques in a somewhat simplified framework. Jones' quasi-2D treatment for low aspect-ratio wings is a remarkably powerful and insightful tool which historically has also provided a framework for understanding the results and trends of more exact numerical studies.

Advances beyond Jones' theory, especially as applied to

*This work was supported by the AFOSR under Grant Nr. AFOSR-86-157. Earlier phases of the research were also supported by NASA Langley under Grant Nr. NAG-1-658.

†Professor, Associate Fellow, AIAA

‡Research Assistant, Member, AIAA

‖Research Assistant

¶Member, AIAA. Present address: Northrop Aircraft 1 Northrop Ave., Dept. 3812/82, Hawthorne, California 90250

delta wings, began with the recognition by many authors [2], [3], [4], [5] of the need for a vortex wake structure above the suction surface of the wing. (Fig. 1) The role of this wake pattern, somewhat idealised here in the figure, is to provide means of establishing smoother flow (a "Kutta condition") at the wing edges than that arising in the original Jones treatment. The resulting modifications provide predictions more commensurate with real flows at large but finite Reynolds Nr. One can view such a double wake structure as the result of a form of leading-edge separation occurring along each of the swept edges.

In this paper we discuss the self-consistent development of the wake pattern above a low aspect-ratio delta wing at modest angle of attack in the context of its effect on slender wing theory. In particular, we undertake to include in our treatment the presence of embedded cores of distributed vorticity, or regions of reduced total pressure, near the end of each wake trace as illustrated in Fig. 2. The physical reasons for the presence of these embedded regions are discussed briefly in the next Section. We will find in later Sections that the effect of embedded low-total-pressure regions on the development along the wing of various flow quantities, including static pressure, requires careful attention. A self-consistent procedure for determining these parameters in the slender-wing limit is developed in this paper and compared with the classical case of purely potential flow. In addition, we derive criteria for determining the size and evolution of the vortex cores. However, in this paper we do not consider the possibility of vortex breakup. Some of our recent work on that subject will be reported elsewhere.

2 Wake Formation in Potential Flow

2.1 Development of Wakes with Total Pressure Loss

In Reference [6] the self-consistent development of vortex patterns above slender delta wings in large-amplitude unsteady motion is discussed from the point of view of analysing the cross-flow pattern at each chordwise station. In that work, however, the wakes are treated ideally, as if they were simply vortex sheets of complex shape, with no total pressure loss in the flow. The focus there is on determining interactively the shapes of the two required wakes as viewed in successive cross-flow planes. The distribution of vorticity along them is determined so as to maintain smooth flow along the wing leading edges. The method extends the classical literature [2], [3], [4], [5] so as to allow for severe wing motion during maneuver. Non-linear self-consistent vortex wake evolution is explicitly included.

As pointed out in that paper, such a model of the wake structure is somewhat too idealised, in that the development during wake roll up of vortex cores at finite Reynolds numbers, with attendant regions of distributed total pressure loss, is not addressed. Similarly, the related occurrences of secondary separation "bubbles," which arise due to localised separation of the wing boundary layers, and the phenomena of vortex breakup, are explicitly omitted.

In the course of the non-linear evolution of the (ideal, inviscid) vortex-sheet patterns as in [6], the wakes generally tend to "coagulate," with the vortex traces spiralling in on themselves and "rolling up." (See Fig. 2) If this is the case and the Reynolds number is finite (no matter how large), viscous dissipation and smearing out of the vorticity must become important at some stage as the contortions of the ideal wake traces become more and more intricate. The result, as sketched in Fig. 2, is the creation of a region of smeared-out vorticity in the "core" of each wake. (Multiple cores can also occur.) In these core regions, a corresponding embedded region of total pressure deficit is created. Both numerical and experimental evidence exists for such embedded regions; see, for example, references [7], [8], [9], [10], [11].

2.2 Coordinate System: A 'Time-Analogy' Approach

Although the wakes may partially roll up into "cores" as discussed above, we still require a careful treatment of those portions of the wake which remain thin and sheet-like, with negligible total pressure loss across them. For example, the strength of the cores must change as they move downstream over the wing, not least because of chordwise variations in wing geometry. Thus, sheet-like portions of each wake can be regarded as "umbilicals" feeding each core (see Figures), and to these the analysis of [6] applies almost without change.

In the present paper, however, we wish to take advantage of a form of the time-analogy approach inherent in the classical Jones-Munk treatment of slender wings and bodies. [1], [12] For simplicity in the present discussion we take the wing to be a delta of planar geometry and in steady motion at small, constant angle of attack, omitting the radical maneuvers discussed in [6].

Jones suggested an observation coordinate frame fixed in the still atmosphere through which the wing being observed penetrates during its flight. Extending the ideas of Munk, Jones pointed out that if the wing was slender enough (i.e., of low aspect ratio) an observer fixed in this frame would see, in a "cross-flow plane" oriented normal to wing surface, a quasi-2D, but unsteady, flow pattern. The unsteadiness would arise, for example, because the observer would see, in the cross-flow plane, a wing trace "growing" in span according to

$$b(t) = \frac{\mathcal{AR}}{2} z = U_\infty \cos\alpha \frac{\mathcal{AR}}{2} t \approx U_\infty \frac{\mathcal{AR} t}{2} \qquad (2.1)$$

In addition, in Jones' scheme, the wing would appear to be plunging at constant rate $U_\infty \sin\alpha \approx U_\infty \alpha$.

As illustrated in Fig. 3, we adopt in this paper the Jones "time-analogy" view, with the exception that we "stop" the apparent plunging by including a countering cross-flow

velocity (from the left, in Fig. 3) of magnitude $U_\infty \sin\alpha$. Thus, in the cross-flow observation plane, the origin of the $z-y$ frame remains fixed on the wing center line as the wing passes through.

It is in describing the evolution of the two wake traces that the time analogy approach has its greatest appeal. In the spirit of Jones' low aspect-ratio-limit treatment, the potential flow solution in the observation plane at each instant represents an instantaneous solution of Laplace's Equation corresponding to the boundary conditions of the moment. But these now include not only the apparently growing wing trace, but also the developing wakes (or wake traces) emenating from the wing edges. Moreover, at any instant t the outer portions of each wake trace, including and approaching the cores, carry with them the "history" of the wing's penetration of our observation plane; the vorticity in those parts of the wake were generated at times previous to t.

When the wing is in steady flight at angle of attack α, we can relate time variations seen in the present observation frame to chordwise variations referred to in [6] through the transform

$$\frac{\partial}{\partial t} = U_\infty \cos\alpha \frac{\partial}{\partial z} \approx U_\infty \frac{\partial}{\partial z} \tag{2.2}$$

2.3 Convection of Ideal Wakes

The mathematical description of the non-linear convection and evolution of ideal wakes is contained in Reference [6] and will not be repeated here. However, a synopsis of the general approach is useful.

In formulating the ideal wake model the only concession to the existence of viscous-related phenomena is to enforce a Kutta condition - i.e., smooth flow - at each edge of the wing trace. Once an element of circulation has been shed, in that model, the wake is treated in the inviscid limit. Thus each increment of vorticity is convected in accordance with the inviscid Helmholtz relation.

Moreover, the ideal treatment requires that each wake trace be "force-free" along its entire length. The wake vorticity then convects at the local flow velocity. In the cross-flow plane this convection velocity at any point on the wakes is the sum of the cross-flow component of the free stream velocity, $U_\infty \sin\alpha$, and the "induced" velocities associated with all the neighboring vorticity on the wing trace and in the port and starboard wakes.

Owing to the wake history, each element of a specified wake trace (i.e., port or starboard) can be identified according to the time it emanated from the wing edge. Denoting this time as $\bar{\lambda}$, the two wake traces at each instant t are streaklines along which $\bar{\lambda}$ varies from 0 at the far reaches of the wake trace to t at the wing trace ends. (See Fig. 4) Hence the incremental circulation, $d\Gamma$, can be written

$$d\Gamma = \frac{d\Gamma}{d\bar{\lambda}} d\bar{\lambda} . \tag{2.3}$$

We make use of Eq. (2.3) in writing out the "wake-history" integrals below. In [6] it is shown that $\bar{\lambda}$ is a "purely-convected" quantity, acting as a label for a given circulation element in the wake.

2.4 Determining the Vortex Strength Distribution in Ideal Wakes

The net circulation in the cross flow plane is zero for all times by Kelvin's Theorem;

$$\Gamma^{STBD} + \Gamma^{PORT} + \Gamma^{TRACE} = 0 . \tag{2.4}$$

where Γ^{TRACE} is the cross-flow circulation of the wing trace, and Γ^{STBD}, Γ^{PORT} refer to the starboard and port wake traces. From the symmetry of the problem with zero roll angle we see that

$$\begin{aligned} \Gamma^{STBD} &= -\Gamma^{PORT} \\ \Gamma^{TRACE} &= 0 . \end{aligned} \tag{2.5}$$

(See Fig. 4) (For cases involving asymmetric maneuver Γ^{TRACE} must be worked out, and will not generally vanish.)

In complex-variable notation the quasi-2D cross-flow velocity associated with the wakes is, with $Z \equiv z + iy$

$$\begin{aligned} U_{\text{wake}} - iV_{\text{wake}} &= W_{\text{wake}}(Z) \\ &= \frac{1}{2\pi i}\left\{ \int_0^t d\bar{\lambda} \left\{ \frac{\frac{d\Gamma^{PORT}}{d\bar{\lambda}}}{Z - Z_*^{PORT}} \right\} \right. \\ &\left. + \int_0^t d\bar{\lambda} \left\{ \frac{\frac{d\Gamma^{STBD}}{d\bar{\lambda}}}{Z - Z_*^{STBD}} \right\} \right\} . \end{aligned} \tag{2.6}$$

In writing Eq. (2.6) we have made use of Eq. (2.3). In addition, $Z_*^{PORT}(\bar{\lambda})$ and $Z_*^{STBD}(\bar{\lambda})$ are the instantaneous complex locations in the cross flow plane (z, y) of the vorticity elements in the port and starboard wake traces, respectively.

For our chosen reference frame, the boundary condition of no flow through the wing trace is written

$$U|_{\text{wing trace}} = 0, \quad -\frac{b}{2} \le y \le \frac{b}{2}, \quad z = 0 . \tag{2.7}$$

In Eq. (2.7) y is the instantaneous spanwise coordinate, and $\frac{b}{2}$ is the semispan at the specified t. (Fig. 4).

We define the complex velocity $W_0 \equiv U_0 - iV_0$ to be that which would occur if there were no wakes. In that case, imposition of boundary condition Eq. (2.7) in the presence of the cross flow $U_\infty \sin\alpha$ leads to a discontinuous part of the velocity at the wing trace, ΔV_0:

$$\Delta V_0|_{\text{trace}} = -2U_\infty \sin\alpha \frac{y}{\sqrt{\frac{b^2}{4} - y^2}} . \tag{2.8}$$

This is Jones' classical result in the limit of small angle of attack, $\sin\alpha \simeq \alpha$. It is also singular at the wing edges.

Next, we introduce the complex velocity $W_1 \equiv U_1 - i V_1$ to represent the flow field associated with the additional vorticity at the wing trace needed to continue to satisfy Eq. (2.7) in the presence of W_{wake} as given by Eq. (2.6). Using the theory of conjugate functions we find

$$\Delta V_1|_{\text{trace}} = \frac{2\tan\beta}{\pi} \oint_{-\frac{\pi}{2}}^{\frac{\pi}{2}} \frac{d\tau \left(-U_{\text{wake}} \cos\tau\right)}{\cos\tau - \cos\beta} . \qquad (2.9)$$

where ΔV_1 is the jump in V_1 at the wing trace. In Eq. (2.10) the "angle variable" β is

$$y = \frac{b}{2}\sin\beta \qquad (2.10)$$

with β being $\frac{\pi}{2}$ and $-\frac{\pi}{2}$ at the port and starboard wing edges, respectively.

The wing-edge singularities in these additional "wake-induced" terms must exactly cancel the singularities as given in Eq. (2.8) at both edges of the wing if the Kutta-conditions are to be satisfied.

In Eq. (2.9) U_{wake} can be written down in terms of the wake integrals in (2.6). Cancellation of the singularities at both wing edges $\left(y = +\frac{b}{2},\ -\frac{b}{2}\right)$ then requires

$$U_\infty \sin\alpha = Re\frac{i}{\pi}\left\{\int_0^t d\bar{\lambda}\left\{\frac{\frac{d\Gamma^{PORT}}{d\bar{\lambda}}}{\sqrt{(Z_v^{PORT})^2 + \frac{b^2}{4}}}\right\} + \int_0^t d\bar{\lambda}\left\{\frac{\frac{d\Gamma^{STBD}}{d\bar{\lambda}}}{\sqrt{(Z_v^{STBD})^2 + \frac{b^2}{4}}}\right\}\right\} . \qquad (2.11)$$

This equation provides us with the means to calculate the rate at which vorticity is shed from the wing edges while satisfying both Kutta conditions. Its derivation is analogous to that used by Wagner [13] in developing an integral equation for the wake vorticity in unsteady airfoil problems. For this reason we refer to Eq. (2.11) as the "Cross Flow Wagner Integral Equation".

The left hand side of Eq. (2.11) is known, being simply the cross-flow component of the free stream.[1] Operationally, on the computer the use of Eq. (2.11) is relatively straightforward, except for finding the initial incremental vortex elements shed at the instant the point of the delta pierces the cross flow plane (i.e., at $t = 0$). Difficulties arise there since the kernel of the *rhs* is singular. An effective method for treating this critical first moment can be developed in analogy with the method given in [14]. After the procedure has been properly started it proceeds without further difficulty. Once the strength of a vortex element has been determined by Eq. (2.11) at the instant it leaves the wing trace, that strength, as measured by its incremental circulation, remains unchanged as the element convects in the wake. Throughout the evolution of the wake we "track" the locations of the elements by the method of [6] and develop a "history" of the wake vorticity density. Thus all the information needed to carry out the wake integrations (such as in Eq. (2.11)) is present except for that part which depends on the elements currently being shed into each wake. Eq. (2.11) then determines these additional entries so that the edge flow remains smooth.

[1] The *lhs* of Eq. (2.11) is really a step function, being zero for $t < 0$ and $U_\infty \sin\alpha$ thereafter. For the present case, if α is limited to small angles of attack, $U_\infty \sin\alpha \approx U_\infty \alpha$.

2.5 Extension of the Cross-Flow Wagner Integral Equation to Flows with Distributed Vorticity

Eq. (2.11) can be reformulated to incorporate wakes in which there are regions of smeared out vorticity as well as "ideal" regions. As an intermediate step in this reformulation we simply write the expression for the wake "induced" velocity components in terms of integrals taken over the instantaneous lengths of the umbilicals (i.e., those portions of the wake which are thin and sheetlike) and over the areas of the vortical cores. (See Fig. 5) Along the umbilicals the incremental circulation is written

$$d\Gamma = \frac{d\Gamma}{d\ell} d\ell \qquad (2.12)$$

where $d\ell$ is the differential length measured along the instantaneous trace. In the cores the incremental circulation is given by

$$d\Gamma = \Omega dA \qquad (2.13)$$

where Ω is the vorticity density and dA the differential area. (See Fig. 5) Recalling that the Biot-Savart law applies as well to distributed vortical regions we obtain the "induction" equation

$$W_{\text{wake}} = U_{\text{wake}} - iV_{\text{wake}} = \frac{1}{2\pi i}\left\{\int_{L^{PORT}_{\text{umb}}} d\ell\left\{\frac{\frac{d\Gamma^{PORT}}{d\ell}}{Z - Z_v^{PORT}}\right\} + \int_{L^{STBD}_{\text{umb}}} d\ell\left\{\frac{\frac{d\Gamma^{STBD}}{d\ell}}{Z - Z_v^{STBD}}\right\} + \int_{A^{PORT}_{\text{core}}} dA\left\{\frac{\Omega^{PORT}}{Z - Z_v^{PORT}}\right\} + \int_{A^{STBD}_{\text{core}}} dA\left\{\frac{\Omega^{STBD}}{Z - Z_v^{STBD}}\right\}\right\} \qquad (2.14)$$

where "L_{umb}" and "A_{core}" represent integrations along the umbilicals and over the areas of the cores respectively.

Since the shapes and strengths of the umbilicals are not known *a priori* we again use the concept of history integrals and ideal wake tracking and obtain:

$$W_{\text{wake}} = U_{\text{wake}} - iV_{\text{wake}} = \frac{1}{2\pi i}\left\{\int_{\bar{\lambda}_{\text{junct}}}^{t} d\bar{\lambda}\left\{\frac{\frac{d\Gamma^{PORT}}{d\bar{\lambda}}}{Z - Z_v^{PORT}}\right\} + \int_{\bar{\lambda}_{\text{junct}}}^{t} d\bar{\lambda}\left\{\frac{\frac{d\Gamma^{STBD}}{d\bar{\lambda}}}{Z - Z_v^{STBD}}\right\} + \int_{A^{PORT}_{\text{core}}} dA\left\{\frac{\Omega^{PORT}}{Z - Z_v^{PORT}}\right\} + \int_{A^{STBD}_{\text{core}}} dA\left\{\frac{\Omega^{STBD}}{Z - Z_v^{STBD}}\right\}\right\} . \qquad (2.15)$$

The lower limit of the history integrals $\bar{\lambda}_{\text{junct}}$ denotes the circulation element of the ends of the umbilicals at the juncture with the cores while the upper limit t pertains to the vorticity currently entering the wake at the wing edges. The value of $\bar{\lambda}_{\text{junct}}$ increases in time as vorticity from the umbilicals "feed" the cores, and must be determined. (See § 5).

Applying the boundary condition of no flow through the wing trace Eq. (2.7), and enforcing the Kutta conditions we obtain in a manner analogous to that of § 2.4:

$$
\begin{aligned}
U_\infty \sin\alpha = \\
& Re\frac{i}{\pi}\left\{\int_{\bar{\lambda}_{\text{junct}}}^{t} d\bar{\lambda}\left\{\frac{\frac{d\Gamma^{PORT}}{d\bar{\lambda}}}{\sqrt{(Z_\bullet^{PORT})^2+\frac{b^2}{4}}}\right\}\right. \\
& +\int_{\bar{\lambda}_{\text{junct}}}^{t} d\bar{\lambda}\left\{\frac{\frac{d\Gamma^{STBD}}{d\bar{\lambda}}}{\sqrt{(Z_\bullet^{STBD})^2+\frac{b^2}{4}}}\right\} \\
& +\int_{A_{\text{core}}^{PORT}} dA\left\{\frac{\Omega^{PORT}}{\sqrt{(Z_\bullet^{PORT})^2+\frac{b^2}{4}}}\right\} \\
& \left.+\int_{A_{\text{core}}^{STBD}} dA\left\{\frac{\Omega^{STBD}}{\sqrt{(Z_\bullet^{STBD})^2+\frac{b^2}{4}}}\right\}\right\}. \qquad (2.16)
\end{aligned}
$$

Denoting the net circulation in the core as Γ_{core}, and that in the umbilical as Γ_{umb}, the total circulation in the wake is written

$$\Gamma_{\text{wake}} = \Gamma_{\text{core}} + \Gamma_{\text{umb}} \,. \qquad (2.17)$$

As pointed out in the Introduction the formation of embedded vortical regions is dependent on the action of viscosity no matter how large the Reynolds number. In those regions the ideal wake tracking method is no longer directly applicable. Therefore we need to size and locate each core and determine its vorticity distribution before the extended integral equation Eq. (2.16) can be helpful to us. We show in Section 6 that one must consider the role of viscous interaction between the cores and surrounding flow and also include criteria to determine the rate at which vorticity is removed from the umbilical. A sample calculation, including the sizing of the cores, is described there.

3 Slender Wing Expansion

3.1 Ordering in the Slenderness Parameter: Formal Procedure.

Suppose we fix ourselves in a reference frame defined by $\underset{\sim}{\xi}_x, \underset{\sim}{\xi}_y, \underset{\sim}{\xi}_z$; where $\underset{\sim}{\xi}_x$ and $\underset{\sim}{\xi}_y$ are the unit vectors in the cross-flow plane depicted in Fig. 3, and $\underset{\sim}{\xi}_z = \underset{\sim}{\xi}_x \times \underset{\sim}{\xi}_y$ is aligned with the center-line of the wing. In this reference frame the wing appears to travel in the $-z$-direction at a speed $U_\infty \cos\alpha$. In addition there is the steady cross-flow, $U_\infty \sin\alpha$ described above.

We write the velocity vector $\underset{\sim}{v}$ in the form

$$\underset{\sim}{v} = \underset{\sim}{v}_\perp + w\underset{\sim}{\xi}_z \qquad (3.1)$$

where

$$\underset{\sim}{v}_\perp = (u,v) = u\underset{\sim}{\xi}_x + v\underset{\sim}{\xi}_y \qquad (3.2)$$

are the cartesian velocity components in the cross-flow plane. Similarly, if $\underset{\sim}{\Omega} \equiv \text{curl}\ \underset{\sim}{v}$ is the vorticity,

$$\underset{\sim}{\Omega} = \Omega_z\underset{\sim}{\xi}_z + \underset{\sim}{\Omega}_\perp \qquad (3.3)$$

where

$$
\begin{aligned}
&\nabla_\perp \times \underset{\sim}{v}_\perp = \Omega_z\underset{\sim}{\xi}_z = \left(\frac{\partial v}{\partial x} - \frac{\partial u}{\partial y}\right)\underset{\sim}{\xi}_z \,;\ \nabla_\perp \equiv \underset{\sim}{\xi}_x\frac{\partial}{\partial x} + \underset{\sim}{\xi}_y\frac{\partial}{\partial y} \\
&\underset{\sim}{\Omega}_\perp = (\Omega_x, \Omega_y) \,;\ \Omega_x = \frac{\partial w}{\partial y} - \frac{\partial v}{\partial z} \,;\ \Omega_y = \frac{\partial u}{\partial z} - \frac{\partial w}{\partial x} \qquad (3.4)
\end{aligned}
$$

We next introduce the slenderness parameter, ϵ, characterising the wing aspect ratio, $\mathcal{AR}$. We can then write

$$\left|\frac{\partial}{\partial z}\right| / |\nabla_\perp| = 0(\epsilon) \,. \qquad (3.5)$$

In the light of Eq. (3.5), the order of magnitude of various terms in Eqs. (3.1) through (3.4) can be worked out. Based on the time-analogy approach discussed in Section 2.2, chordwise variations are related to time variations as in Eq. (2.2). Eq. (3.5) is then equivalent to

$$
\begin{aligned}
\left|\frac{\partial}{\partial t}\right| / (U_\infty |\nabla_\perp|) &= \cos\alpha\, 0(\epsilon) \\
&= 0(\epsilon) \qquad (3.6)
\end{aligned}
$$

since U_∞ is of order unity. Note also that div $\underset{\sim}{\Omega} = 0$, so

$$\frac{\partial \Omega_z}{\partial z} = -\nabla_\perp \cdot \underset{\sim}{\Omega}_\perp \qquad (3.7)$$

and consequently

$$|\underset{\sim}{\Omega}_\perp| / |\Omega_z| = 0(\epsilon) \,. \qquad (3.8)$$

Eqs. (3.4), (3.5) and (3.8) then imply

$$\frac{w}{|v_\perp|} = 0(\epsilon) \,. \qquad (3.9)$$

The above corresponds to the standard procedure showing how slenderness is employed to make approximations for low $\mathcal{AR}$ wings; the technique is used throughout this paper.

3.2 Flow Quantities in the Cross-Flow Plane Through First Order.

§ 3.1 establishes a formal procedure for calculating the magnitude of various flow quantities under the slenderness approximation. One begins by considering the cross-flow plane. In this section we make use of slenderness to derive the basic governing equations in that plane, including first-order "time"-variations in the time-analogy.

The continuity equation in incompressible flow is

$$\nabla \cdot \underset{\sim}{v} = 0 \,. \tag{3.10}$$

Since $\frac{\partial w}{\partial z} = 0(\epsilon^2)$ Eq. (3.10) reduces to

$$\frac{\partial u}{\partial x} + \frac{\partial v}{\partial y} \equiv \nabla_\perp \cdot \underset{\sim}{v}_\perp = 0 \,. \tag{3.11}$$

through first order in ϵ. This can be satisfied at any instant using a streamfunction $\psi(x, y; t)$ such that

$$\underset{\sim}{v}_\perp = (v_x, v_y) = \nabla_\perp \psi \times \underset{\sim}{\hat{e}}_z \tag{3.12}$$

to the required order. (Note that $\underset{\sim}{v}_\perp = U_\infty \sin\alpha \, \underset{\sim}{\hat{e}}_z \approx U_\infty \alpha \underset{\sim}{e}_z$ far away from the wing trace in the cross-flow plane.) The z-component of the vorticity is then, to the same order,

$$\Omega_z = -\nabla_\perp^2 \psi \,. \tag{3.13}$$

The unexpanded momentum equation in the "inviscid" regions described in the Introduction can be written as

$$\frac{\partial \underset{\sim}{v}}{\partial t} + \underset{\sim}{v} \cdot \nabla \underset{\sim}{v} = -\frac{1}{\rho} \nabla p \,. \tag{3.14}$$

Again using slenderness, Eq. (3.14) becomes, through first order,

$$\frac{\partial \underset{\sim}{v}_\perp}{\partial t} + \underset{\sim}{v}_\perp \cdot \nabla_\perp \underset{\sim}{v}_\perp = -\frac{1}{\rho} \nabla_\perp p \,. \tag{3.15}$$

Here, "ρ" is the (constant) fluid density and "p" the static pressure. Eq. (3.15) can also be written as [15]

$$\frac{\partial \underset{\sim}{v}_\perp}{\partial t} + \underset{\sim}{v}_\perp \times \Omega_z \underset{\sim}{\hat{e}}_z = -\frac{1}{\rho} \nabla_\perp \left(p + \rho \frac{v_\perp^2}{2} \right) \tag{3.16}$$

or

$$\frac{\partial \underset{\sim}{v}_\perp}{\partial t} + \Omega_z \nabla_\perp \psi = -\frac{1}{\rho} \nabla_\perp P_{\perp_0} \tag{3.17}$$

through first order in ϵ. Here, $v_\perp$ is the magnitude of $\underset{\sim}{v}_\perp$, and $P_{\perp_0} \equiv p + \rho \left(\frac{v_\perp^2}{2} \right)$ is the cross-flow "total" pressure in the incompressible limit, through first order in ϵ.

When the flow is irrotational, as in the "outer" flows discussed in § 1, Eq. (3.17) can be treated in the usual way. Replacing $\underset{\sim}{v}_\perp$ by $\nabla_\perp \phi$ and noting $\Omega_z = 0$, we have

$$\nabla_\perp \frac{\partial \phi}{\partial t} = -\frac{1}{\rho} \nabla_\perp P_{\perp_0} \tag{3.18}$$

or

$$\frac{P_{\perp_0}}{\rho} + \frac{\partial \phi}{\partial t} = \frac{P_{\perp_0}(\infty)}{\rho} = \text{const} \tag{3.19}$$

for irrotational flow. Note that in this frame of reference, therefore, the quantity $P_{\perp_0}$ is discontinuous wherever ϕ or $\frac{\partial \phi}{\partial t}$ is discontinuous, as on the umbilical vortex sheets in the wakes and on the wing trace. Application of Eq. (3.19) on both sides of the umbilical at the juncture (Fig. 6) yields

$$\frac{\Delta P_{\perp_0}}{\rho} \equiv \frac{P_{\perp_0}^+ - P_{\perp_0}^-}{\rho} = \frac{\partial}{\partial t}(\phi^- - \phi^+) = \frac{\partial \Gamma_{\text{core}}}{\partial t} \,. \tag{3.19a}$$

The usefulness of this equation will be seen in § 5.

Utilising Eq. (3.11), we also have $\nabla_\perp^2 \phi = 0$, defining the usual potential problem in the cross-flow plane, [1], [12].

By contrast, in the "inner" vortical embedded regions (see § 1), even if they are essentially inviscid, we must adopt a somewhat different approach. Using Eq. (3.12), we can rewrite Eq. (3.17) in this case as

$$-\frac{1}{\rho} \nabla_\perp P_{\perp_0} = \Omega_z \nabla_\perp \psi + \nabla_\perp \left(\frac{\partial \psi}{\partial t} \right) \times \underset{\sim}{\hat{e}}_z \tag{3.20}$$

In exploring how to use this relation, it is helpful to note its implications in zeroth order: if

$$P_{\perp_0} = P_{\perp_0}^{(0)} + 0(\epsilon)$$
$$\Omega_z = \Omega_z^{(0)} + 0(\epsilon)$$

then, since $\frac{1}{|\psi|} \frac{\partial \psi}{\partial t} = 0(\epsilon)$

$$\Omega_z^{(0)} \nabla_\perp \psi = -\frac{1}{\rho} \nabla_\perp P_{\perp_0}^{(0)} \,.$$

This implies $P_{\perp_0}^{(0)} = P_{\perp_0}^{(0)}(\psi)$ to zeroth order, and consequently $\Omega_z^{(0)} = \Omega_z^{(0)}(\psi)$ as well. In fact,

$$\Omega_z^{(0)}(\psi) = -\frac{1}{\rho} P'_{\perp_0}(\psi) \tag{3.21}$$

can be taken as a lowest-order characteristic feature of an embedded vortical region. It implies that the "total pressure", $P_{\perp_0}$, tends to vary only across (instantaneous) streamlines, but is constant along them, corresponding to the Bernoulli result in lowest order. In this order, one could also determine ψ by solving

$$\nabla_\perp^2 \psi = -\Omega_z^{(0)}(\psi) \tag{3.21a}$$

with appropriate boundary or matching conditions, provided one knew $\Omega_z^{(0)}(\psi)$. (See [16] and [17] and § 4).

The presence of the "perturbation" term involving $\frac{\partial \psi}{\partial t}$ in Eq. (3.20), however, can have a profound influence on this conclusion, especially for recirculating embedded flows. For such flows the dominant part of $\nabla_\perp \left(\frac{\partial \psi}{\partial t} \right)$, particularly if Ω_z is changing locally in time, is itself in the $\nabla_\perp \psi$-direction. This, in turn, implies first-order variation of $P_{\perp_0}$ along "streamlines". But if the flow is in fact recirculating, $P_{\perp_0}$ must be cyclic (see § 4), requiring either that $\frac{\partial \psi}{\partial t} = 0$ in the embedded region, or that an appropriate cyclic average of $\frac{\partial \psi}{\partial t}$ around the recirculation path must vanish. Physically, for recirculating embedded regions large enough to be essentially inviscid, this observation corresponds to the statement that the local angular momentum cannot change other than by transport or storage of that quantity in a given control volume. (Recall that lines of constant ψ, as treated here, are "instantaneous streamlines" only: through first order there is generally a flux across them.)

To illustrate in a simple example, we consider a circular embedded region with solid-body flow, $v_r = 0$, $v_\theta = \frac{\omega_0 r}{2}$, $\Omega_z = \omega_0(t)$, where r is measured from the epicenter of the

convecting core. In that case, $\psi = -\frac{\omega_0 r^2}{4} + \psi_0(t)$, and $\nabla_\perp \frac{\partial \psi}{\partial t} \cong -\left(\frac{\dot{\omega}_0 r}{2}\right) \ell_r$, where $\dot{\omega}_0 \equiv \frac{d\omega_0}{dt}$. Since $\underset{\sim}{\ell}_r \times \underset{\sim}{\ell}_s = -\underset{\sim}{\ell}_\theta$, we recover from Eq. (3.20)

$$-\frac{1}{\rho}\nabla_\perp P_{\perp_0} = -\frac{\omega_0^2 r}{2}\underset{\sim}{\ell}_r + \frac{\dot{\omega}_0 r}{2}\underset{\sim}{\ell}_\theta . \qquad (3.22)$$

In this case, for an embedded, recirculating circular flow we must conclude that $\dot{\omega}_0 = 0$, since $\frac{\partial P_{\perp_0}}{\partial \theta} = 0$. For such a simple embedded flow, therefore, (see § 5) we would find Ω_s = constant, independent of time and space throughout the confined region, even though that confined region itself may grow in time.

In the general case, application of the cyclic constraints ideas discussed in § 4 provides information on the cross-streamline variation of $P_{\perp_0}$. For the circular-flow case, as in Eq. (3.22), the radial variation of $P_{\perp_0}$ is determined, provided we can determine ω_0. In either case, on matching the inner with the outer flow, one determines the static pressure within the core as well.

4 Embedded Cross - Flow Regions: Cyclic Constraints, and The Sheath Model

4.1 Cyclic Constraint: Low-Shear-Stress Recirculating Regions

Determining the distribution of the vorticity and the corresponding total pressure loss within embedded flow requires considerations special to the recirculatory nature of the flows within them [16], [17]. Introduction of "cyclic constraints" at finite Reynolds number to account for the recirculating feature of the streamlines in the presence of viscosity is a key to determining $\Omega_s(\psi)$ within the cores. The following illustrates the construction of typical cyclic constraint conditions.

The full Helmholtz equation which includes viscous effects (sometimes called the dissipative Helmholtz equation) is given by

$$\frac{\partial \underset{\sim}{\Omega}}{\partial t} + \underset{\sim}{v} \cdot \nabla \underset{\sim}{\Omega} = \underset{\sim}{\Omega} \cdot \nabla \underset{\sim}{v} + \nu \nabla^2 \underset{\sim}{\Omega} \qquad (4.1)$$

Using the slenderness approximation, the z-component of Eq. (4.1) becomes

$$\frac{\partial \Omega_s}{\partial t} + \underset{\sim}{v}_\perp \cdot \nabla_\perp \Omega_s = \nu \nabla_\perp^2 \Omega_s + 0(\epsilon^2) \qquad (4.2)$$

The first two terms on the left-hand side of (4.2) are of order ϵ and unity respectively; and the dissipation term on the right-hand side is of $0\left(\frac{1}{Re}\right)$, when Re being the Reynolds number. One solution to Eq. (4.2) is $\Omega_s = 0$, representing potential flow. When the flow is rotational and in the absence of strong shear stress, $\Omega_s = F(\psi)$ satisfies Eq. (4.2) to seroth order. (Note $F(\psi)$ is equivalent to $\Omega_s^{(0)}(\psi)$ in (§ 3.2).) The $0\left(\frac{1}{Re}\right)$ and $0(\epsilon)$ terms can be accounted for by writing

$$\Omega_s(\psi, \ell) = F(\psi) + f(\psi, \ell) \qquad (4.3)$$

where ℓ is a measure of the distance along a streamline, and f is of higher order than F. With this substitution for Ω_s, Eq. (4.2) becomes

$$\frac{\partial F}{\partial t} + \underset{\sim}{v}_\perp \cdot \nabla f = \nu \nabla_\perp^2 F; \qquad (4.4)$$

correct to $0\left(\frac{1}{Re}\right)$ and $0(\epsilon)$. Eq. (4.4) can be rewritten as

$$|\nabla_\perp \ell| \, v_\perp \frac{\partial f}{\partial \ell} = \nu \nabla_\perp^2 F - F' \frac{\partial \psi}{\partial t} . \qquad (4.5)$$

When the streamlines (lines of constant ψ) "connect" to infinity, or to any region of known flow conditions, $P_{\perp_0}(\psi)$ and hence $\Omega_s^0(\psi)\,(\equiv F(\psi))$ are determined. Solution of Eq. (3.13) with appropriate boundary conditions then proceeds as usual and determines the flow to lowest order.

On the other hand, for an embedded region of distributed vorticity, the streamlines are not connected to an outer, known region, and the above standard treatment is not applicable. In such regions, since the instantaneous streamlines close on themselves to lowest order, a different requirement must be met which will turn out to determine the flow. This new requirement states that, for purposes of physical continuity, the integral over a closed streamline of the variation of any property along that particular streamline must vanish. In other words, the embedded flow has to be cyclic. When this cyclic constraint is applied to $f(\psi, \ell)$, it implies

$$\oint d\ell \, \frac{\partial f(\psi, \ell)}{\partial \ell} = 0 \qquad (4.6)$$

where the integral is to be taken along closed streamlines. Eqs. (4.5) and (4.6) then yield

$$\nu \oint \nabla_\perp^2 F \frac{d\ell}{v_\perp |\nabla_\perp \ell|} - F' \oint \frac{\frac{\partial \psi}{\partial t}}{v_\perp |\nabla_\perp \ell|} = 0 \qquad (4.7)$$

Defining $ds_\ell \equiv d\ell / |\nabla_\perp \ell|$, $\Gamma(\psi) \equiv \oint v_\perp ds_\ell$, $\tau(\psi) \equiv \oint ds_\ell / v_\perp$ and also noting $\nabla_\perp^2 F = F' \nabla_\perp^2 \psi + F'' |\nabla_\perp \psi|^2 = -FF' + v_\perp^2 F''$, Eq. (4.7) becomes

$$\nu \left[\Gamma F'' - \tau F F'\right] - F' \left(\oint \frac{ds_\ell \frac{\partial \psi}{\partial t}}{v_\perp} \right) = 0 \qquad (4.8)$$

in the low-shear-stress region of the embedded flow in the cross-flow plane.

Interpretation of Eq. (4.8) through first order in ϵ, i.e., including the $\frac{\partial \psi}{\partial t}$ term, provides additional information. This term is equivalent to the $\frac{\partial \psi}{\partial t}$ term discussed in connection with the momentum balance in Eq. (3.20) for embedded flows, which we recognised there as being associated with the flux of angular momentum across the instantaneous recirculating streamlines, ψ = const. It can be argued, in fact, that in large Reynolds number (low-shear-stress) regions the integrated $\frac{\partial \psi}{\partial t}$ term of Eq. (4.8),

being $0(\epsilon)$, is inherently much larger than the term proportion to "ν", which is $0\left(\frac{1}{Re}\right)$. In that case we must impose the separate constraint

$$F' \oint \frac{ds_\ell \frac{\partial \psi}{\partial t}}{v_\perp} = 0 \,. \qquad (4.8a)$$

Unless $F'(\psi)$ is strictly zero this implies, as in § 3, that any part of $\frac{\psi_t}{|\nabla \psi|}$ which is not simply periodic in the cyclic variable s_ℓ must vanish. Again, for simple core shapes, one concludes that the mean vorticity density tends to be time independent in embedded recirculatory regions. Finally, note that when Eq. (4.8a) applies separately, the remaining cyclic constraint is in the form originally treated by Batchelor:

$$\nu \left[\Gamma F'' - \tau F F''\right] = 0 \,, \qquad (4.8b)$$

corresponding to a strictly two-dimensional embedded vortical flow with recirculating streamlines.

For the simple core geometries that tend to be observed the practical solution of Eq. (4.8b) is essentially F = constant, [16], [17]. Only very weak variation about this condition can be found for reasonable distributions of $\Gamma(\psi)$ and $\tau(\psi)$ in such geometries. However, the conclusion F = constant, or essentially so, does not mean that the core flow is circular or "solid-body". In [17], for example, a range of elliptical embedded vortical regions, together with detailed variations of F about its dominant constant value, were studied. But the primary feature of these embedded regions remains that F is essentially constant in space in the low-shear-stress regime. Our conclusions from Eq. (4.8a) then provide the additional information that F is constant in time as well.

4.2 The Sheath Model and Cyclic Constraints in General

In the absence of any viscosity-dominated regions whatsoever, Kelvin's theorem would not allow a vortical but essentially inviscid core to be embedded in an irrotational flow. This then implies, under the high Re assumption, the presence of a viscous sheath surrounding the core in order to impart vorticity to the flow entrained into the core.

Using this sheath model we can complete the determination of the total pressure distribution in the cross-flow plane. On account of Eqs. (3.19) and (3.20), a difference in the evolution of total pressure, $P_{\perp_0}$, inside and outside the core is inevitable. The sheath plays the role of redistributing $P_{\perp_0}$ at the core edges, thus smoothing out any otherwise forbidden "jumps" in $P_{\perp_0}$. Moreover, the length around the perimeter of the cores needed for the viscous action to provide a specified change of $P_{\perp_0}$ grows with some power of the Reynolds number [17]. This fact, combined with the required sheet strengths of the umbilicals, will be used in § 5 to determine the core sizes as they develop.

An example involving both the application of Batchelor's cyclic constraint and the redistribution of total pressure by the viscous sheaths is illustrated in [17]. In that work a model for the leading edge separation and reattachment over a two-dimensional plate is developed. The study utilises Eq. (4.8b) to deduce the form of vorticity in the embedded core regions. The model for the viscous sheath consists of a shear layer made up of two sub-layers. (See Fig. 7) The inner sublayer, being in direct contact with the embedded region, consists of recirculating flow that incorporates the boundary layer on the upper-side of the plate. In contrast the outer sub-layer, of which a portion is the boundary layer on the underside of the plate, is bounded by the irrotational outer flow.

In this sheath model the outer sub-layer is considered to drive the inner sub-layer via shear stress. One important criterion emerging from this two-layer model is that, to maintain its recirculating nature, the inner sub-layer flow must be given enough energy to overcome viscous dissipation on the plate. In other words, the gain in total pressure of a fluid particle travelling from A through B to C must turn out to exactly balance the loss in the same quantity as the particle completes the cycle by moving from C back to A. This corresponds to an application of the generalised cyclic constraint idea. It is used together with the fact that the static pressure along the outer edge of the sheath is governed by the outer flow to deduce the sheath profile and its peripheral static pressure distribution via an iterative procedure. Figs. 8 and 9 show results obtained for two different Reynolds numbers: streamlines for the external flow are presented in (a) and those for the embedded region in (b). Such results provide a framework from which techniques developed so far can be extended to include corrections for unsteady effects. But in addition, as illustrated in § 5, these ideas provide one of the final links necessary to determine the vortex core evolution.

5 Closure of the Aerodynamic Problem with an Embedded Circular Core

This section illustrates how one can systematically employ the techniques developed in the previous sections to determine the flow in an embedded region based on a simple, but physically revealing model. In particular the role of interaction between the umbilical and viscous sheath is clearly demonstrated. The model consists of a strictly circular core, with a convective epicenter and with a spatially constant, time-invariant vorticity density ω_0. This vorticity distribution is consistent with the results of § 4. A "core" can be said to be present when the structure of a portion of the wake becomes so rolled up as to form a spiral with spacing between successive turns which is comparable to that of an appropriate diffusion thickness of the umbilical sheet feeding it.

Using a simple estimate for the influence of viscosity on the umbilical sheet we find that each circulation element has a thickness which develops as

$$\delta = 4\sqrt{\nu\tau} \qquad (5.1)$$

where ν is the kinematic viscosity of the fluid and τ is the "drift time" associated with that particular wake element. It follows from (5.1) that δ increases monotonically along the umbilical from zero thickness at the wing edge, to a maximum at the point where the umbilical joins the viscous sheath surrounding the core. The drift time at this point is $\tau_{\text{junct}} \equiv t - \bar{\lambda}_{\text{junct}}$ (§ 2). Alternatively (5.1) can be rewritten

$$\delta = \frac{4}{\sqrt{R_{e_c}}}\sqrt{\frac{\tau}{T_0}} \tag{5.1a}$$

and

$$\delta_{\text{junct}} = \frac{4}{\sqrt{R_{e_c}}}\sqrt{\frac{\tau_{\text{junct}}}{T_0}} \tag{5.1b}$$

where R_{e_c} is the Reynolds number based on the wing chord length, $R_{e_c} \equiv \frac{U_\infty \cos\alpha\, c}{\nu}$, and T_0 is the characteristic time of the unsteady crossflow problem $T_0 = \frac{c}{U_\infty \cos\alpha}$.

Having introduced the concept of a diffusion thickness, we proceed to establish a "cut-off" criterion for determining the core formation. We first approximate the rolled-up portion of the ideal wake by a spiral defined by

$$r(\theta) = \frac{r_0\theta}{2\pi} \tag{5.2}$$

where $r(\theta)$ is the distance from the center of the spiral at angle θ, and r_0 is a constant. Denoting the number of encirclements about the spiral centre by N, the relation

$$r_\flat = N r_0 \tag{5.3}$$

is obtained for $N >> 1$. We can now seek a relation between r_0 and δ_{junct} with the aim of establishing the cut-off criterion for the core; that is, determining where and when to replace the ideal wake by an equivalent vortical core. We choose

$$r_0 = \delta_{\text{junct}} \tag{5.4}$$

since in that case one can no longer ignore the effects resulting from the diffusion of vorticity among the vortex elements in the contorted wake region, i.e., the core becomes smeared out and diffused.

Next, recall from § 3 that once a circular core is established at some initial stage, it will have a spatially-constant, time-invariant vorticity, ω_0. The drift time can now be employed to formulate

$$\begin{aligned}\Delta\tau \equiv t - t_{\text{form}} - \tau_{\text{junct}} &= \int_0^{2\pi\left(N-N_{\text{form}}\right)} \frac{d\theta}{\left(\frac{d\theta}{dt}\right)} \\ &= \frac{4\pi\left(N - N_{\text{form}}\right)}{\omega_0}\end{aligned} \tag{5.5}$$

where t_{form} is the time when the core first appears; N_{form} corresponds to N at $t = t_{\text{form}}$. Recall that τ_{junct} is the drift time associated with the vortex element at the umbilical/core juncture at time t. Eqs. (5.3), (5.4), (5.5) can be combined with T_0 and R_{e_c} to give

$$\begin{aligned}\tau_{\text{junct}}^{\frac{1}{2}} - \tau_{\text{junct}}^{\frac{1}{2}}\left(t - t_{\text{form}} + \frac{4\pi}{\omega_0}N_{\text{form}}\right) \\ = -\left(\frac{\pi r_\flat}{c}\right)\frac{\sqrt{R_{e_c}}\sqrt{T_0}}{\omega_0}\end{aligned} \tag{5.6}$$

Additional information relating τ_{junct}, ω_0 and $r_\flat$ can in principle be obtained from a sheath model like that of Ref. [17]. However in this context it suffices to adopt an even simpler model in which the sheath is taken to be of constant thickness equal to that of the umbilical at τ_{juncture}. In this case the total pressure loss around the perimeter of the core is given by

$$\frac{1}{\rho}\Delta p_0 = \frac{\nu U_e}{\delta_{\text{junct}}^2}\Delta\ell \tag{5.7}$$

where U_e is the velocity at the edge of the core $U_e = \frac{\omega_0 r_\flat}{2}$; and $\Delta\ell$ is the perimeter of the core, $\Delta\ell = 2\pi r_\flat$. Recalling from Section (3.2) that the total pressure loss around the core is equal to the rate of change of core circulation, and that for a solid body core,

$$\Gamma_{\text{core}} = \pi\,\omega_0\, r_\flat^2\,, \tag{5.8}$$

we finally obtain

$$\frac{dr_\flat}{dt} = \frac{r_\flat}{32\,\tau_{\text{junct}}} \tag{5.9}$$

In the long run, $t >> \left(-t_{\text{form}} + \frac{4\pi}{\omega_0}N_{\text{form}}\right)$. Eq. (5.6) becomes

$$\tau_{\text{junct}}^{\frac{1}{2}}\left(\tau_{\text{junct}} - t\right) = -\frac{\pi r_\flat}{c}\,\frac{\sqrt{R_{e_c}}\sqrt{T_0}}{\omega_0}\,, \tag{5.10}$$

the unknown parameters being τ_{junct}, $r_\flat$ and ω_0.

Inspection of Eq. (5.10) reveals two limits of the behavior of τ_{junct} which give important insight into the rate of core growth. The first is the one for which

$$\tau_{\text{junct}} \approx t\,. \tag{5.11}$$

This is the limit of a small or very slowly growing core. In this case, using (5.9) the core grows asymptotically as

$$r_\flat \sim \frac{1}{\sqrt{R_{e_c}}}t^{\frac{1}{32}}\,. \tag{5.12}$$

The second limit illustrates the case in which the core is entraining wake vorticity as fast as the umbilical can supply it. For sufficiently large times,

$$\tau_{\text{junct}} \sim \frac{R_{e_c}}{t^2} \tag{5.13}$$

and the core grows according to

$$r_\flat \sim \frac{\omega_0}{\sqrt{R_{e_c}}}t^{\frac{1}{2}}\,. \tag{5.14}$$

Eq. (2.16) allows one to express at any instant the total circulation of the vortex elements lying between any location along the wake and the free end of the wake as a function of the drift time associated with the element at that particular location. Hence there exists a one-to-one correspondence between Γ_{core} and τ_{junct}. Eliminating ω_0 from Eqs. (5.8) and (5.10) then gives $r_\flat$ as a function of τ_{junct}. Such a relation between $r_\flat$ and τ_{junct}, together with Eq.

(5.9), finally determines η_{junct} and r_b. As a result Γ_{core} and ω_0 are determined.

The analysis can also be extended to determine N_{form} since ω_0 is now known and constant in time. This is achieved by projecting backwards in time to $t = t_{form}$. Eqs. (5.6), (5.8), (5.9) are then solved in much the same way as before, the unknowns now being N_{form}, r_b, η_{junct} instead of ω_0, r_b, η_{junct}. Once N_{form} is obtained, t_{form} is determined.

Once the shape, location and circulation distribution of each wake has been determined, the information is at hand to calculate the loading and force on the wing. Eq. (2.15) is used to find the induced velocity at the wing trace associated with the wake. Eq. (2.9) then serves to determine the discountinuous part of the tangential velocity required to satisfy the boundary condition Eq. (2.7) of no flow through the trace. This is added to the "wake free" velocity jump ΔV_0 given by Eq. (2.8). Then the unsteady Bernoulli Equation determines the instantaneous loading at each point on the trace, (as in [6]) which can be integrated to yield the normal force on the wing per unit chord. Hence the local force coefficient (i.e., the force per unit chord normalised by the dynamic pressure and the local span) is given by

$$C_n = \frac{\pi \mathcal{AR}}{2} \sin\alpha + \text{ wake history effects} \qquad (5.15)$$

where the first term is Jones' classical wake free contribution and where the wake history effects are calculated by the integrals just cited.

This result emphasises that the forces depend not only on the local angle of attack and spanwise growth of the trace but also on the cumulative effects of all events in the evolution of the wakes up to that point. This would imply a change in the magnitude and distribution of the normal force across the chord which will have a substantial effect on the wing's overall lift, drag, and moment.

References

1. Jones, R.T., "Properties of Low-Aspect-Ratio Pointed Wings at Speeds Below and Above the Speed of Sound." NACA Report 835.

2. Adams, Mac, "Leading-Edge Separation from Delta Wings at Supersonic Speeds." J. Aeron. Sci., *20*, Reader's Forum, June 1953.

3. Edwards, R.H., "Leading-Edge Separation from Delta Wings." J. Aeron. Sci., *21*, Reader's Forum, Feb. 1954.

4. Cheng, H.K., "Remarks on Non-Linear Lift and Vortex Separation." J. Aeron. Sci., *21*, Reader's Forum, March 1954.

5. Brown, C.E., and Michael, W.H., Jr., "Effects of Leading-Edge Separation on the Lift of a Delta Wing." J. Aeron. Sci., *21*, Oct. 1954.

6. McCune, J.E., "Interactive Aerodynamics of Wings in Severe Maneuver." To be included in Proceedings of Workshop II on Unsteady Flow, United States Air Force Academy, July 28-30, 1987. To be published.

7. Hoeijmakers, H.W.M., *Numerical Simulation of Vortical Flow*, MP 86032 U, NLR, 1986.

8. Powell, K.G., "Vortical Solutions of the Conical Euler Equations." M.I.T. Ph.D. Thesis, June 1987.

9. Earnshaw, P.B., "An Experimental Investigation of the Structure of a Leading Edge Vortex." Aero. Res. Coun., Lond., Rep. No. 22, 876.

10. Thomas, J.L., Taylor, S.L. Anderson, W.K., "Navier-Stokes Computations of Vortical Flows Over Low Aspect Ratio Wings." AIAA 87-0207, January 1987.

11. Newsome, R.W., Kandil, O.A., "Vortical Flow Aerodynamics — Physical Aspects and Numerical Simulation." AIAA 87-0205, January 1987.

12. Munk, M., "The Aerodynamic Forces on Airship Hulls." NACA Report 184.

13. Wagner, H. "Dynamischer Auftrieb von Tragflugeln," Zeitschr. f. Agnew. Math. u. Mech. (ZAMM), *5*, 17, 1925.

14. Scott, Matthew T., "Nonlinear Airfoil-Wake Interactions in Large Amplitude Unsteady Flow," M.I.T. Master's Thesis, June, 1987. See also: Scott, M. and McCune, J.E., AIAA Paper Nr. 88-0129, AIAA 26th Aerospace Sciences Meeting, Reno NV, Jan., 1988.

15. Lamb, Sir Horace, *Hydrodynamics*, 6th Ed., Dover Publications, N.Y., 1945.

16. Batchelor, G.K., "On Steady Laminar Flow with Closed Streamlines at Large Reynolds Number." Journal of Fluid Mechanics, Part II, p. 177, 1956.

17. Weissbein, D. "Embedded Vortical Regions in Otherwise Irrotational Flows." M.I.T. S.M. Thesis, June 1987.

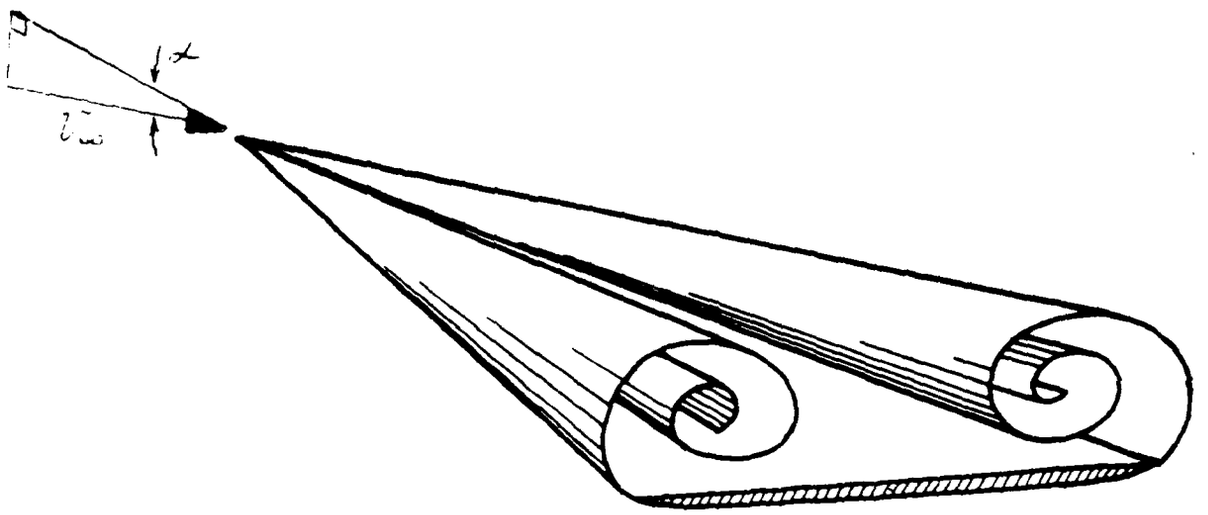

(a)

Vortex wake Structure above Suction Surface of Wing

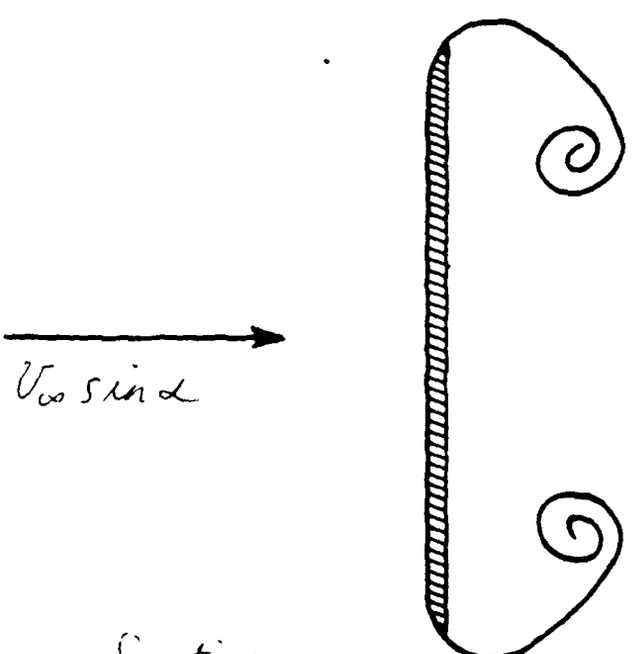

(b)

Cut-away Section Showing Wing and Wake traces

Fig. 1

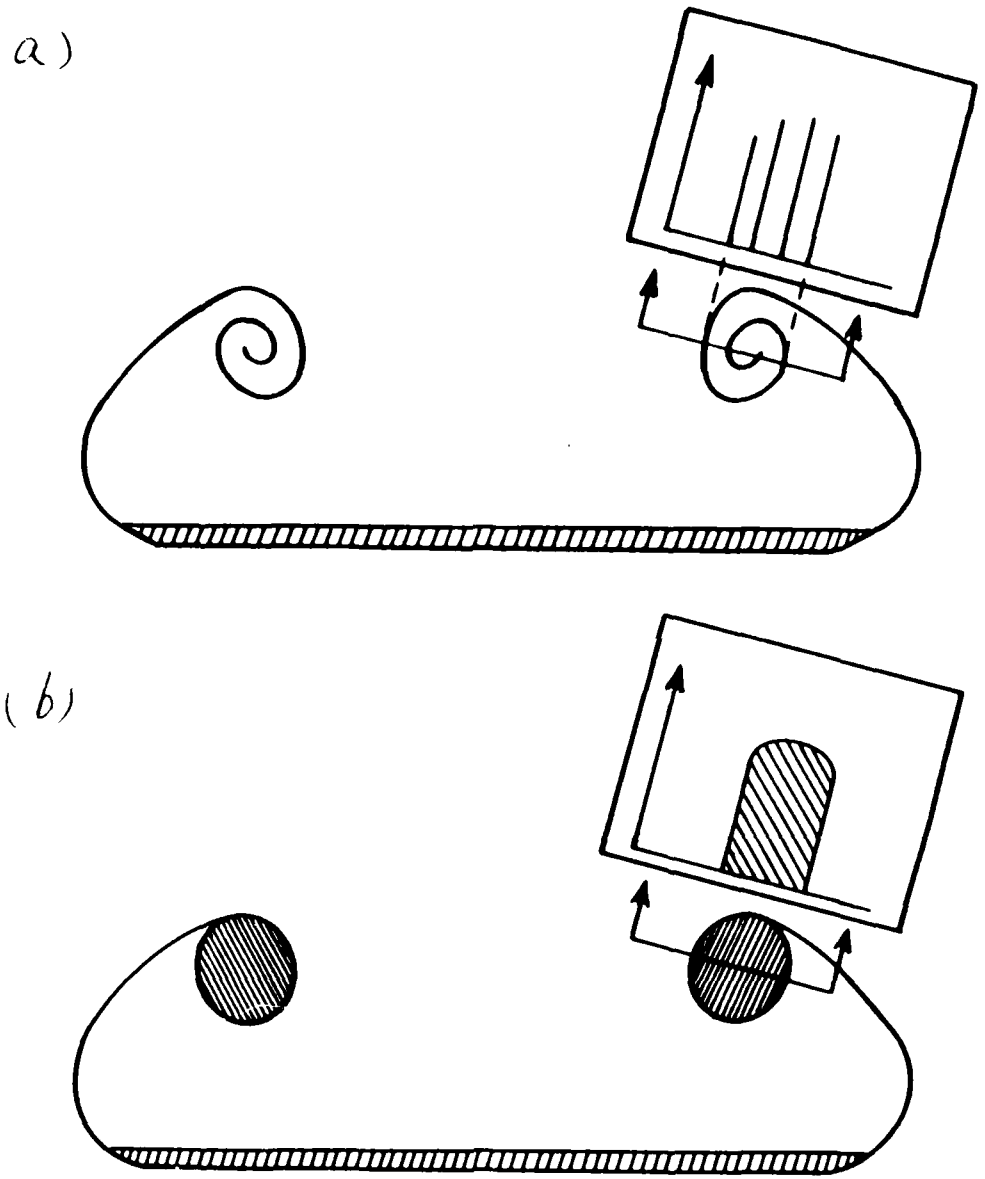

Fig. 2 Replacement of the Ideal Wake Structures(a) by Cores with Distributed Vorticity

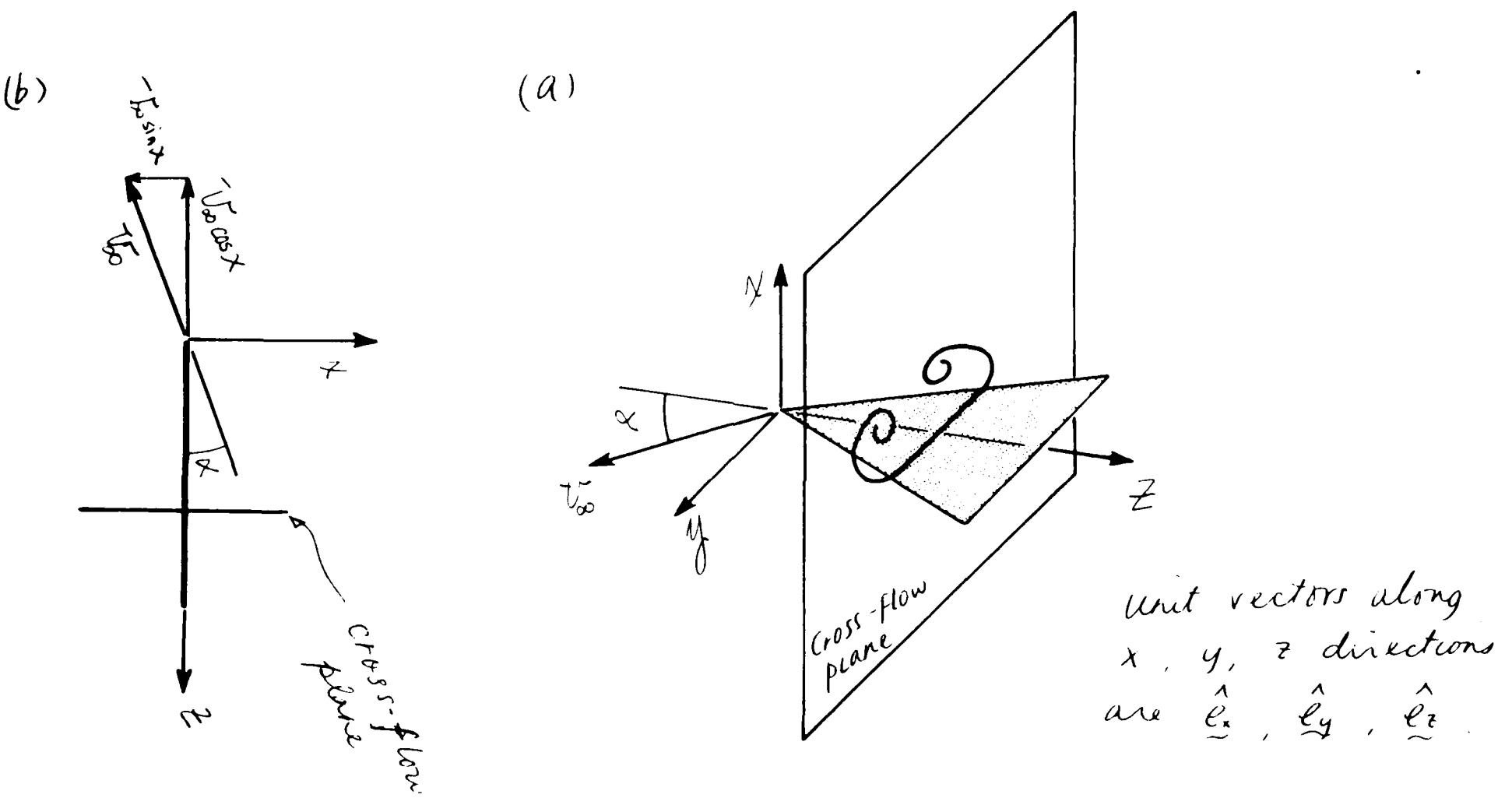

Fig. 3 Illustration of the Time Analogy:
(a) Wing penetrating Cross-Flow Plane
(b) Side View

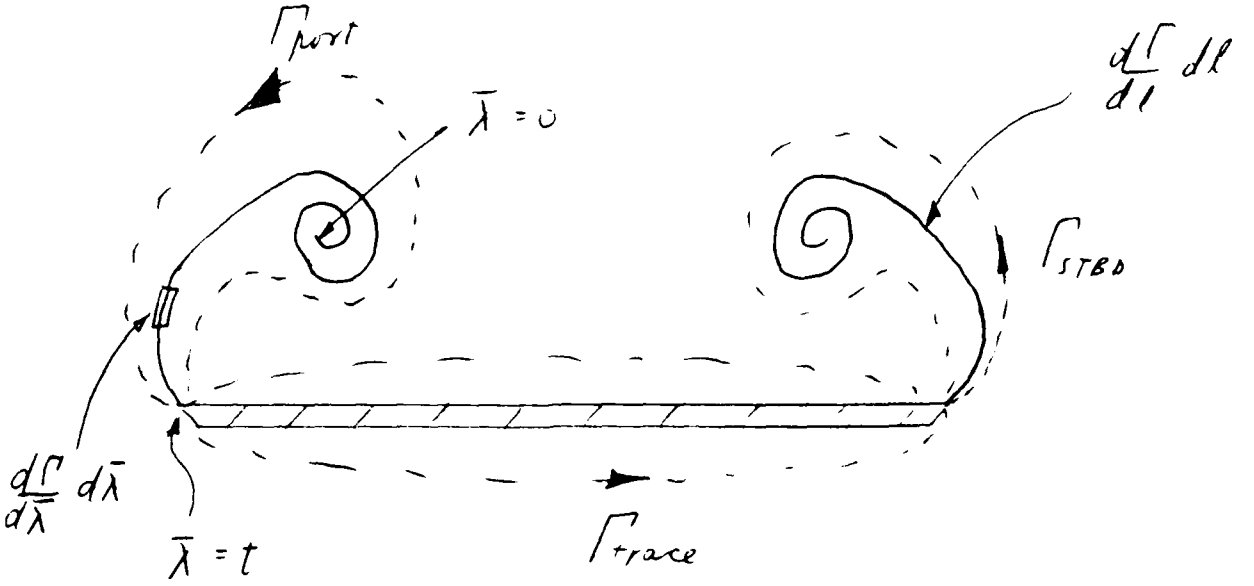

Fig. 4 Relations of Γ_{trace}, Γ_{port} and Γ_{STBD}

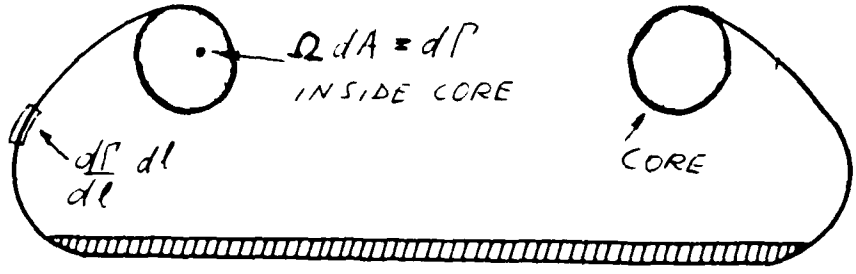

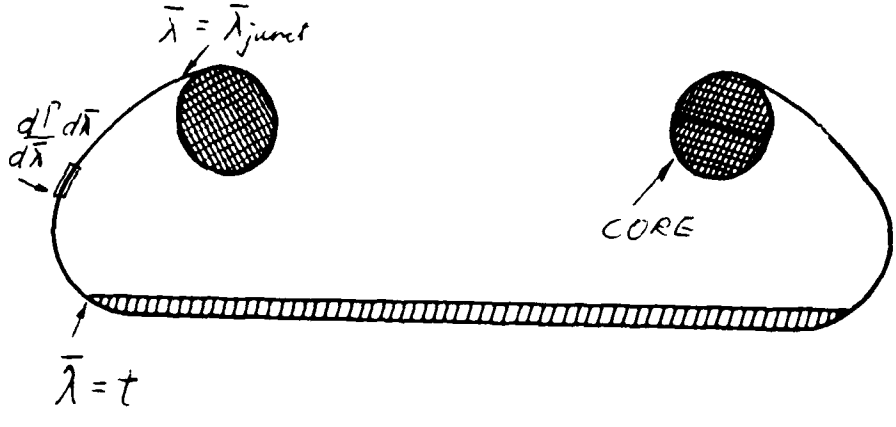

Fig 5 Figures showing λ, Γ and Ω inside core

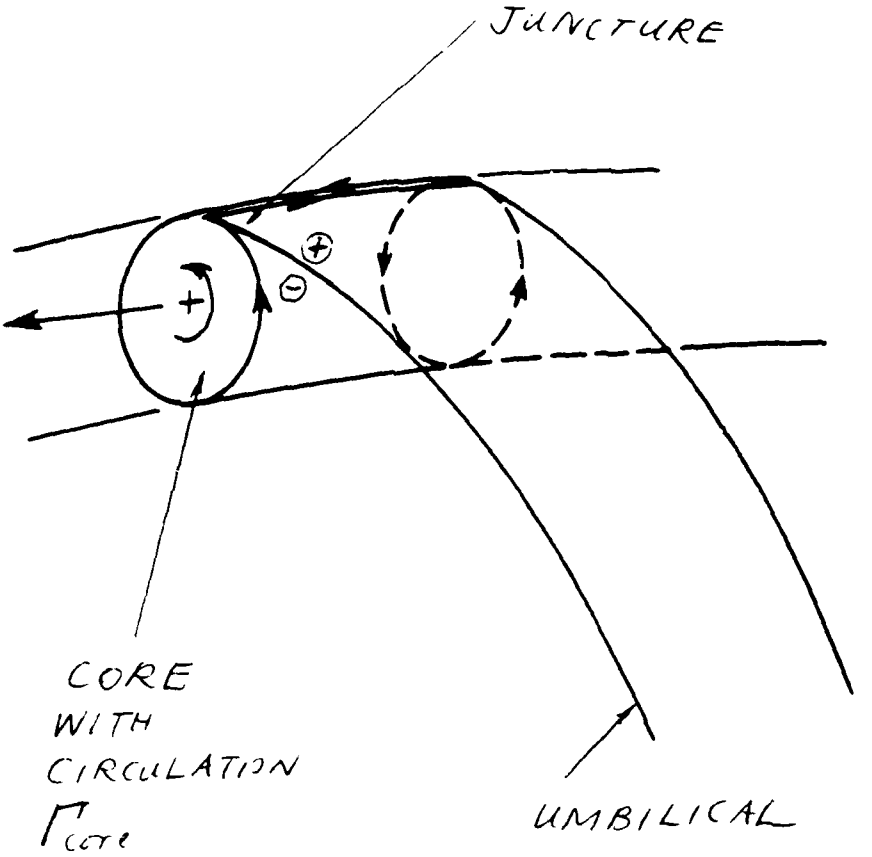

Fig 6. CORE AND UMBILICAL SEEN IN THE FRAME OF THE WING

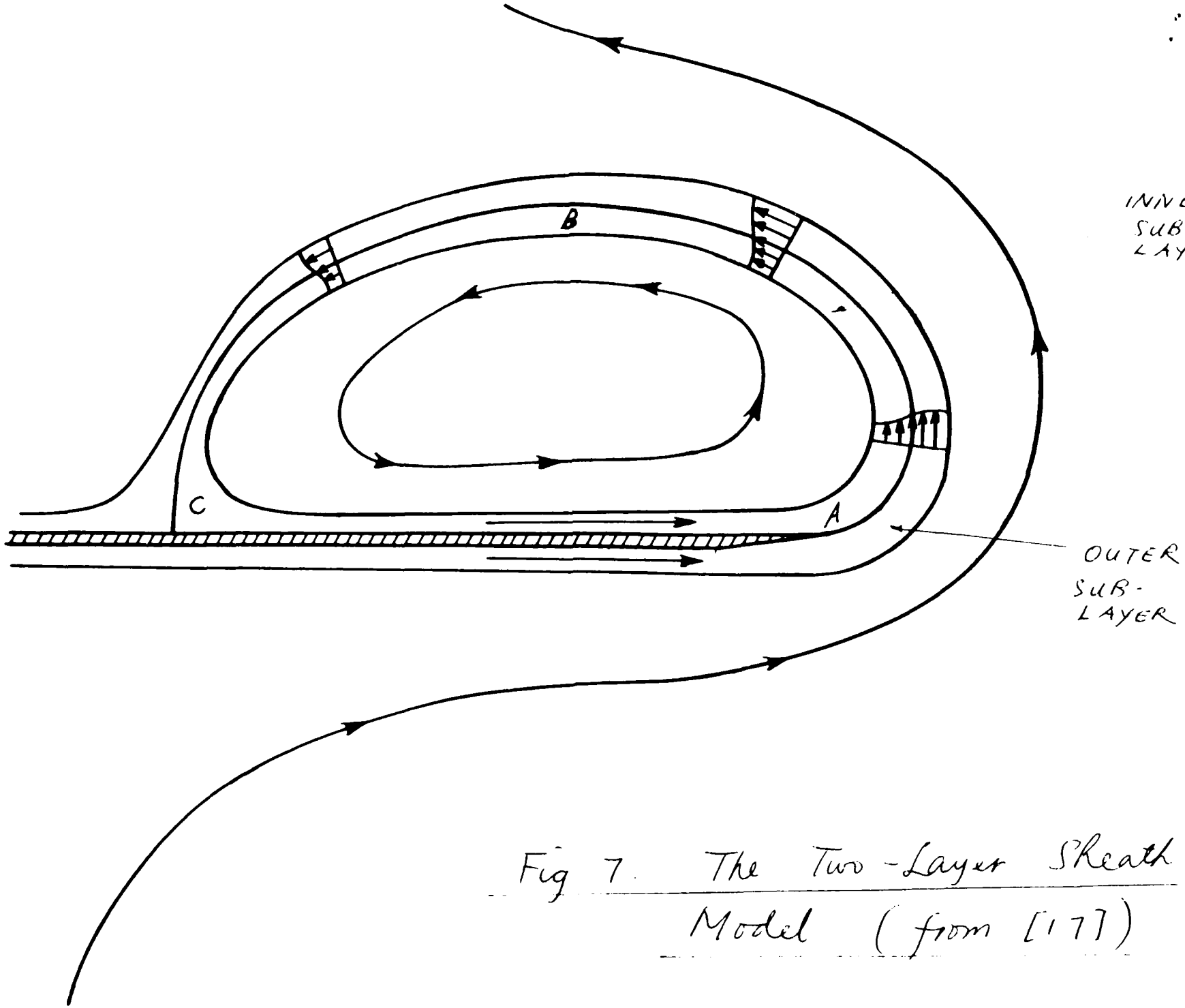

Fig 7 The Two-Layer Sheath Model (from [17])

Fig. 8 Bubble streamline pattern for $R_x = 10000$ (from [17])

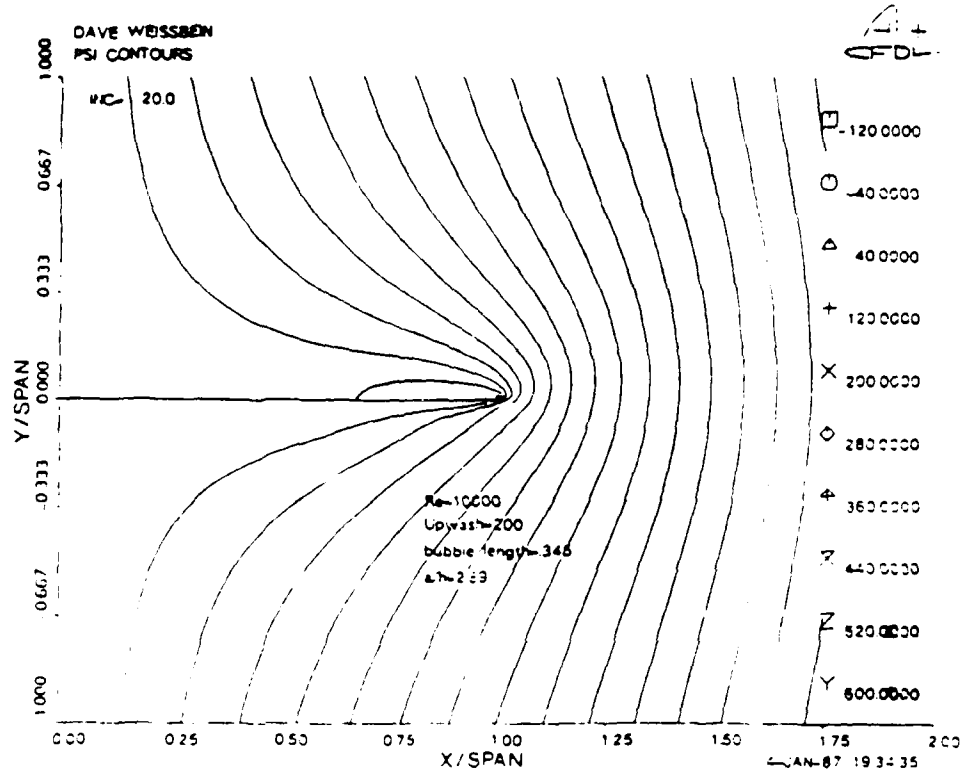

Figure 6.6a Cross-flow streamlines of leading edge separation bubble for $Re = 10000$

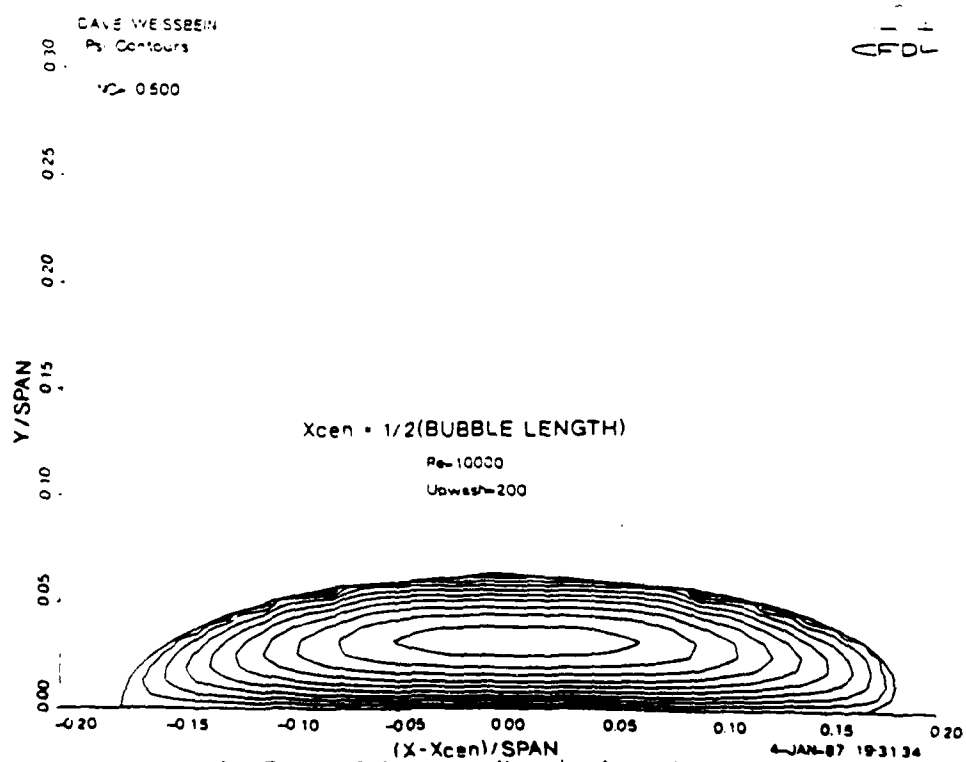

Figure 6.6b. Detail of the streamlines in the embedded region, $Re = 10000$.

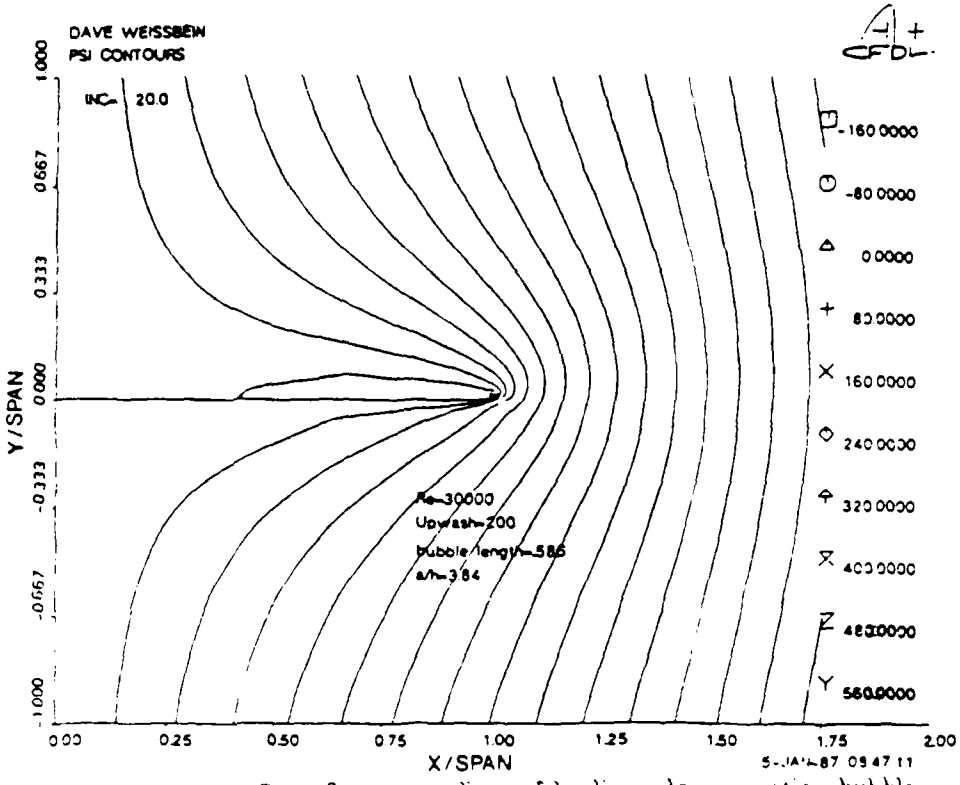

Figure 6.9a Cross-flow streamlines of leading edge separation bubble for $Re = 30000$.

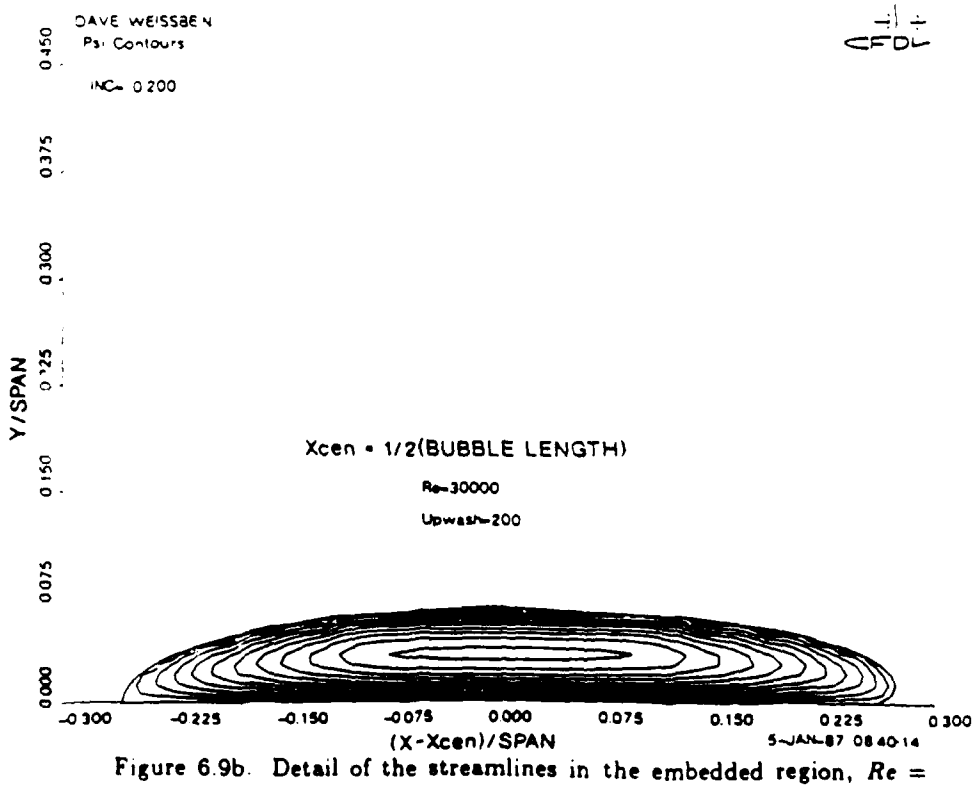

Figure 6.9b Detail of the streamlines in the embedded region, $Re = 30000$.

END

DATE

FILMED

3-88

DTIC